UNIVERSITY OF LIVERPOOL

Developing a CFD informed approach for subchannel analysis investigations for a wire-wrapped fuel bundle experiment

Venkata Ravindra Mallela Viswa (201462952)

Supervisors:

Prof. Bruno Merk, Dr Ming Li, Prof. Stephen Graham

June 2022

Table of Contents

Abstract

Project FAITH, which is part of the UK government funded Advanced Manufacturing and Materials (AMM) phase 2 nuclear innovation programmes, provided an excellent opportunity to develop skills in nuclear thermal hydraulics area. The project aimed at exploring modular building techniques for a sodium rig that can be used to conduct Generation IV reactor thermal-hydraulics experiments within the UK. To achieve this, two rigs, one using water (Rig - 1) and the other one using sodium (Rig - 2) have been proposed using modular technology.

A subchannel code called CTF has been used to model the Rig-1 facility which is being built at NNL's Workington facility in a modular manner by Cammell Laird, a ship building company. To gain confidence and build expertise on using the CTF code, two validation activities have been studied. The first validation activity is performed against PSBT benchmark data where the boundary and operating conditions are that of pressurised water reactors involving multiphase, while the second validation activity is on PNNL experimental studies in which the measurements were made on the flow regimes similar to single-phase flow inside a Gen IV sodium cooled fast reactor. Both these validation activities offered invaluable experience and confidence in using CTF for practical problems to assure successful qualification in code usage.

Rig-1 configuration along with its operating conditions makes it a non-standard case for analysis from CTF, not least due to the geometry that has fuel pins with wire wrapped around them, arranged in a triangular lattice in a hexagonal pipe. A method has been developed wherein CFD studies were performed for the operating Reynolds numbers, N_{Re} ($5000 \leq N_{Re} \leq 100000$) on Rig – 1 and frictional loss coefficients were obtained from the analysis. These frictional loss coefficients were linked in the subchannel code, CTF replacing its standard frictional correlations for pressure drop estimates.

The method has been tested on various pin arrangements ranging from square array to triangular array to the current Rig-1 design that has a hexagonal pipe with 7 fuel pins with wire wrapped around them, replicating fuel rod structure inside a sodium cooled fast reactor. The CTF results with its standard frictional correlations have over predicted the pressure drops (as compared to CFD results) by about 25% for square or triangular subchannels and around 6% for Rig-1 geometry with wire wraps. However, when this novel method of applying frictional coefficients (obtained from CFD) in CTF code, the results of pressure drop from CTF matched excellent with CFD results by overpredicting only about 0.5%.

This improved CTF model can also be used to perform a range of parametric studies which includes slight variations in the geometry (due to manufacturing tolerances etc.) and their effects on the flow at a quicker turnaround time. In addition to this, the frictional coefficients obtained from 7-pin, can also be used for 19-pin and 37-pin configurations, thus CTF modelling capabilities are further expanded.

List of publications

Paper Submitted for 4th International Conference on Nuclear Power Plants: Structures, Risk, Control & Decommissioning (NUPP 2022): 19-20 September 2022, ONLINE

Title: OFF-SITE MODULAR MANUFACTURE AND DIGITAL TWIN FOR FAST REACTOR EXPERIMENTS

Project FAITH, Fuel Assembly Incorporating Thermal Hydraulics

Authors: M Bankhead, J Willgress, B Merk, V Ravindra

MDPI Journal Articles:

1. CTF and FLOCAL Thermal Hydraulics Validations and Verifications within a Multiscale and Multiphysics Software Development

Authors: Sebastian Davies, Ulrich Rohde, Dzianis Litskevich, Bruno Merk, Paul Bryce, Andrew Levers, Anna Detkina, Seddon Atkinson and Venkata Ravindra

2. DYN3D and CTF Coupling within a Multiscale and Multiphysics Software Development (Part I)

Authors: Sebastian Davies, Dzianis Litskevich, Ulrich Rohde, Anna Detkina, Bruno Merk, Paul Bryce, Andrew Levers and Venkata Ravindra

List of figures

List of tables

CHAPTER 1: INTRODUCTION

1.1 Forward

Project FAITH (Fuel Assembly Incorporating Thermal Hydraulics) originated from the (Department for Business, Energy & Industrial Strategy) BEIS programme, "Advanced Materials and Manufacturing Phase Two". The objective is to explore modular building techniques for a sodium rig that can be used to conduct Generation IV reactor thermal-hydraulics experiments within the UK. To achieve this, two rigs, one using water (Rig-1) and the other one using sodium (Rig-2) have been proposed using modular technology.

Cammell Laird (CL) are involved in design and manufacture of these modular assemblies with the support from National Nuclear Laboratory (NNL). The construction of these rigs is multi-phased. During the initial phase, a water-based fuel assembly rig will be built to carry out isothermal experiments. Water is considered as the working fluid because of its ease of handling, minimum safety hazards, low cost, ready availability with well-defined properties and characteristics. The knowledge and experience gained from building and operating this water rig will be applied to the design and build activities for the sodium rig. Hence, the study of the water rig will be a treated as an important initial step towards understanding the thermal hydraulics behaviour of sodium in liquid metal fast reactors (LMFR) subchannels. Although, Prandtl number (Pr) cannot be matched to sodium, using flow Reynolds number (Re), it is possible to replicate some of the flow regimes that are experienced in LMFR as its rheological properties are not too different from sodium, so Reynolds numbers can be matched quite easily. The definitions of Prandtl number and Reynolds number are as given below with typical SI units provided for each property:

$$\mathrm{Pr} = \frac{momentum\ diffisivity}{thermal\ diffusivity} = \frac{(\mu/\rho)}{\left(k/_{C_P}\rho\right)} = \frac{C_p\mu}{k}$$

$$\mathrm{Re} = \frac{inertial\ forces}{viscous\ forces} = \frac{\rho vL}{\mu}$$

where:

μ = dynamic viscosity of the fluid (kg/m-s)

ρ = density of the fluid (kg/m³)

k = thermal conductivity of the fluid (W/m-K) or (W/m-°C)

C_P= Specific heat capacity of the fluid (J/kg-K) or (J/kg-°C)

L = characteristic linear dimension (m)

v = velocity of the fluid with respect to the object (m/s)

Table 1-1 lists some of the physical properties of light water at a representative temperature of 315°C and pressure of 155 bar that correspond to primary loop in a pressurised water reactor while the liquid sodium physical properties are reported at 535°C and 1 bar. The orders of magnitude difference in Prandtl number between water and liquid sodium can be seen clearly from the values of around 1 for light water and around 225 times less for liquid sodium as compared with water.

Table 1-1: Physical properties of water and liquid sodium with Prandtl number

Reactor Coolant	Reference Temperature (°C) and Pressure (bar)	Density (ρ) (kg/m³)	Dynamic Viscosity (μ) (kg/m-s)	Thermal Conductivity (k) (W/m-°C)	Heat Capacity (C_P) (J/kg-°C)	Prandtl Number
Light water	315°C and 155 bar	704	0.000087	0.5	6270	1.091
Liquid sodium	535°C and 1bar	817.7	0.000228	65.88	1260	0.00436

Whilst the objective of the project FAITH is to investigate and understand the fundamental aspects of fluid flow and heat transfer mechanisms for a liquid sodium system, many other associated challenges will need to be considered when applying this knowledge within an industrial environment. As this involves lot of fundamental research that also needs to be applied to industrial problems, it is intended that this MPhil programme will facilitate a close collaboration between NNL and the UK academic network, particularly with university

of Liverpool such that NNL staff can upskill and expand the capability on thermal hydraulics area and apply this knowledge in an industrial setting.

One of the objectives of the FAITH programme is to upskill the UK R&D skills base in sodium technology to replace skills that were lost, due to the winding down of the UK's world leading research in this area in the 1990's. Furthermore, the UK, being a founding member of the Generation IV International Forum (GIF), has responsibility to take lead in developing research necessary to test the feasibility and performance of fourth generation nuclear systems, and to make them available for industrial deployment by 2030. Research and development on sodium-cooled fast reactors (SFR) is one of the six reactor technologies identified by GIF. The FAITH project represented an opportunity to develop skills in nuclear thermal hydraulics vis-à-vis SFR. The MPhil project described in this report was developed from this opportunity and represents one contribution FAITH is making to re-establishing UK expertise.

1.2 Gap analysis relating to water rigs & sodium rigs

The proposed rigs of both Rig-1 (water as working fluid) and Rig-2 (sodium as working fluid) from Project FAITH have 7 fuel rods or pins with wire wrapped around each of them, further arranged in a triangular lattice in a hexagonal duct. This is the typical arrangement of central section of fuel rods in a sodium cooled fast reactor assembly. Figure 1-1 shows 19-pin arrangement with wire wrapped around each of them in a hexagonal duct. The left image shows the top cross-sectional view depicting the arrangement of interior, corner and side rods whilst the right image shows the side view of the fuel pin with the helical wire wrapped around. Depending on the number of rings of rods that are used in the fuel assembly, the total number of rods keep changing. For example, in Figure 1-1, the number of rings of rods are 2, and this makes the total number of rods as 19, while the interior, corner and side rods are 7,6 and 6 respectively.
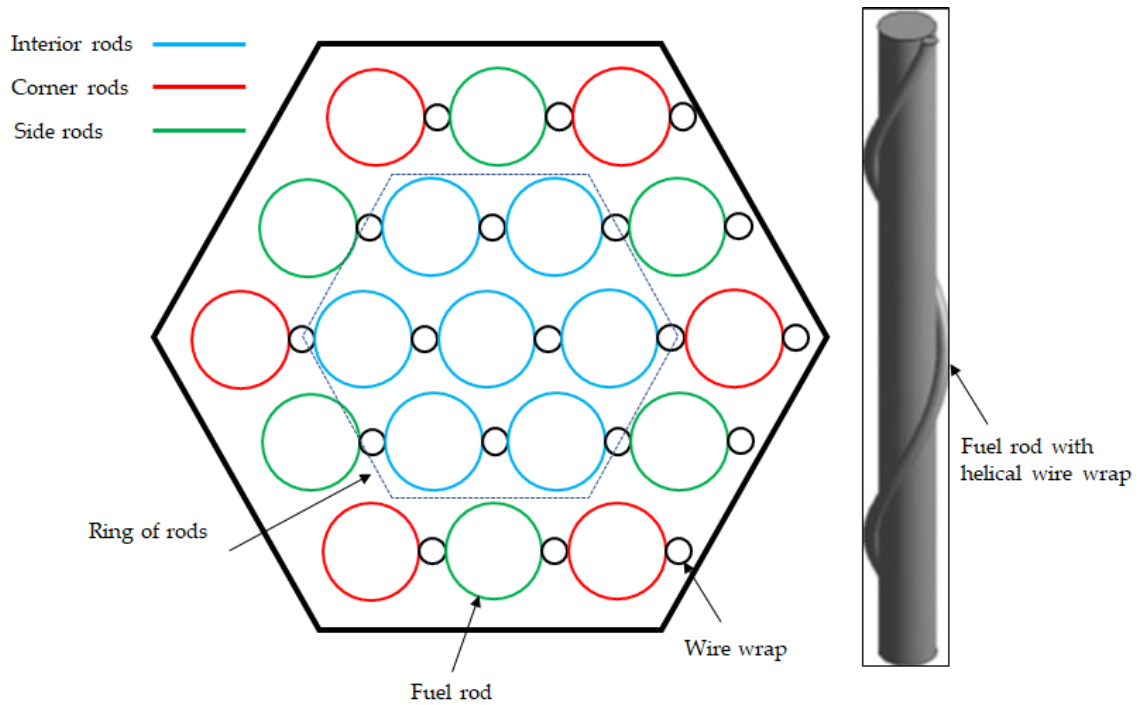
Figure 1-1: Wire-wrapped assembly and fuel configuration with 19 pins

The following table (see Table 1-2) summarises the theoretically possible number of rods in a hexagonal fuel assembly as a function of number of ring rods. The table lists number of possible interior, corner and side rods. The first thing that can be noticed is that the corner rods is always 6 (when there are more than one ring of rods) while the number of side rods is $6 \times (n-1)$. The total rods can be computed using the expression: $\sum_n 6n + 1$ where n is the number of rings of rods.

Table 1-2: The maximum number of theoretically possible number of rods in a hexagonal fuel assembly as a function of 'Ring Count' (Masterson 2019)

Rings of Rods	Interior Rods	Corner Rods	Side Rods	Total Rods
1	7	0	0	7
2	7	6	6	19
3	19	6	12	37
4	37	6	18	61
5	61	6	24	91
6	91	6	30	127

n	Same as total rods for (n-1) rings of rods	6	6 × (n-1)	$\sum_n 6n + 1$

The actual number of fuel rods for a sodium cooled fast reactor fuel assembly in the core typically ranges between 169- 271 (IAEA, 2006 #72). It is not practical to build rigs that comprise these many hundreds of rods; a few studies in the literature have focussed on representative minimum number of pins that are needed to understand the behaviour of the core. (Rolfo et al. 2012) studied the flow characteristics for several fuel pin/rods arranged in a hexagonal duct. The authors have looked at 7, 19, 61 and 271 fuel pin configurations computationally. (Gajapathy et al. 2009) have investigated for 7, 19 and 37 fuel pin configurations numerically. The detailed computational studies from these two different papers have concluded that the number of fuel pins away from the centre does not influence greatly on the flow features towards the centroid of the core where only seven pins are present in a hexagonal lattice. This suggests that the rigs in project FAITH adapted 7-fuel pin configuration in a hexagonal duct is evidently a practical way forward backed up by the literature.

There are a few researchers who did experiments on either square or hexagonal configurations with different fuel pin configurations such as 5 × 5 or 4× 4 pin arrangement for square and 7 or 19 or 61 pins for hexagonal; these studies will be discussed in detail in the subsequent sections.

1.2.1 Measurements on square subchannels

The authors in (Chang, Kim & Song 2014; Dominguez-Ontiveros & Hassan 2009; Ikeda & Hoshi 2007; Shen, Cao & Lu 1991) have looked at square pin configurations with an objective to measure either lateral or axial velocities, however none of these authors measured the pressure drops. (Shen, Cao & Lu 1991) investigated 4× 4 type of assembly in a square with spacer grid, and measured velocities in only in lateral direction at a fixed Reynolds number of 14200 using Laser Doppler Velocimeter (LDV). The authors have studied the effects of blade angles of spacers on the rate of mixing and concluded that larger angles produce greater mixing, but caused non-uniform mixing. (In 1999) developed a computational fluid dynamics (CFD) model representing the setup by (Shen, Cao & Lu 1991) and concluded that the CFD

simulation can be used to analyse the effect of the open blades on the crossflow mixing. The rest of the authors used 5 × 5 square pin arrangement with spacer grid, but the Reynolds number that was fixed for the test was different among them and even the velocity measurement techniques were different among them. (Ikeda & Hoshi 2007) found measuring velocities using LDV was challenging due to the number of rods and the associated small gaps among them within the experimental setup. They developed a rod-emended fibre LDV to measure both the axial and cross-flow velocities. (Dominguez-Ontiveros, Estrada-Perez & Hassan 2010; Dominguez-Ontiveros & Hassan 2009) also performed experiments on 5 × 5 square pin arrangement with spacer grid, however they used Time Resolved Particle Image Velocimetry (TR-PIV) to provide their experimental database for CFD simulations. (Li et al. 2019) recently performed measurements on a 5 × 5 rod bundle with spacer grids with the latest techniques such as Laser Induced Fluorescence (LIF), a non-intrusive method of measuring concentration and temperature in the flow. Their measurements also aimed at providing benchmark data for CFD codes validation studies. (Chang, Kim & Song 2014) measured both axial and lateral velocities within the subchannels using 2D LDV. All of these research work indicates that there are several flow visualisation and full-field measurement techniques were used in rod bundle channels but predominantly PIV and LDV techniques were used to perform quantitative analysis and further to get high precision data.

1.2.2   Measurements on triangular subchannels

(Nguyen et al. 2017; Vaghetto et al. 2017) performed experiments on 61-pin wire wrapped fuel pins arranged in a hexagonal lattice measuring for both velocities and pressure drops. The ratio of pitch to diameter of their rod bundle is 1.19 which is close to 1.2 for the proposed Rig-1 by project FAITH. However, the other difference worth mentioning is that their wire wraps do not physically contact the other surrounding rods or pins unlike for the proposed Rig-1. The velocity measurements and flow structures near wall regions were reported using PIV for a fixed Reynolds number of 19,000 by (Nguyen et al. 2017). The pressure measurements were reported for the Reynolds number range of 250-19000 by (Vaghetto et al. 2017). (Bertocchi, Rohde & Kloosterman 2019) in their recent work considered 7-pin wire wrapped fuel pins in a hexagonal duct. The experiments were carried out for a range of Reynolds numbers from 4400-21600. As with the experimental setup by (Vaghetto et al. 2017), the wire wraps do not touch the neighbouring pins directly. It is also noted that the

pitch to the diameter ratio of fuel pins for this setup is 1.11. The authors only presented flow details around the central rod using PIV technique, however the pressure measurements were not performed by them. At the time of writing this thesis, it is anticipated that CL and NNL will use non-intrusive instrumentation for the measurements of velocity and pressure for Rig-1.

1.2.3 Views on developed correlations from the literature

The majority of the pressure drop experiments and friction factor correlations for rod bundle configurations were developed before 1990. A semi-empirical model to estimate the pressure losses in a hexagonal array of wire-wrapped pins in the turbulent flow regime is developed by (Novendstern 1972). (Rehme 1973) performed experiments on a wide range of geometrical parameters, for example, involving pitch to diameter ratio from 1.125 to 1.417, and number of pins ranging from 7 to 61. All of these studies aimed at pressure drop correlations within the Reynolds number ranging between 1000 to 30000. (Cheng & Todreas 1986) came up with their hydrodynamic models for subchannel friction factors, mixing parameters in a 37-pin fuel bundle, covering laminar, transition and turbulent flow regimes. Specific correlations for subchannel and bundle friction factors, flow split, enhanced eddy diffusivity and the peripheral wire induced swirl velocity were presented by these authors. (Chun & Seo 2001) and (Bubelis & Schikorr 2008) have revisited these existing correlations and following their detailed assessments, both have come up with different conclusions. (Chun & Seo 2001) concluded that correlations from the work of (Cheng & Todreas 1986) are the best fit which is generally called Cheng and Todreas Correlation (CTD), whereas (Bubelis & Schikorr 2008) concluded that (Rehme 1973) is the best fit. This could perhaps be due to different data sets and accompanying assessing methods used by the researchers. However, (Chen, Todreas & Nguyen 2014) have clarified in their work about the contradicting conclusions between those famous correlations. This contraction is due to the simplified Cheng-Todreas model described in (Bubelis & Schikorr 2008) is not same as the one originally published by (Cheng & Todreas 1986) as incorrect parameter related to the wire lead length was used which lead to the conclusions. Furthermore, they provided recommendations to the designers regarding the most appropriate correlations that have to be used as fit for purpose depending on their application.

Even though there are many ongoing research programmes related to rod bundle experiments on sodium fast cooled reactors in China, France, India and Russia, there is only a little published data available in the literature which can be directly compared with the CFD simulation data. This could perhaps be due to the associated challenges accessing the flow regions within a tightly packed hexagonal rod bundle with wire wraps. The majority of the liquid metal cooled fast reactors employ wire wraps in place of spacers between the individual pins for various reasons including structural integrity, enhanced flow mixing, heat transfer etc. However, wire wrappers produce higher pressure drops as compared to bare rods. While at low Reynolds number this increase in pressure may be marginal, it becomes significantly higher at high Reynolds number. These wire wraps in general have close contact with the neighbouring pins within the hexagonal arrangement. New thermal hydraulic experiments are currently under preparation in Germany, Italy, and the USA to address these challenges and further provide accurate flow representations using the state-of-the-art measurement techniques. Republic of Korea maintains a large-scale component facility for sodium cooled fast reactors to provide benchmark data (both separate and integral effect test data) for verification & validation (V&V) of thermal hydraulics design codes and safety analysis system codes (Kim et al. 2016). The results produced by Sodium Test Loop for Safety Simulation and Assessment-1 (STELLA-1) were used for V&V of computer codes. Here in the UK, BEIS is planning to base Britain's first thermal hydraulics test facility in Anglesey, North Wales. In the absence of reliable CFD-comparable data from the measurements, CFD techniques are increasingly in use by the thermal hydraulics researchers/engineers. As a result, the focus is now shifting towards high-fidelity CFD approaches such as large eddy simulation (LES) and direct numerical simulation (DNS) which can be used to verify the numerical output from the standard Reynolds-Averaged Navier-Stokes (RANS) approaches ((Merzari et al. 2016).

1.3   Objective and scope of the thesis

The overall objective of this MPhil project is to support the rig related work (be it water or liquid sodium as coolant) being carried out by CL from a thermal hydraulics standpoint and thereby contribute to the research and developmental activities regarding Generation IV reactor technology within the UK. While achieving this objective, the overarching aim of the project FAITH i.e., upskilling and expanding capabilities in the domain of thermal hydraulics will also have been met.

The scope adapts pure computational studies on Rig-1 geometry using a subchannel code called CTF and a Computational Fluid Dynamics (CFD) solver namely Ansys Fluent. The detailed capabilities of these codes are explained at length in the next chapter. It is recognised and accepted by the nuclear industry that the subchannel codes (such as CTF) are efficient at predicting the performance details of nuclear reactor core at subchannel level in fast and effective manner specially for Light Water Reactors (LWR). However, the codes have certain limitations in the way they predict the flow behaviour around the regions within the subchannels for certain configurations of the geometry, for instance, triangular arrangement of fuel rods in a hexagonal pipe without/with wire wrapped around the fuel rods. This is because of the complex nature of flow in certain regions where the wire is helically wound around the rod, subsequently causing secondary flows. On the other hand, CFD codes (such as Ansys Fluent) can potentially resolve all the detailed flow features involving flow separation, boundary layer flows and turbulent mixing etc. but computationally intense, expensive and time consuming even for steady-state analysis.

Studies in this work address how to account for these complex flow effects in subchannels with minimum CFD studies that are required to generate enough information (for example, pressure loss coefficients) which can be further fed back into subchannel codes. Taking the required information from the CFD codes, the subchannel codes can be more reliably used for various useful investigations in thermal hydraulic analysis of nuclear reactor core. As a result, the values of safety margins of different thermal hydraulic systems can be improved.

1.4   Organisation of the thesis

This thesis is divided into 3 major parts. The first part consists of initial two chapters which are Chapter 1 and Chapter 2. Introduction, background and motivation to the research problem were discussed in Chapter 1 and Chapter 2 presents subchannels codes, CFD codes and their limitations based on the way they are adapted in the nuclear industry. The second part contains two different validation activities. The first one being the validation activity which involves building and running CTF model of the rig with the operating conditions where the measured data was made available from Pressurised Water Reactor Sub-channel and Bundle Tests (PSBT) benchmark exercise. The details of this study are presented Chapter

3. In Chapter 4, the second validation activity is reported. This validation study is about modelling the 2 × 6 rod bundle experimental flow conditions that are representative of sodium cooled fast reactors using CTF. The final part consists of computational activities that are carried out in support of Rig-1 using both subchannel and CFD codes which are presented in Chapter 5 while the Chapter 6 summarises the conclusions and future work.

CHAPTER 2: CODES AND METHODS

2.1   Introduction

The details of subchannel codes, CFD codes in the context of subchannel analysis during this work have been discussed in this chapter following a brief introduction on the different levels of quality used for CFD analysis.

The hierarchy of CFD approaches, subchannel codes and system level codes using lumped parameter models is shown in the pyramid in Figure 2-1. As can be seen, Direct Numerical Solution (DNS) yields the most accurate solution followed by Large Eddy Simulation (LES). This is because DNS method solves for the Navier-Stokes equations numerically without any turbulence model resolving the whole range of spatial and temporal scales of the turbulence. LES method still tries to resolve some the eddies with the mesh. Reynolds Averaged Navier-Stokes solution (RANS) follows these two and then subchannels codes find their place between RANS and system level codes. It is evident from the figure that the complexity, computational costs, resolution of physics, model mesh size and accuracy will increase as we move from system codes to DNS. But using DNS and LES is impractical for the subchannel analysis due to their disadvantages which are discussed in detail in the later part of this chapter, RANS has limited appeal despite the wider availability of turbulence models. This is due to the required computational costs and the model mesh size are still enormous at fuel assembly level and core level(Yu et al. 2017).
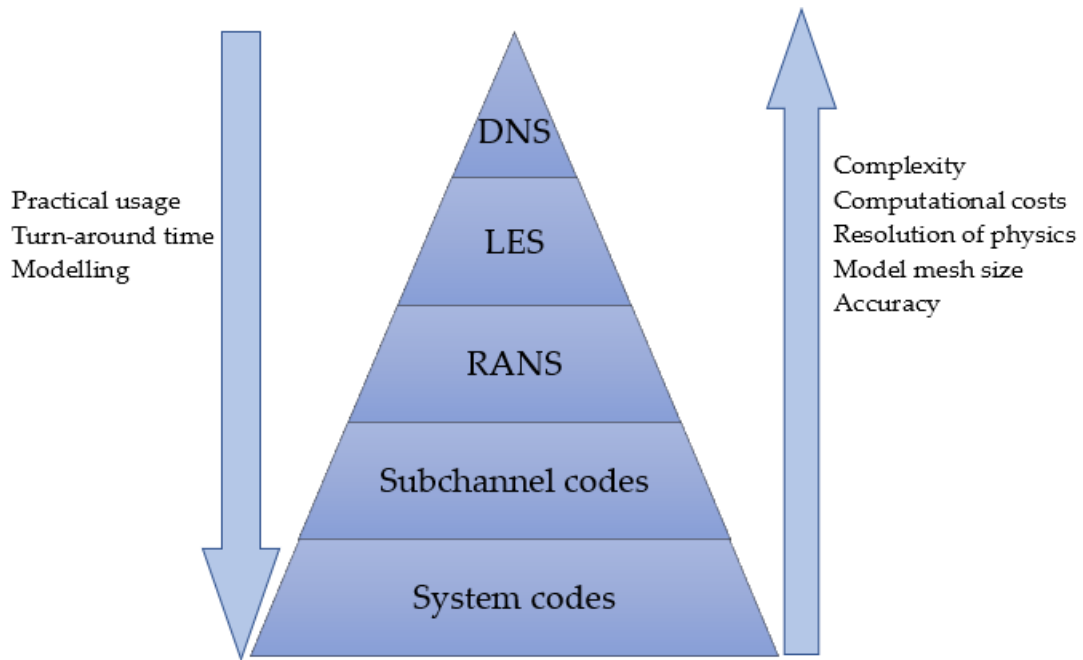
Figure 2-1 The pyramid of different CFD approaches, subchannel codes and system codes in the context of subchannel flow analysis for fuel assembly and reactor cores

2.2   CTF subchannel code

CTF is an improved version of Coolant-Boiling in Rod Arrays – Two Fluids code (COBRA-TF), which is a thermal hydraulic subchannel analysis code capable of calculating reversed flow, counter current flow and cross-flow in light water reactor (LWR) analysis. This code was originally developed using FORTRAN 77 during 1980 by PNNL (Pacific Northwest National Laboratory)(Salko Jr et al. 2019), and later had been in use by many institutions and further the capabilities of the code were enhanced by Pennsylvania State University (PSU) by their Reactor Dynamics and Fuel Modelling Group (RDFMG) and eventually renamed COBRA-TF as CTF (Salko Jr et al. 2019). Some of the enhancements include translation from fixed to free format coding, enhanced input-error checking, implementation of better numerical schemes etc (Sung et al. 2015). Nuclear Regulation Commission (NRC) has been the major sponsor of all these developmental activities around this code. Currently, CTF is being maintained and developed by PSU and North Carolina State University (NCSU) trying to expand its capabilities for Water-Water Energetics Reactors (VVER), Small Modular Reactors (SMR)using light water and Fast Breeder Reactors (FBR) using sodium as coolant.

The purpose of the code is to study the performance and accident scenarios of nuclear reactor core from the thermal hydraulics standpoint. It uses a two-fluid, three-field (i.e., fluid film, fluid droplets and vapour) modelling approach with provision for both three-dimensional (3D) cartesian and subchannel coordinate formulations for fluid flow and heat transfer solutions in fuel rod bundles and reactor cores.

Geometric modelling involves a rod bundle which is divided into subchannels whose boundaries are defined by adjacent walls and/or rod surfaces. CTF also includes capabilities for modelling fuel rods, electric heater tubes, and walls using a finite-difference form of the heat conduction equation (Salko Jr et al. 2019), however, the emphasis has been placed on modelling the flow field within the scope of this MPhil. A typical square subchannel is shown in for a 3 × 3 rod bundle in a square pipe in Figure 2-2 (a). As can be seen in the image from Figure 2.2 (a), there are three different types of subchannels namely corner, centre and side. The corner subchannels are shown in red colour, green colour represents centre subchannels while blue colour indicates side subchannels. Figure 2.2 (a) also depicts the radial mesh for a CTF, where each radial element is equal to the size of the corresponding subchannel. It can be said from the Figure 2.2 (a) that the total number of radial elements are 16 that consists of corner, centre and side subchannels regions. These flow channels are subsequently divided axially to form discrete control volume or axial mesh elements. Figure 2.2 (b) shows an axial uniform mesh for CTF for a case where there are no spacers along the flow. There is freedom for the user to refine the axial mesh unlike the radial mesh which is limited by the number of subchannels. A typical non-uniform mesh can be seen in Figure 2.2 (c). The image shows that in the locations where spacers are present, the mesh is refined in the axial direction.

The governing equations describing the conservation of mass, momentum and energy are solved on these discrete control volumes numerically(Salko Jr et al. 2019). Solution of these equations provides the flow rates (axial and lateral) and enthalpy values within each of the computational cells or mesh elements.

| (a) Radial mesh | (b) Axial mesh – no spacers | (c) Axial mesh – spacers |
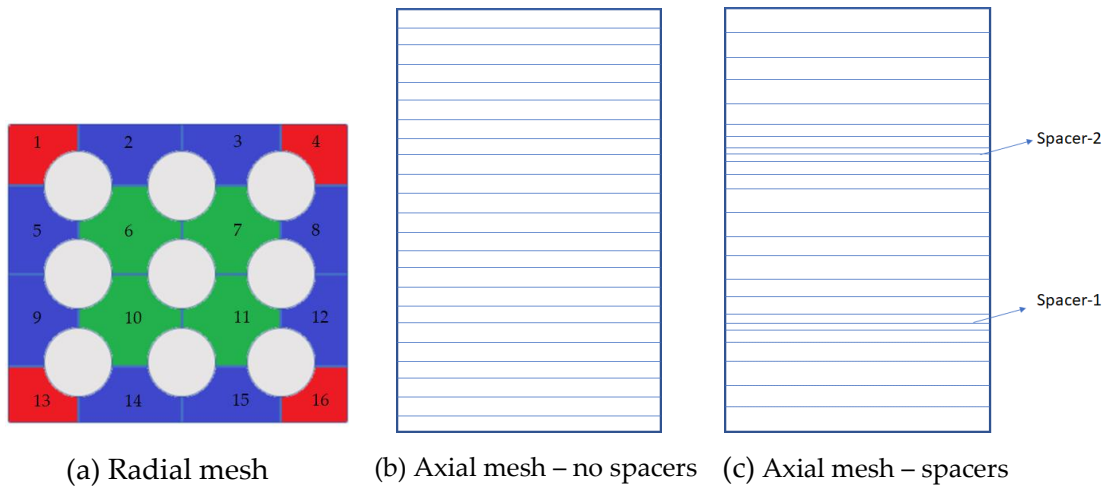
Figure 2-2 Typical CTF meshes for 3 × 3 rod bundle in a square pipe in radial as well as in axial direction

In addition to geometric input requirements, boundary conditions have to be applied such as: -

- Rod power

- Inlet flow rate and temperature,

- Outlet pressure

- Input correlations for friction factors, void drift and turbulent mixing(Beus 1972)

The CTF output consists of parameters such as subchannel flow rate, temperature, enthalpy, pressure and fuel rod temperatures mapped onto a user-specified mesh and written to files in a format suitable for visualisation. Besides the pure fluid dynamics, a fuel rod model is incorporated in CTF, which allows to simulate the heat transfer within the rod, the gap and the clad to deliver the cladding surface temperature for the fluid dynamics solution.

2.3   CFD code – ANSYS Fluent

Computational Fluid Dynamic (CFD) is the branch of science that mathematically models the underlying physical phenomena involving fluid flow, heat and mass transfer processes to provide a computational solution using a wide range of numerical schemes (Patankar 2018; Versteeg & Malalasekera 2007). In theory, CFD finds application wherever there is fluid present, i.e., process industries, automobile, aerospace, nuclear etc. Within nuclear industry, CFD methods have been widely used both in light water reactors and liquid

metal cooled fast reactors, providing greater insight into the complex issues of thermal hydraulics analysis thus contributing to the CFD aided modelling in technology development and design (*Summary Review on the Application of Computational Fluid Dynamics in Nuclear Power Plant Design* 2022). The power of CFD in calculating the local effects for multi-dimensional problems can be used to improve the code predictions of either system level or lumped parameter model approaches. This has to be done via coupling of CFD codes with system codes which has been the major focus within the nuclear industry recently (Aumiller, Tomlinson & Bauer 2001; Toti 2018). One such application has been attempted in this current study.

Modelling transitional and turbulent flows which are prevalent in subchannel flows especially for Gen IV reactors using hexagonal rod bundles with wire wrapped around the fuel rods has remained still the major challenge. The choice of turbulence model in CFD modelling determines the accuracy of the solution. The numerical models of a turbulent flow can be classified broadly as: DNS, LES and RANS. DNS resolves all fluid motions (both spatial and temporal scales of turbulence) within the flow and thus the computational domain needs to accommodate for the smallest and the largest turbulent eddy. Consequently, it is highly expensive to use it (considering fine grids and the required small-time scales) in practice; however, it is currently predominantly used in academic research. In LES, the large eddies of the turbulent flow are explicitly solved while the small eddies are approximated. LES is still computationally expensive to run but more affordable to implement than DNS for industrial problems. Both LES & DNS give substantially more information on flow details (on length & time scales) than an engineer requires for the design studies. RANS employs a wide range of turbulence models wherein Reynolds stresses tensor from turbulent fluctuations is computed within the fluid momentum. The effect of turbulence on the mean flow is captured through different selectable models which is sufficient to understand the turbulent flow characteristics in practice. Various RANS turbulent models include: Standard k-ε, Realizable k-ε and Reynolds Stress Model (RSM), Re-Normalisation Group (RNG), Shear Stress Transport (SST) k-ω. All these turbulent models along with wall functions for capturing the effects at the near wall region are widely used in the nuclear industry.

There is no unique model that can be used for all the flow problems appearing in a nuclear reactor. There are strengths and weaknesses and recommended best practice guidelines are available widely in the open literature and also in the ANSYS Fluent theory & user manuals (Fluent 2021). While these RANS models can be used to capture the flow effects well, still there are challenges to use these CFD approaches in the context of subchannels flows at fuel assembly level involving large number of fuel pins, and also at reactor core level not least due to the complexities of fast acting transients in multi-phase flows. This is where the subchannel codes and system codes find huge advantage over CFD approaches and make the case for their use within the range that these codes have been validated. In the present study, the input parameters for subchannel codes have been obtained from CFD RANS approach to improve the accuracy of predictions from the subchannel codes which will be discussed in following chapters.

ANSYS – Fluent software has been used for the current study because of its wider capabilities in terms of handling complex geometries, well documented & validated physical models with excellent user & theory manuals (Fluent 2021). Another motivating factor is that ANSYS Fluent is one of the most widely used codes in the nuclear safety community (Podila & Rao 2015). As with any other CFD commercial code, there are 3 major stages within ANSYS Fluent: Preprocessing, Solving and Postprocessing and it is worth mentioning that all these three stages are strongly interconnected to yield a solution that is physically meaningful. Creation of geometry, mesh or grid generation, defining material properties and boundary conditions come under preprocessing stage. During solving stage, the governing equations of transport equations for mass, momentum, energy, species and any other transport variable with the defined physical models such as turbulence, radiation, combustion will be solved on mesh/grid. The solver needs a few settings such as initialisation, solution control, monitoring and convergence criteria. The final stage is postprocessing where all the field variables can be plotted using X-Y plots, contours, velocity vectors, streamlines etc. when the converged solution is ready.

CHAPTER 3: PSBT VALIDATION STUDIES

3.1   Introduction

It is vital to get good hands on experience using thermal hydraulic codes and also ensure predictions by user are reasonable. As a confidence building exercise, a validation study has been undertaken using the CTF thermal hydraulics subchannel code. As part of this validation exercise, a CTF model will be compared against existing experimental data on Pressurised Water Reactor Sub-channel and Bundle Tests (PSBT). This chapter describes the experimental set-up and how the simulation results from CTF compare with the measured data from the experiments.

3.2   Experimental details and geometry

PSBT benchmark consists of two phases, with each phase consisting of different exercises. The Phase I is the void fraction benchmark, and Phase II is the departure from nucleate boiling (DNB) benchmark. Void fraction measurements and DNB tests were performed under the conditions similar to PWR thermal-hydraulic conditions including steady states and the transients such as power increase, flow reduction, depressurisation and temperature increase.

Data consists of sub-channel experiments and rod bundle experiments where the void fraction in each experiment is measured by gamma-ray transmission method (Rubin & Avramova 2011a; Rubin, Avramova & Velazquez-Lozada 2016a; Rubin et al. 2012; Specifications 2012). The gamma-ray transmission method measured the density of the flow, and later void fraction was derived from the density measurements for the gas-liquid two-phase flow. This is a non-intrusive technique and thus no obstruction to the flow. The steady state bundle benchmarking exercise is aimed at providing validation data for verifying various numerical codes. Simulations have been performed using CTF for rod bundle size of 5 × 5 which was the PSBT rig configuration and with a PWR rated conditions which are shared in the subsequent section of this chapter.

The images of the test section for rod bundle void distribution measurement and the cross section of the test vessel are as shown in Figure 3-1 and Figure 3-2. The experiments were carried out on a number of cases with various geometrical configurations (Rubin &

Avramova 2011a). However, the validation study focusses on only one of the configurations named B5. Figure 3-1 represents test section for rod bundle void distribution measurement; the rig is approximately 4m high, with an effective heated length of 3.658m. This heated length i.e., the portion of the rod where the electrical heating was applied to simulate the heat generation from a fuel rod, is divided into three sections, namely upper, middle and lower measuring at 3.177m, 2.669m and 2.216m, respectively. The total power supplied to the rod bundle ranges from about 1MW to approximately 3.3MW for the test cases considered here. CTF model includes only the heated length of the test section. A cross section through the rig can be seen in the image given in Figure 3-2. The image shows the 5 × 5 rod bundle surrounded by flow channel, which is surrounded by flow shroud. This whole unit is enclosed in a test vessel. However, the CTF model only includes the 5 × 5 rod bundle with just internal boundary of flow channel without its metal thickness. Table 3-1 summarises key geometrical properties of the test assembly. The first column in the table lists various components of the test section such as number of heated rods including type of power shape profile of the rods while the second column gives the respective quantities. It can be noticed from the Table 3-1 that uniform axial profile is used for this configuration whilst the radial power shape type is A which is defined in the subsequent section.

The various types of spacers used in the test rig are shown in Figure 3-3 and the number of different spacers used, including their positions along the axial length from the bottom of the heated length are presented in Table 3-2. Figure 3-3 demonstrates three types of spacers: simple, non-mixing or no mixing vane and mixing vane. Table 3-2 shows that there are only two non-mixing spacers which are at either ends of the test rig whilst the simple and mixing vane spacers keep alternating each other in their arrangement within the heated section.

The experimental data includes measurements of void fraction (chordal averaged over the four central subchannels) at three axial elevations (see Figure 3-1) along the bundle length and graphical images of the bundle void distribution.
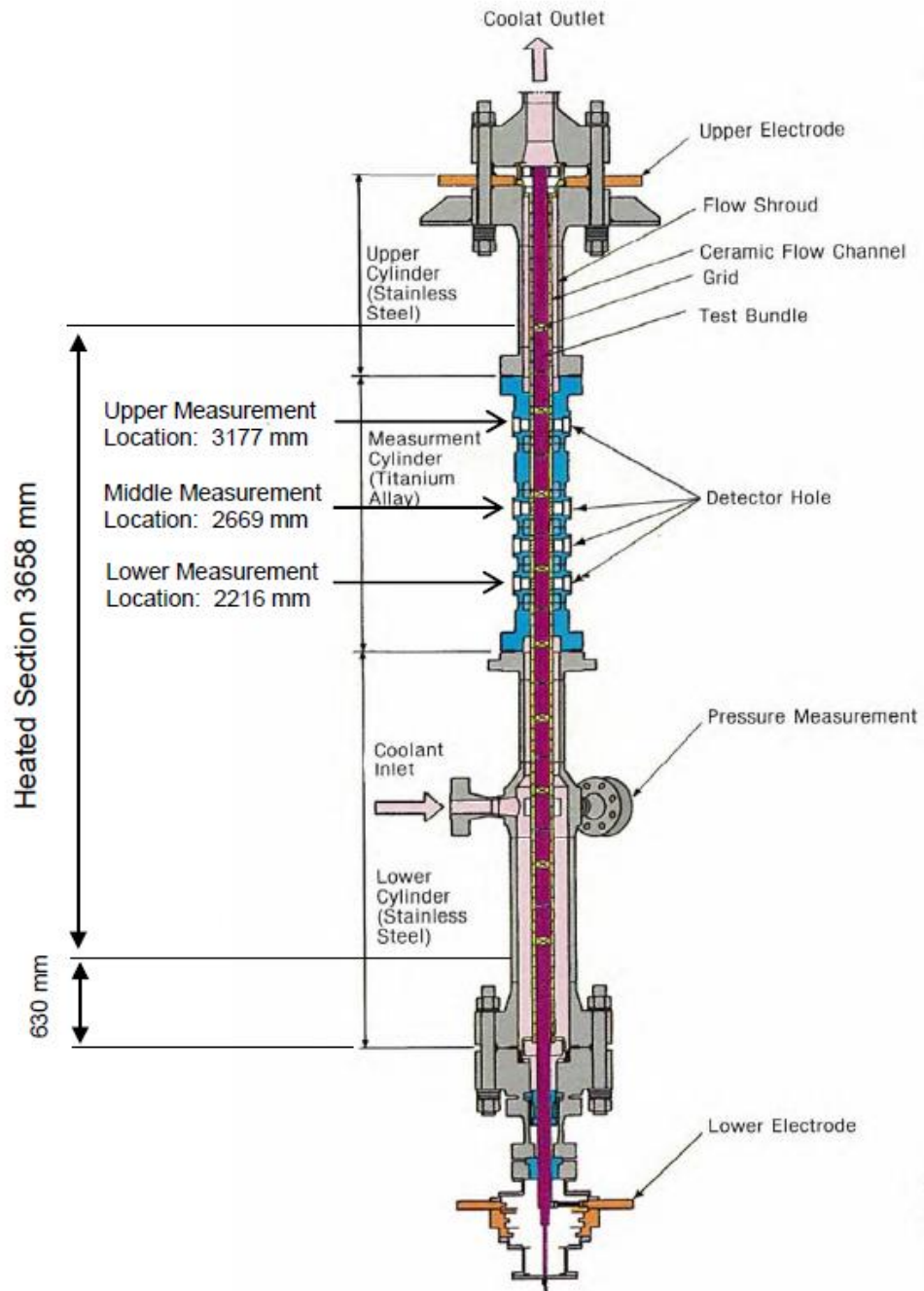
Figure 3-1: Test section for Rod Bundle Void Distribution Measurement (Rubin & Avramova 2011a)
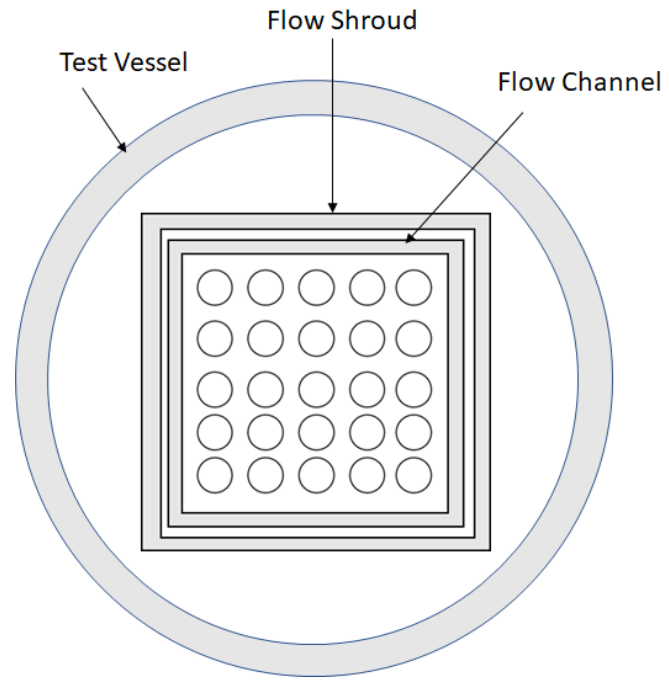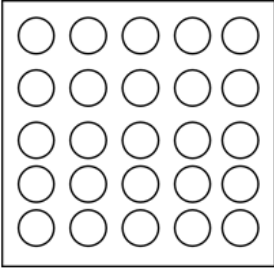
Figure 3-2: Cross Section of Test Vessel (Rubin & Avramova 2011a)

Table 3-1: Geometry and power shapes details for test assembly B5

Item	Data
Assembly	B5
Rods array	5×5
Number of heated rods	25
Heated rod outer diameter (mm)	9.50
Heated rod thickness (mm)	0.65
Heated rod pitch (mm)	12.60
Heated rod material	Inconel 600
Axial heated length (mm)	3658
Flow channel inner width (mm)	64.9
Radial power shape	A
Axial power shape	Uniform
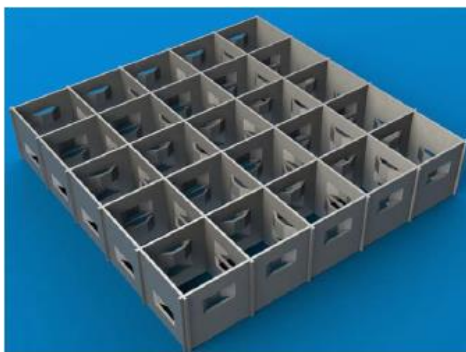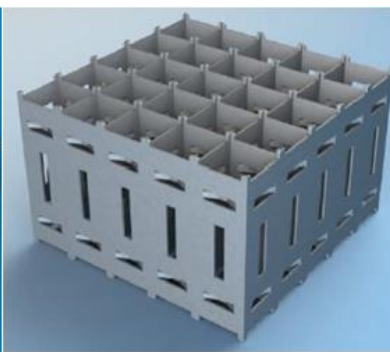
Simple Spacer   No Mixing Vane   Mixing Vane
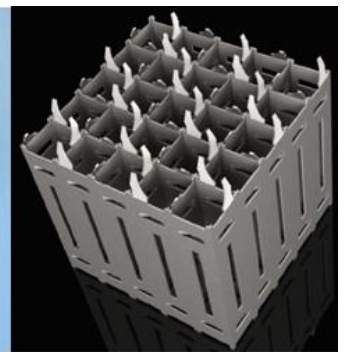
Figure 3-3: Images of various spacers used in the test rig

Number of mixing vane spacers	7
Number of non mixing vane spacers	2
Number of simple spacers	8
Mixing vane spacer location (mm)	471, 925, 1378, 1832, 2285, 2739, 3247
Non-mixing vane spacer location (mm)	2.5, 3755
Simple spacer location (mm)	237, 698, 1151, 1605, 2059, 2512, 2993, 3501

3.3   Boundary conditions

The test matrix operating conditions are similar to the rated conditions as in a PWR. As part of benchmarking exercise, the test conditions reported in Table 3-3 have been considered for analysis as they cover full range of operating pressures and temperatures. All of these validation cases are for assembly configuration B5. The actual number of test conditions are much more than that is reported here and the details can be found in (Rubin & Avramova 2011a). As can be seen from the Table 3-3, the operating conditions vary quite a lot from inlet temperature to operating pressure, power and inlet mass flux. These conditions cover the range of typical operating conditions in pressurised water reactors.

Radial power distribution between the rods in 5 × 5 rod bundle arrangement is as shown in Table 3-4. Each cell value in the Table 3-4 represents relative power for the rod in that position. It can be clearly seen that higher powers have been applied for the central rods while the corners and side rods have less powers. A uniform axial power is applied for all the rods.

Table 3-3: Test conditions for steady-state void measurement

Run No	Pressure (bar)	Mass flux (10^6 kg/m²h)	Power (kW)	Inlet Temperature (°C)
5.1221	165.036	11.00	3000	292.3
5.1222	165.016	10.98	2998	297.3
5.2111	145.286	15.08	3296	291.9
5.2112	145.178	14.98	3294	296.8
5.2442	147.07	4.99	2000	263
5.2332	146.92	7.94	2523	287.8
5.3441	122.799	5.00	2014	247.9
5.3442	122.711	5.00	2013	257.7
5.4562	98.2921	2.02	1016	214.3
5.6321	48.2487	7.87	3000	173.5
5.6322	48.131	7.86	3000	183.6
5.6552	49.2	2.00	1028	159.1

The heated section of the 5 × 5 rod bundle was modelled in CTF with 36 subchannels and 25 rods following the geometric arrangement of the experiment as given in Figure 3-4. The geometry was later axially discretised into 36 nodes, and these nodes were distributed non-uniformly in the axial direction accounting for spacers' locations. This makes the total number of computing cells as 1296 (36×36).
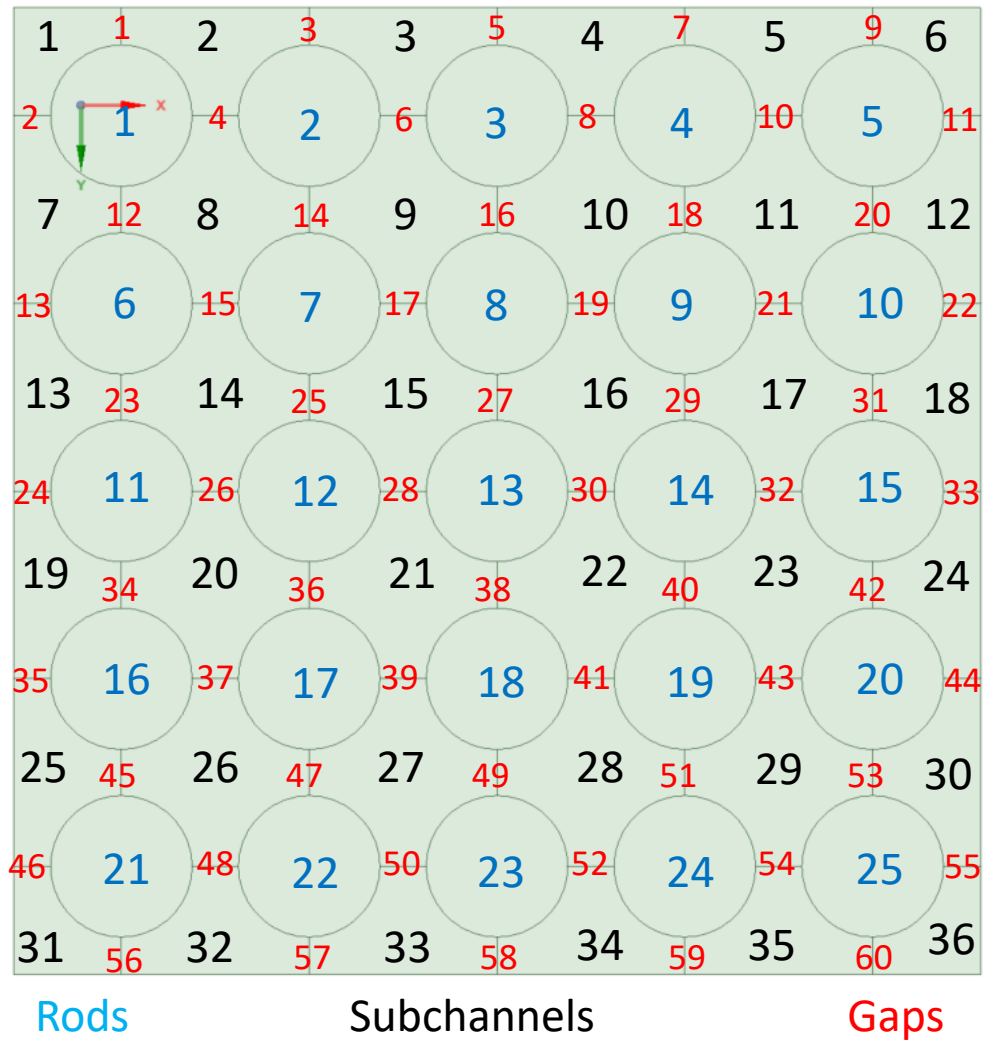
Figure 3-4: CTF mesh notations: Rods, Subchannels and Gaps

Nominal flow area and wetter perimeter are specified for each subchannel in the input file. The area and perimeter are assumed to be constant within each cell. Transverse flow connections are specified between subchannels to complete the multidimensional mesh of the region. These connections are termed as gaps as shown in Figure 3-4. These gaps are defined by the width of the flow path between two subchannels and the distance between the subchannels' centroids.

The spacers are not explicitly modelled in the CTF simulations, but pressure loss coefficients have been used to account for momentum loss. These pressure loss coefficients are provided in (Rubin & Avramova 2011a) and are reported in Table 3-5. The performance of these spacers differs in the way they offer pressure drop across them and in particular for mixing spacers, they aid in mixing, creating local turbulence.

The salient modelling parameters for CTF are summarised in Table 3-6. It can be seen from Table 3-6 that the side walls are maintained adiabatic; this means not losing heat to the surroundings and hence zero heat flux. The fuel rods have been modelled as hollow tubes as the conduction through the rods is not of interest for the current work. Also, the complete geometry is modelled without any assumptions on the symmetric nature of either flow or geometry. Mass flow rate boundary condition with specified temperature has been applied at the inlet while the outlet is open to atmospheric pressure and temperature. Heat flux values have been imposed on the rods based on test specification (input power). Turbulence mixing and void drift has been accounted by single phase turbulent mixing coefficient and with a Beus two phase multiplier ((Beus 1972). Semi-Implicit Method for Pressure-Linked Equations (SIMPLE) has been adapted to solve the conservation equations (Patankar).

Table 3-4:Radial Power Distribution, Type A

0.85	0.85	0.85	0.85	0.85
0.85	1.00	1.00	1.00	0.85
0.85	1.00	1.00	1.00	0.85
0.85	1.00	1.00	1.00	0.85
0.85	0.85	0.85	0.85	0.85

Table 3-5: Bundle average spacer pressure loss coefficients

Spacer type	Loss coefficient
Simple spacers	0.4
Non-mixing vane spacers	0.7
Mixing vane spacer	1.0

Table 3-6: Important modelling parameters in CTF

Type	Details
Axial nodalisation	36 nodes in axial direction with 36 subchannels. This makes the total number of computational nodes as 36 ×36 = 1296
Boundary conditions	Inlet: Mass flow rate and coolant temperature Outlet: Pressure and temperature (temperature influences only when there is back flow, otherwise no effect) Wall: Heat flux based on the test specification for rods, and for side walls, it is adiabatic (this means zero flux)
Cross – flow models used (void drift and turbulence models)	Nucleate boiling: Thom correlation (Thom et al. 1967) DNB: W-3 correlation (Beus 1972; Tong 1967, 1972) Turbulent mixing and void drift: Single phase turbulent mixing coefficient and Beus two phase multiplier (Beus 1972)
Wall heat transfer and rod conduction	The walls are adiabatic and the rods are modelled as hollow tubes
Symmetry	No symmetry, full 3D model considered and sub channel approach is adopted
Components of pressure drop	Friction loss Form loss applied for spacer grids Gravity

	Pressure equation is solved by iterative Krylov solver (Salko Jr et al. 2019)
Numerical algorithm	Semi-Implicit Method for Pressure-Linked Equations (SIMPLE) to solve the conservation equations
	The steps of the SIMPLE algorithm, taken from (Patankar).

3.4   Results and discussions

The results presented here in this section are two types:

✓ Code to experimental data comparison
✓ Code to code comparison

Where there is measured data available such as void fraction, the CTF results are compared with experimental data in addition to the other codes. The mean errors $\bar{\alpha}$ and standard deviation σ of these errors are reported using the following definitions of mean and standard deviation. Due to the way the mean error defined here, the positive and negative values cancel each other out to give a single value of mean error. To remedy this, standard deviation of these errors, σ also presented here.

$$\bar{\alpha} = \frac{\sum_{n=1}^{N} \alpha^n}{N} \qquad (1)$$

Where the void fraction error for test case n is represented as:

$$\alpha^n = \left(\alpha^n{}_{code} - \alpha^n{}_{exp}\right) \qquad (2)$$

$$\sigma = \pm\sqrt{\frac{\sum_{n=1}^{N}(\alpha^n - \bar{\alpha})^2}{N-1}} \qquad (3)$$

The absolute values of void fractions at different heights measured along the heated section are presented in the following figures (see Figure 3-5, Figure 3-6 and Figure 3-7) and compared against the measured values. Figure 3-5 shows the bar charts of experimental void

fraction values in black whilst the red coloured bars indicate the CTF void fraction values for Upper measurement. Figure 3-6 and Figure 3-7 follow the same colour notation except the data plotted in Figure 3-6 is for Middle measurement while the data in Figure 3-7 referes to Lower measurement. At higher operating pressures of the order of 150 bar and above and with inlet temperatures up to 290°C, there seems to be little or no vapour reported experimentally, however, CTF has predicted vapour formation albeit at low levels. This could perhaps be due to the 4% uncertainty in void fraction measurement as reported in Table 3-7.

Table 3-7: Estimated accuracy for void fraction measurements (Rubin, 2012 #2)

Quantity	Accuracy
Process parameters	
Pressure	1 %
Flow	1.5 %
Power	1%
Fluid temperature	1 Celsius
Void fraction measurement	
CT measurement	
Gamma-ray beam width	1 mm
Subchannel averaged (steady-state)	3% void
Spatial resolution of one pixel	0.5 mm
Chordal measurement	
Gamma-ray beam width (centre)	3 mm

Gamma-ray beam width (side)	2 mm
Sub-channel averaged (steady-state)	4% void
Sub-channel averaged (transient)	5 % void

The higher mass flux at these conditions perhaps causing low vapour formation, with the reported measured void fractions are around 0.05. At these low levels of actual vapour formation, CTF seems to have overpredicted the void fraction values. However, at lower operating pressure (less than 150 bar) and temperatures, combined with lower mass flux values has yielded higher values of void fraction at all the heights from measurements. CTF simulations have clearly underpredicted under these operating conditions for majority of the cases at all the heights. Both the results indicate that most of the void fraction is at the upper region of the test section, reaching up to 0.75 for the lowest operating conditions of pressure (around 50 bar), temperature (up to 160°C), mass flux (2×10^6 kg/m²h) and power (1.028MW). Equally, for the highest operating conditions of pressure, temperature, mass flux and power, there is the least or no amount of void fraction formed from upper region to the lower region of the test section.
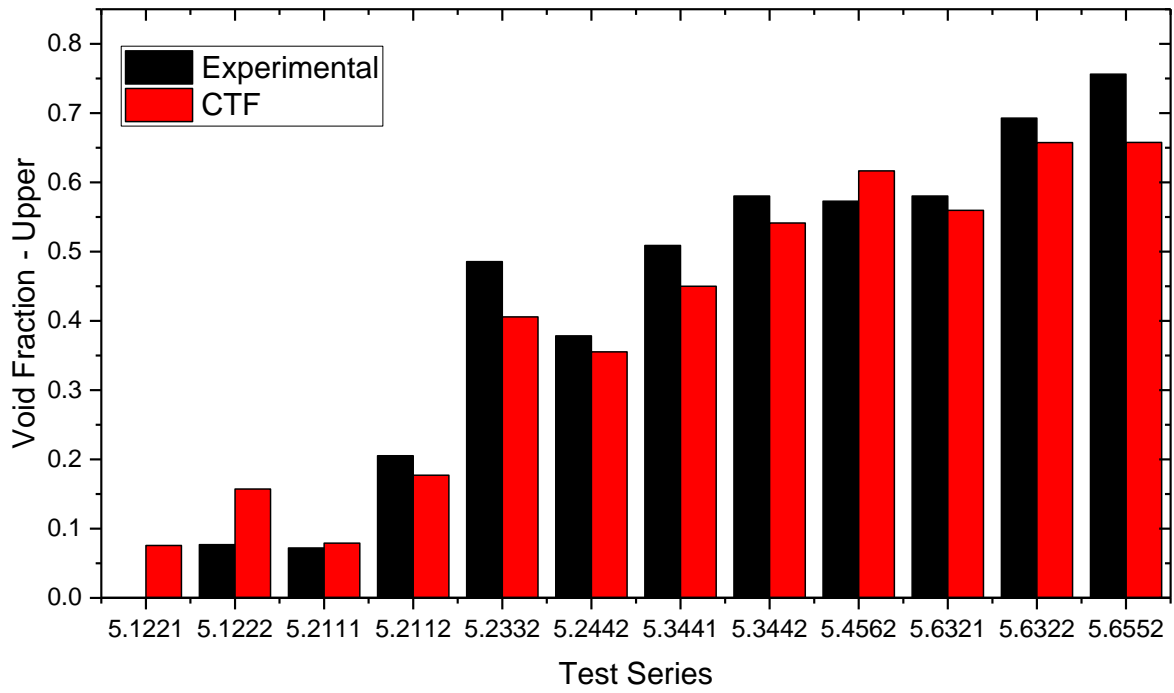
Figure 3-5: Void fraction comparison CTF vs Experiment (Upper measurement)
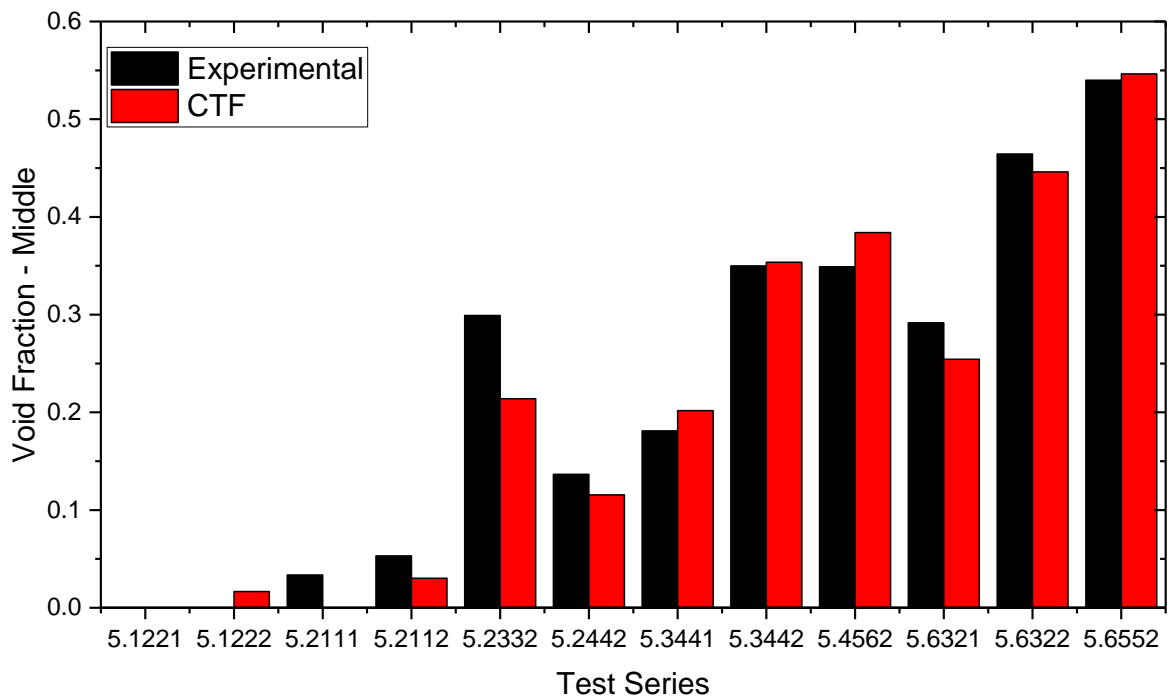
Figure 3-6:Void fraction comparison CTF vs Experiment (Middle measurement)
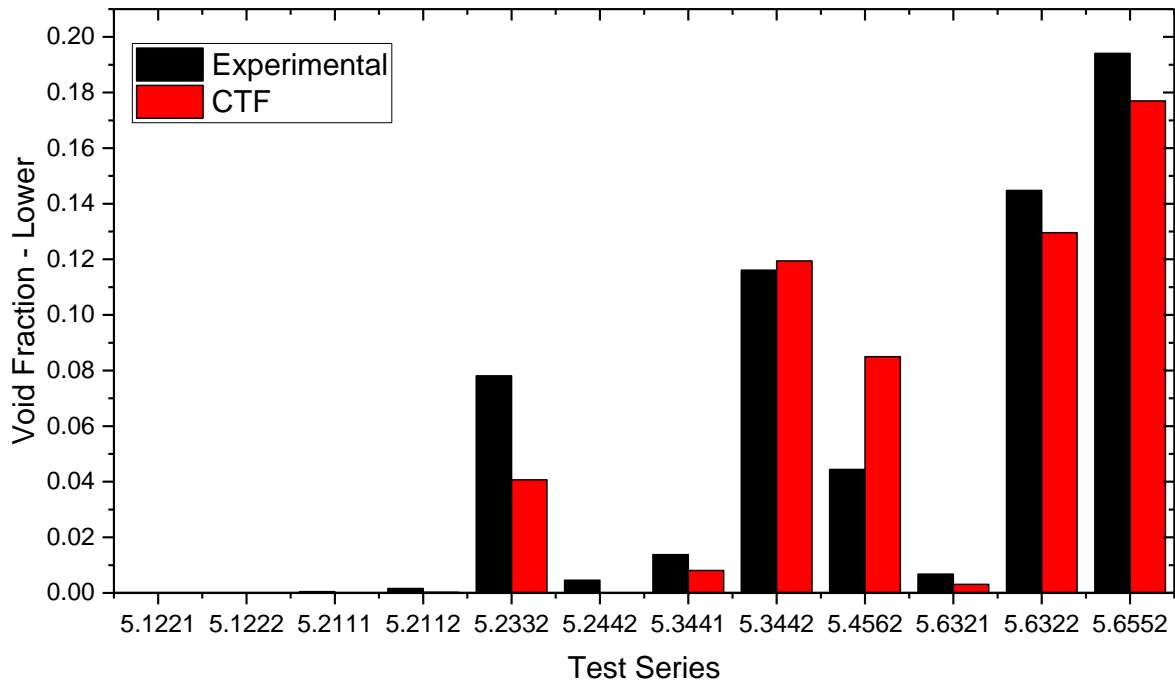
Figure 3-7: Void fraction comparison CTF vs Experiment (Lower measurement)

The mean errors for various heights i.e., Upper, Middle and Lower as calculated from the equation (1) are plotted in Figure 3-8 while the standard deviation (calculated from equation (3)) of the errors is shown in Figure 3-9. The negative values of mean errors indicate that the simulations have underpredicted the void fraction values, however, the lower values of less than around -0.01 imply that difference between the experimental values and the predicated values from the simulations is not significant. In general, the lower values of mean errors and standard deviation as compared to many other industrial codes indicate that the CTF predictions have fared better than the others for the void fraction parameter. For instance, the codes used by KIT (SUBCHANFLOW) and AREVA (F-COBRA-TF) are very similar to CTF, however they ended up predicting a positive mean of around 0.05, overpredicting the results as compared to experimental values.
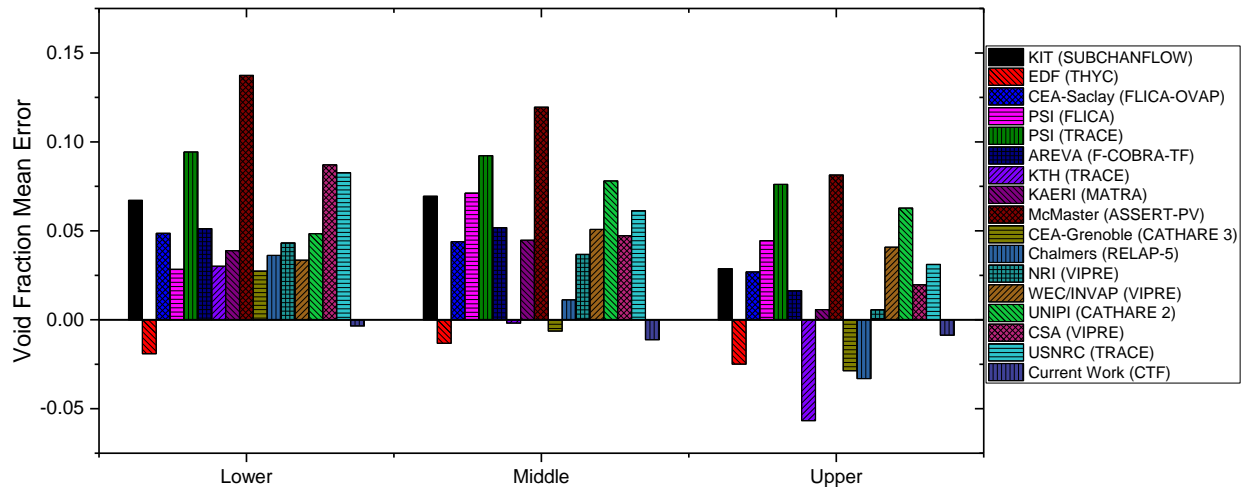
Figure 3-8: Mean error at different heights, where measurements are made
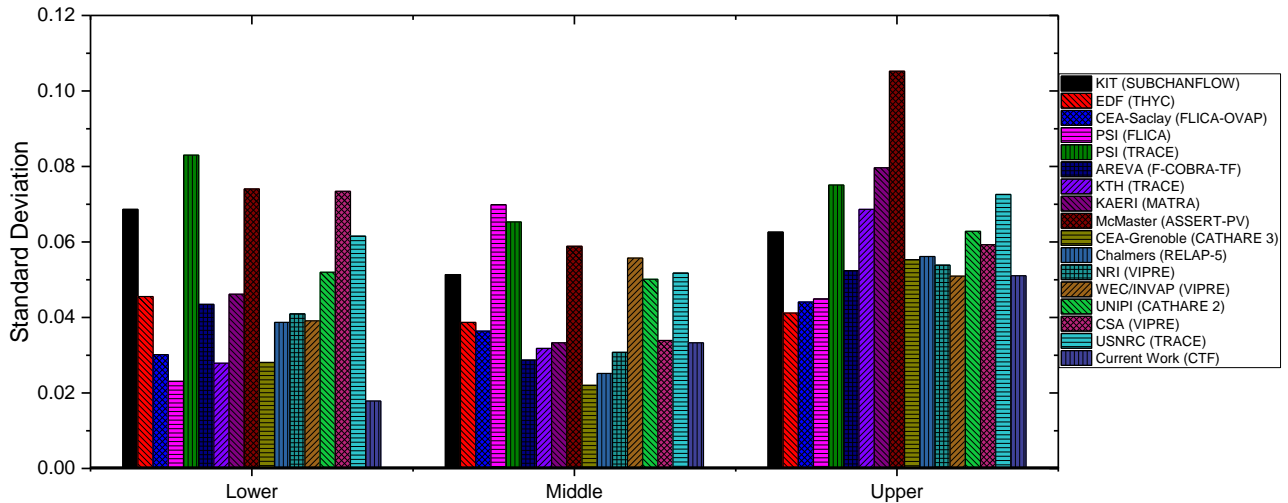
Figure 3-9: Standard deviation of the error at different heights, where measurements are made

The following figure (Figure 3-10) shows the CTF results for the void fraction against the experimental measurements for various test cases simulated as presented in the Table 3-3. On the X-Y plot, the X-axis refers to the void fractions from measurements and CTF results are plotted on Y-axis. The solid blue triangles indicate the CTF results for the upper region, the solid red circles represent CTF results for middle region and the solid black squares show the void fraction date from CTF for the lower region of the test section. There is also another solid red line that can be noticed with the legend name as Y=X which indicates that any point lying on this Y=X line indicates that the simulated results are in perfect agreement with the measured data. The points that lie below this Y=X line indicate the underpredicted data while

the data points that lie above this Y=X line refers to overpredicted data from the simulations as compared to the measured values. Essentially, the Figure 3-10 containing this X-Y data captures the summary of what was discussed using the bar charts, reiterating the fact that majority of the simulation data points were under predicted and these data points correspond to lower operating pressures and temperatures as discussed before.
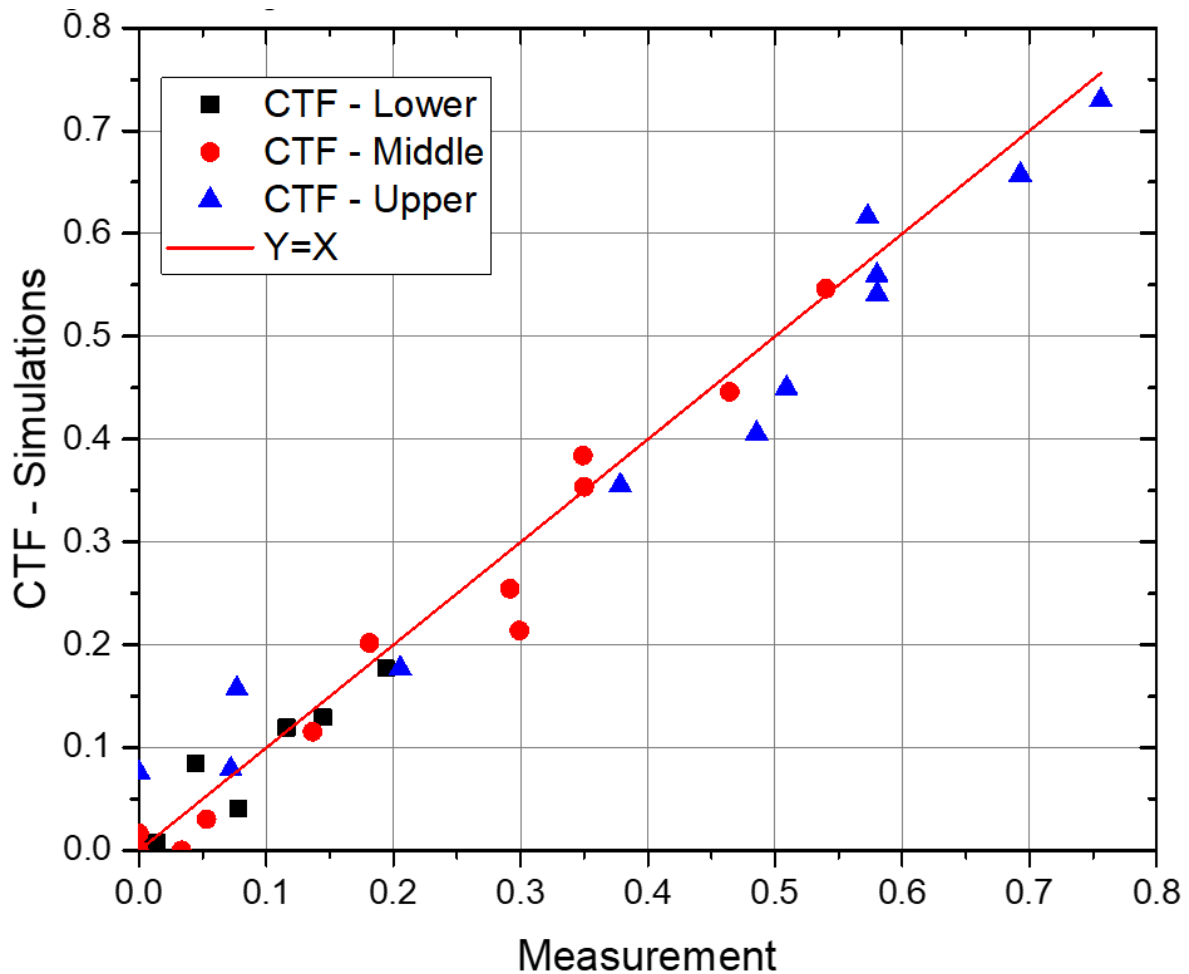
Figure 3-10: Void fraction comparisons at different regions with measurements

The measured data from the experiments is not available for pressure drop for the test rig and hence the predictions from CTF for pressure drop across the bundle for different test points are compared against the values from other commercial codes. Not all the commercial codes that have reported void fraction, have included pressure drop values in their published data. Hence, the CTF simulation data has only been compared with the codes which have published the pressure drop values from their simulations. These comparisons are shown in

41

the bar chart (see Figure 3-11). The bars correponding to the CTF results from the current work have been pointed out with a solid arrow mark for clear demarcation.

Overall, in the absence of pressure data from the measurements, it can be confidently ascertained that the CTF results effectively aligned with other codes. At higher operating pressures, the predicted pressure drop from the CTF simulations is around 2.5 bar for test points 5.2111 and 5.2112, while the maximum pressure drop predicted is around 3.25 bar for these two test points; this is by Paul Scherrer Institute (PSI) which have used TRACE for their analysis, which is a system level software. Clearly, TRACE used by KTH (Swedish: Kungliga Tekniska Högskolan) Royal Institute of Technology has resulted in a different pressure drop values for these test points, and the values are around 2.8 bar. This clearly indicates that the user has a significant role in operating these nuclear codes. It is vital that the user has sufficient experience in handling the codes especially while carrying out calibration exercises like these discussed here.

It is also worth nothing that the pressure drop values reported by Karlsruhe Institute of Technology(KIT) (SUBCHANFLOW) has similar values ranging from about 2.5 bar (test point 5.2111) at higher operating pressures to around 0.25 bar (test point 5.6552)at lower operating pressures. This could be that the two similar codes i.e., SUBCHANFLOW and CTF maybe using similar frictional correlations towards pressure drop predictions.
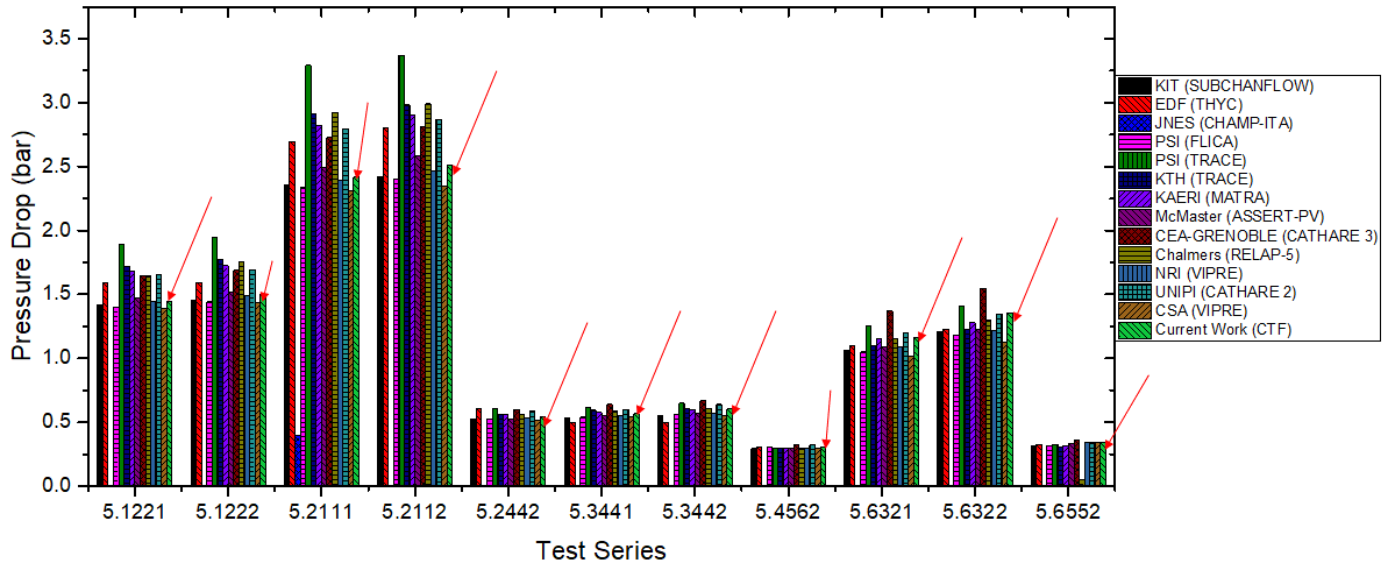
Figure 3-11: Pressure drop comparison with other commercial codes

3.5   Conclusions

Based upon the validation work on PSBT test matrix using CTF, the following conclusions can be drawn:

1. For test points when the operating pressure is high (around 150bar) and at high temperatures (higher than 290°C), the maximum observed void fraction is only less than around 0.2 in the test rig. For these cases, the CTF results of void fraction does not correspond well with the measurements. However, when there is significant void fraction observed experimentally (as high as 0.75), which relate to lower operating pressures (50 bar) and temperatures (in the range of around 160°C to 184°C), CTF results have underpredicted the void fractions for majority of the cases.

2. In the absence of pressure drop values from the measurements, CTF results correspond well with other codes in the industry, predicting around 2.5 bar at higher operating pressure of about 150 bar, and around 0.25 bar at lower operating pressure of 50 bar approximately.

3. The validation studies using CTF for the PSBT test matrix proved beneficial in learning and implementing the code for real applications. A robust modelling

43

method developed using CTF, which is verified and validated, providing the required trust on the user's skills in working with the code.

4. Good agreement with test data suggests that the geometry and complex flow effects have been accurately captured using CTF with the described code settings.

5. The comparison of the simulated data with measurements and also with several other industrial codes has reinforced the confidence on applying CTF knowledge.

CHAPTER 4: PNNL VALIDATION ACIVITIES

4.1   Introduction

PSBT studies presented in the previous chapter were inherently multiphase and the CTF code uses several empirical correlations for friction, void drift, turbulent mixing under boiling conditions at high pressures to represent those phenomena. CTF has been predominantly in use & thoroughly validated for Light Water Reactors (LWR) wherein the majority of the flow regimes are multiphase (Salko Jr et al. 2019). The meaning of multiphase flow regime in this context is that the liquid water undergoes phase change to vapour phase under the prevailing conditions of high pressure and temperature. The scope of the current MPhil project is to assess single - phase flow scenarios using CTF at near atmospheric pressures. In addition to this, the thermal hydraulics experiments on the proposed Rig-1 & Rig-2 for Project FAITH will be carried out only in single-phase flow regardless of water or sodium used as working fluid. Single - phase flow means the entire flow regime is in only liquid phase for the present work. In this section, another validation case where CTF has been tested for completely single-phase flow regime has been described.

4.2   Experimental details

The validation case considered in this chapter relates to an experimental work (Quigley, McMonagle & Bates 1977) carried out at PNNL (Pacific Northwest National Laboratory) on a 2 x 6 rod bundle. The rods do not contain wire wraps around them (a radial cross section through the rods and various subchannel can be seen in Figure 4-1). The experimental work obtained fluid temperature and detailed velocity measurements using a one-dimensional Laser Doppler Anemometer (LDA) in combined free and forced convection flows within an electrically heated rod bundle. LDA is a non-intrusive flow measuring technique used for measuring linear velocity. It works on the principle that when a narrow laser beam is focussed on an object, the beam will be reflected back to the source. But when the object is moving, the frequency of the signal received back will differ from that of the original transmitted signal. The difference in frequency that is called Doppler shift becomes a measure of velocity of the object. According to the authors (Quigley, McMonagle & Bates 1977), their study represents one of the first applications of the LDA velocity measurement technique to be applied for mixed free and forced convection in rod bundle flows at that time.

45

The heating of the rod bundle was set up such that non-uniform radial power distributions could be imposed across the bundle. The authors from this work used the data from their experimental work to compare against the predictions from a thermal hydraulics subchannel code called COBRA-IV, which was available at the time when the experiments were carried out. The objective was to see the ability of the COBRA–IV code to predict velocity and temperature distributions in a rod bundle geometry with flows in the mixed, free and forced convection regimes. These regimes are encountered in Gen IV reactors under normal operating conditions, especially for liquid metal fast breeder reactors. Validation studies of the subchannel codes' performance (in general any numerical code's performance) are paramount for regulatory purposes in nuclear reactor core analysis.

4.3   Geometry and boundary Conditions

The cross-sectional view of the 2 × 6 test section and the CTF model are as shown in Figure 4-1 and Figure 4-2 respectively. In Figure 4-1, The fuel pins are represented by the circular regions of which red circles numbered 1-6 are for heating while the blue coloured circles, numbered from 7-12 are for isothermal conditions. The subdivided regions with dotted lines between the bounding walls and the pins and between the pins themselves are called subchannels, numbered from 1-21. The coolant which is liquid water in this case, passes though these subchannels from the base to the top in a vertical direction. The flow is predominantly axial along the height of the fuel pins for isothermal conditions.

Figure 4-2 illustrates the nine windows located at 6-inch interval over the heated length section of 4-foot where visual access for LDA measurements permitted in addition to the access for thermocouple probes. The total number of axial nodes (30) used for the CTF model along the direction of flow can also be seen in the same image. The radial nodes for the CTF model are same as the number of subchannels which are twenty-one that can be seen in Figure 4-1.

The boundary conditions are presented in Table 4-1. From Table 4-1, it can be seen that there are in total five cases of which three of them (Cases 1-3) are non-isothermal and the remaining two are isothermal. Cases 1, 3 and Isothermal-1 correspond to a higher flow rate of 0.00016 m³/s with varying power ratio among them. Cases 2 and Isothermal-2 correspond to

a low flow rate of 0.00008 m³/s with a varying power ratio between them. The entry liquid temperature for all of these cases is approximately 15.6°C.
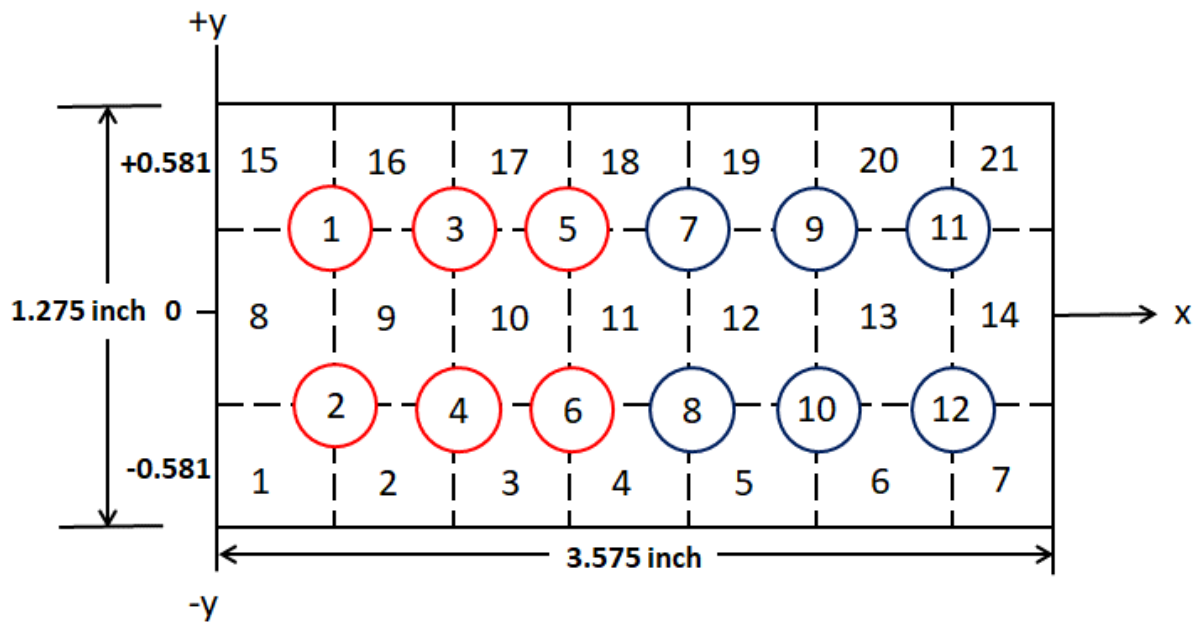
Figure 4-1: CTF Radial modelling of PNNL 2 X 6 test section (Quigley, McMonagle & Bates 1977)

In this thesis work, all of the cases listed in Table 4-1 have been simulated in CTF and some of the results from CTF are compared with the measured data (see from Figure 4-3 to 4.8) and also with COBRA-IV data as reported in (Quigley, McMonagle & Bates 1977). The Case 2 of the experimental set up was modelled by COBRA-TF, a predecessor of CTF, by (Sung et al. 2015) during the evaluation of COBRA-TF code.

The plots presented in Figure 4-3 to Figure 4-8, show how the non-dimensional velocities and temperatures as defined below match with the measured data. The individual plots in these figures are explained in the next section.

Non-dimensional velocity $= \dfrac{U_{local}}{U_{inlet}}$

Non-dimensional temperature $= \dfrac{T - T_{in}}{T_{out} - T_{in}}$
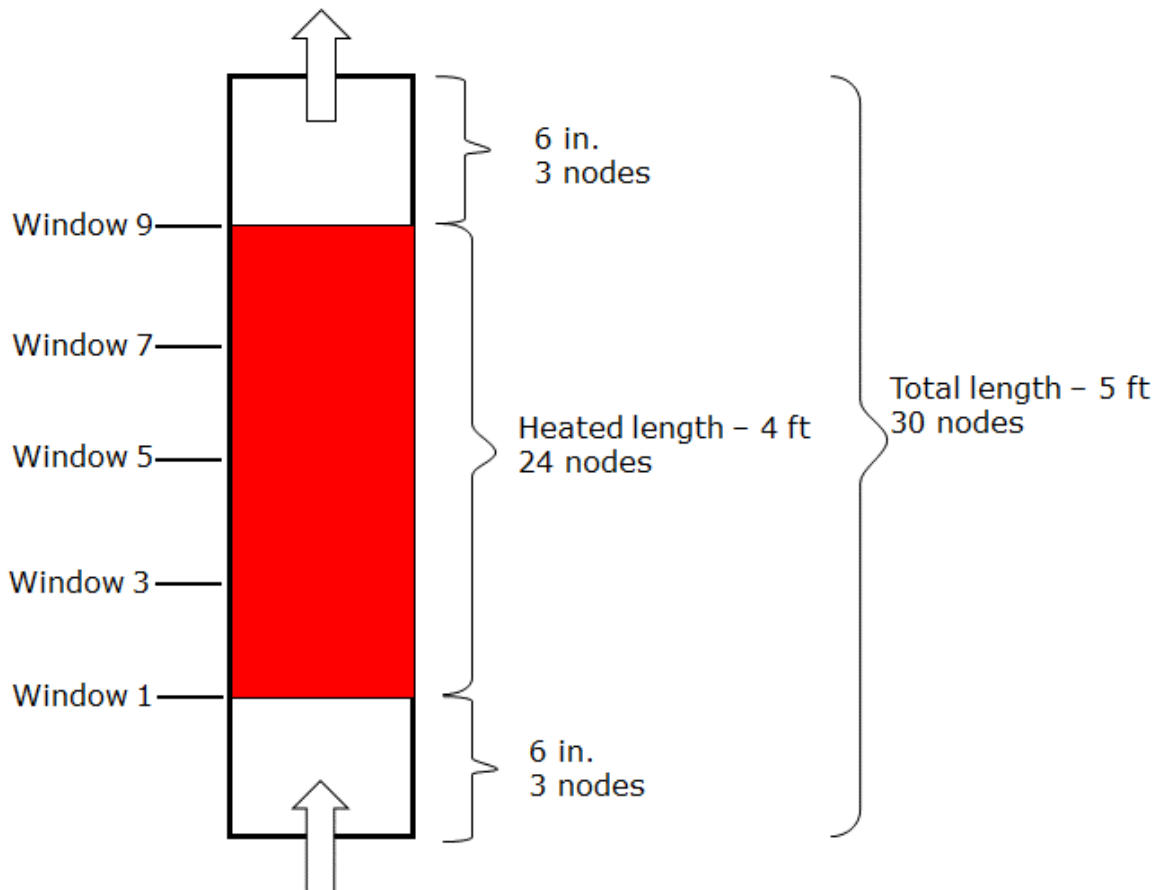
Figure 4-2: Axial schematic of PNNL 2 X 6 LDA measurement windows and CTF meshing (Sung et al. 2015)

Table 4-1: Boundary conditions for various cases

Case no	Flow rate(gpm)	Flow rate(m³/s)	Velocity (ft/s)	Velocity (m/s)	Power ratio	Hot side power, Q_H (kW/Rod)	Cool side power, Q_L (kW/Rod)	T_{inlet} (°C)
1	2.47	0.00016	0.327	0.1	2:1	1.14	0.57	15.6
2	1.25	0.00008	0.164	0.05	1:0	0.91	0.0	15.6
3	2.47	0.00016	0.327	0.1	1:0	1.81	0.0	15.9
Isothermal-1	2.47	0.00016	0.327	0.1	0:0	0.0	0.0	15.6
Isothermal-2	1.25	0.00008	0.164	0.05	0:0	0.0	0.0	15.6

4.4   Results and discussions

In Figure 4-3 and Figure 4-4, the CTF results of non-dimensional velocities for the Case Isothermal-1 are directly overlaid on the measured values for different windows. The x-axis on these plots correspond to the lateral movement of the traverse that is shown with an arrow head on the top right image while the y-axis is non-dimensional velocity as defined in the previous section. The images in top left and bottom left of Figure 4-3 correspond to windows

3 and 1, respectively. Similarly, top left and bottom left of Figure 4-4 correspond to windows 9 and 7, respectively.

From the plots in Figure 4-3 and Figure 4-4, it can be noticed that CTF results of velocity are matching better with measured values at lower heights, this means until about the window height of 5 and less. At the upper regions of heating i.e., window 7 and beyond, the measured values of velocities as can be seen from these plots are not clearly symmetric. Experimentalists in (Quigley, McMonagle & Bates 1977) have attributed this asymmetric nature to the mounting instrumentation of the traverse. These asymmetric details are not included in simulations, and hence all the simulation results are perfectly symmetric. It is also worth noting that the CTF simulation output can only give a single integral value of velocity for the subchannel cell under consideration at any given axial location. It is not possible to get a distribution of velocities within a subchannel.

For Case 1, the non-dimensional results of temperature from CTF are compared directly with experimental measurements and can be found in Figure 4-5. This comparison is carried out at each subchannel over a range of axial positions corresponding to the experimental window positions. The top left image in Figure 4-5 shows results of the simulations for all subchannels, whilst the bottom right image shows results when excluding subchannel-8. The comparison of the CTF data with measurements appears better for all the subchannels presented except for subchannel-8. This could perhaps be due to the presence of mounting accessories for the traverse instrument.

For Case 2, the results of non-dimensional quantities of both velocities and temperatures predicted from the CTF model in this work, are also compared with COBRA-TF by (Sung et al. 2015) in addition to the measured values (see from Figure 4-6 to Figure 4-8). Figure 4-6 represents the comparison of the aforementioned quantities for window 1; Figure 4-7 and Figure 4-8 present the same data for window 5 and window 7 respectively. Overall, the predictions (of velocity and temperature) from both COBRA-TF and CTF codes seem to be aligning with each other well (see from Figure 4-6 to Figure 4-8); however, both are off by a margin (up to 12°C higher prediction for these two codes as compared with experiments) in the vicinity of the wall sub-channel 8, where the experimenters have acknowledged that there is uncertainty in measurements.

Finally, the temperature values from CTF simulations for Case 1, Case 2 and Case 3 are tabulated along with the measurements and COBRA-IV results reported in (Quigley, McMonagle & Bates 1977) (see Table 4-2, Table 4-3 and Table 4-4). The results for Case 1 showed that CTF has always overpredicted the temperature by approximately 3.5°C to 11°C, in the increasing order from window 1 to window 9, for subchannel 8 as compared to the measured values. However, the results for the other subchannels from 9 to 14 showed better comparison with measurements with an over prediction of up to 4°C to an underprediction of around 2°C. There is no set pattern for overprediction or underprediction with regards to windows positions. The temperature results for Case 2 show more pronounced differences between simulations and measurements and Case 3 follows similar trends with few outliers.

For majority of the simulations, the temperature results of CTF have been found to be higher than those predicted by COBRA-IV.
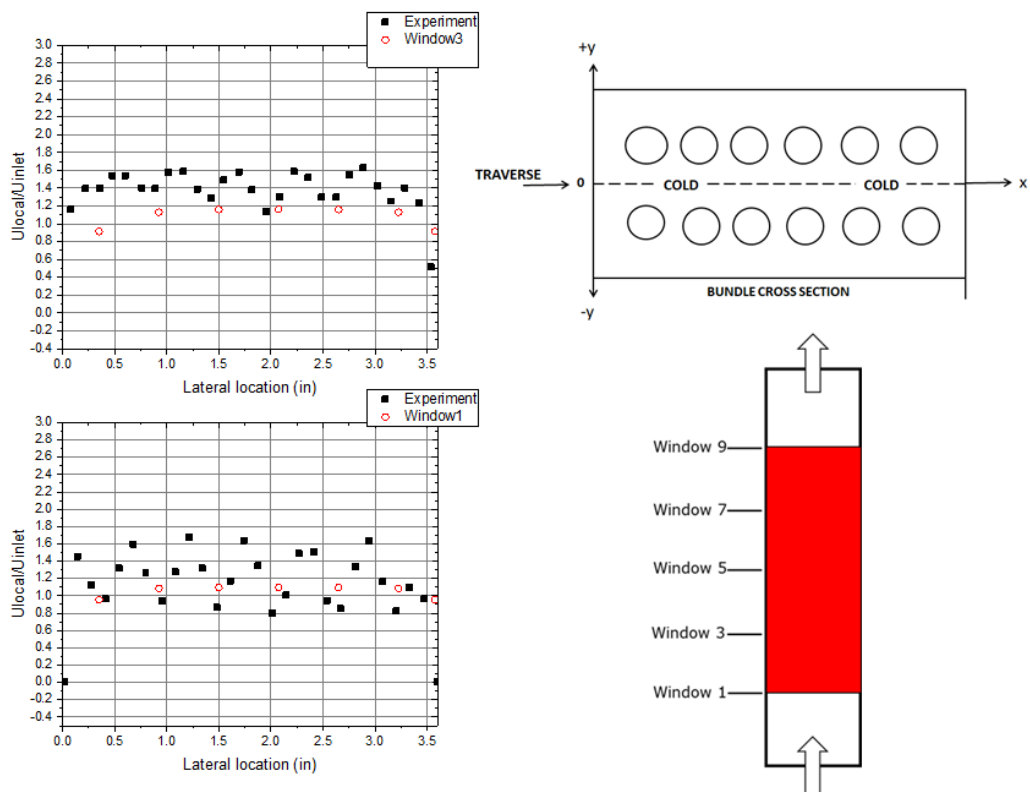
Figure 4-3: Isothermal-1 results - velocity comparison at window 1, window 3 (red hollow circles are CTF results)
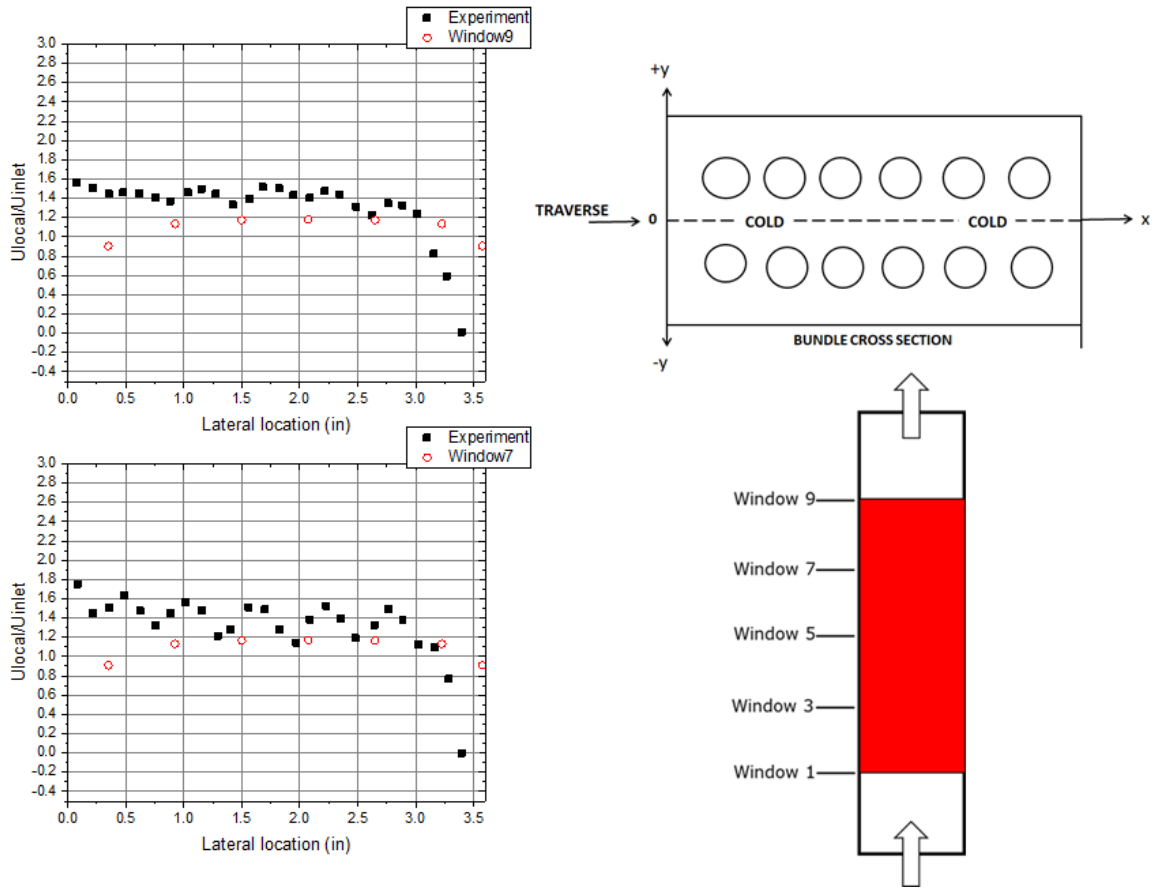
Figure 4-4: Isothermal-1 results: velocity comparison at window 7, window9 (red hollow circles are CTF results)
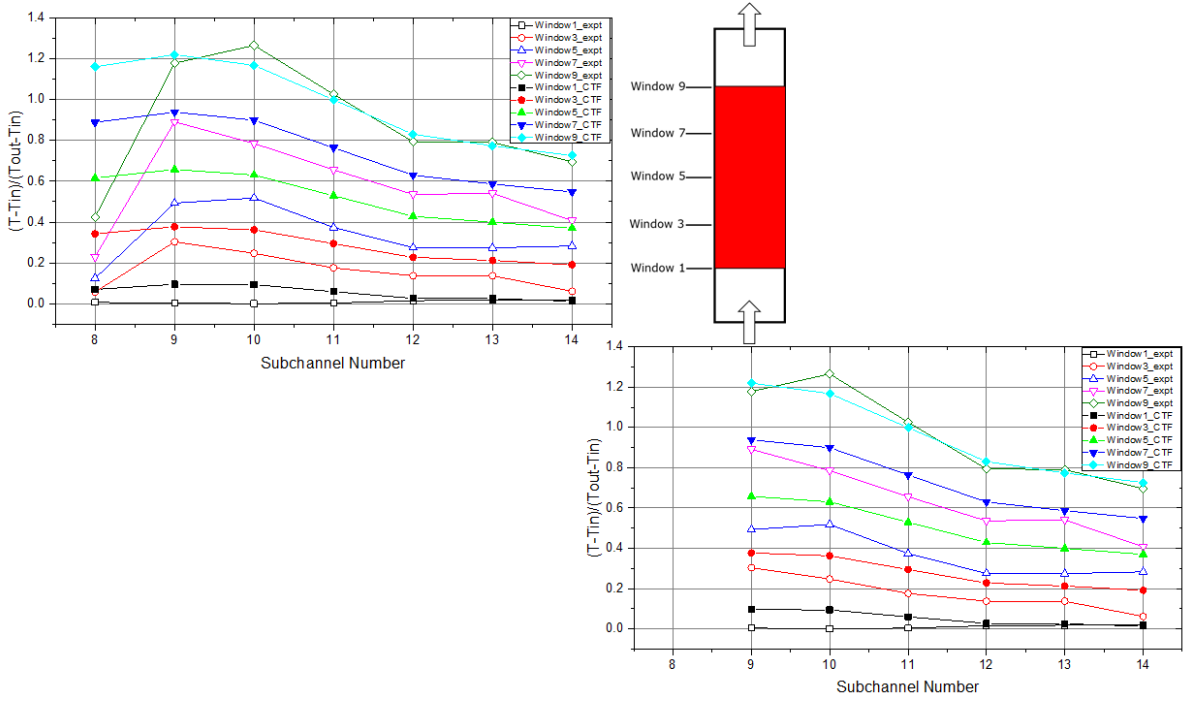
Figure 4-5: Case 1 results measurements vs. CTF predictions (left: Including channel 8, right: excluding channel 8)
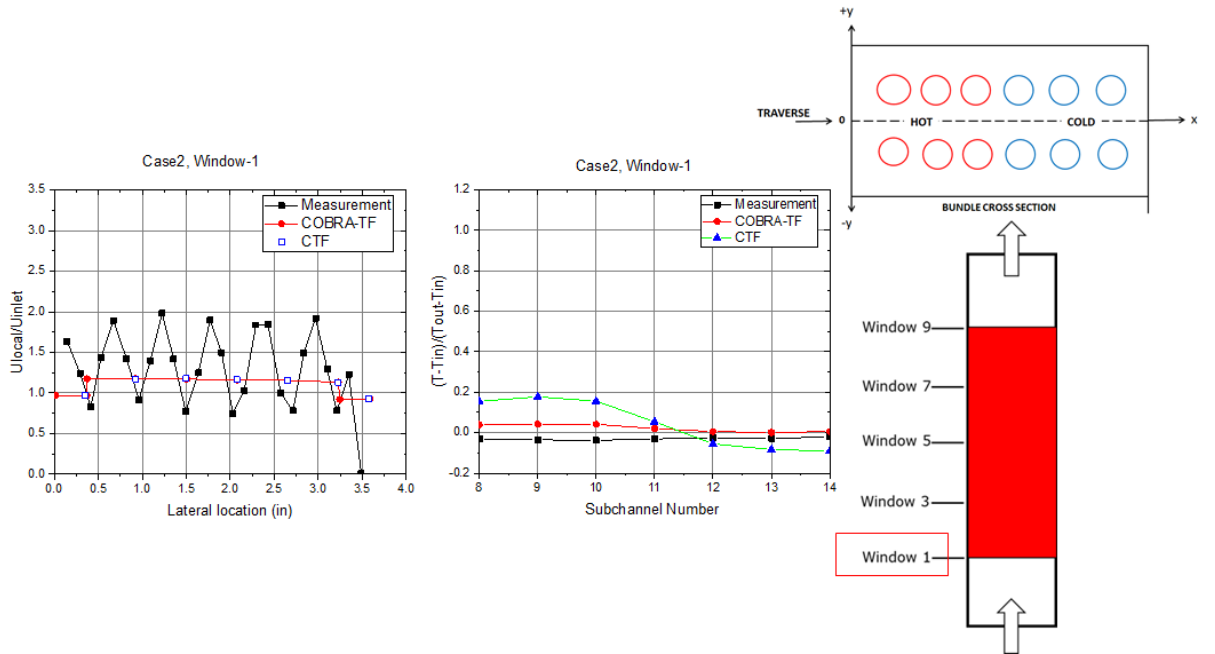
Figure 4-6: Case 2 results for window-1: Velocity (left), Temperature (Right), both are non-dimensional quantities
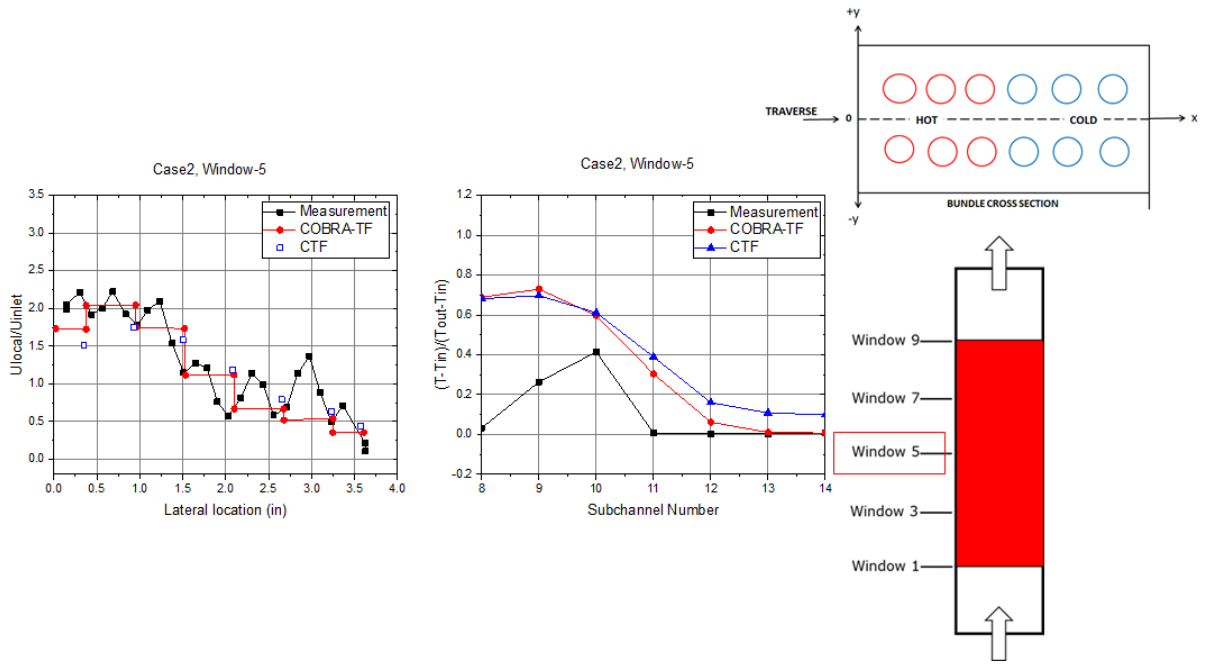
Figure 4-7: Case 2 results for window-5: Velocity (left), Temperature (Right), both are non-dimensional quantities
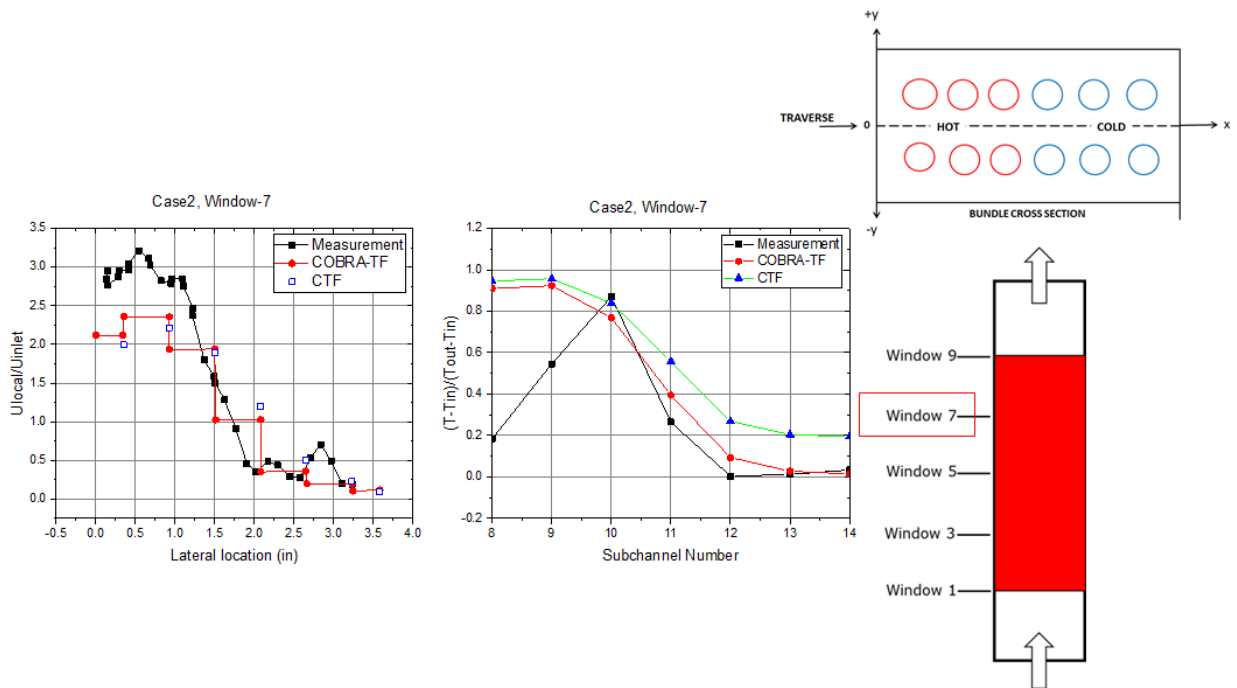
Figure 4-8: Case 2 results for window-7: Velocity (left), Temperature (Right), both are non-dimensional quantities

Table 4-2: CTF results for Case 1 with experimentally measured and COBRA-IV results (colour transition from blue to red indicates temperature increase from low to high)

Window number	Data Type	T_{in}, °C	T_{out}, °C	ΔT, °C $(T_{out}-T_{in})$	Subchannel number						
					8	9	10	11	12	13	14
1	Measured	13.11	30.67	17.56	13.06	13.11	13.17	13.28	13.39	13.39	13.50
	COBRA-IV	15.34	31.13	15.79	15.34	15.34	15.34	15.34	15.34	15.34	15.34
	CTF	15.60	31.35	15.75	16.71	17.11	17.08	16.54	16.02	16.00	15.80
3	Measured	13.44	31.11	17.67	14.44	18.89	17.83	16.61	15.94	15.94	14.56
	COBRA-IV	15.34	31.13	15.79	20.36	20.63	20.53	19.29	18.09	18.11	17.99
	CTF	15.60	31.35	15.75	21.01	21.54	21.31	20.24	19.19	18.94	18.61
5	Measured	16.50	35.33	18.83	18.89	26.00	26.39	23.61	21.83	21.83	21.94
	COBRA-IV	15.34	31.13	15.79	25.11	25.47	25.24	23.03	20.92	20.96	20.92
	CTF	15.60	31.35	15.75	25.30	25.97	25.54	23.94	22.36	21.89	21.42
7	Measured	16.56	33.39	16.83	20.50	31.72	29.78	27.72	25.67	25.78	23.44
	COBRA-IV	15.34	31.13	15.79	29.52	30.08	29.68	26.69	23.91	23.97	24.11
	CTF	15.60	31.35	15.75	29.60	30.40	29.77	27.64	25.52	24.84	24.24
9	Measured	15.61	31.44	15.83	22.39	34.44	35.67	31.89	28.17	28.22	26.67
	COBRA-IV	15.34	31.13	15.79	33.56	34.49	33.89	30.31	27.13	27.22	27.62
	CTF	15.60	31.35	15.75	33.89	34.83	34.01	31.34	28.69	27.79	27.05

Table 4-3: CTF results for Case 2 with experimentally measured and COBRA-IV results (colour transition from blue to red indicates temperature increase from low to high)

Window number	Data Type	T_{in}, °C	T_{out}, °C	ΔT, °C (T_{out}-T_{in})	Subchannel number 8	9	10	11	12	13	14
1	Measured	15.67	33.94	18.28	15.06	15.06	15.06	15.17	15.22	15.22	15.33
	COBRA-IV	15.78	31.94	16.17	15.78	15.78	15.78	15.78	15.78	15.78	15.78
	CTF	15.60	32.16	16.56	18.46	18.84	18.48	16.79	14.99	14.52	14.41
3	Measured	15.89	33.94	18.06	16.00	16.00	20.67	16.00	16.06	16.06	16.17
	COBRA-IV	15.78	31.94	16.17	22.58	22.58	22.04	18.77	15.78	15.78	15.78
	CTF	15.60	32.16	16.56	22.82	23.14	22.25	19.57	16.77	16.11	15.98
5	Measured	15.17	33.56	18.39	15.83	15.83	22.94	15.39	15.22	15.22	15.50
	COBRA-IV	15.78	31.94	16.17	27.47	27.47	26.11	20.88	15.78	15.78	15.78
	CTF	15.60	32.16	16.56	27.19	27.44	26.02	22.35	18.56	17.70	17.55
7	Measured	15.28	33.67	18.39	18.67	18.67	31.22	20.17	15.44	15.56	15.89
	COBRA-IV	15.78	31.94	16.17	31.14	31.14	29.66	22.59	15.78	15.78	15.78
	CTF	15.60	32.16	16.56	31.55	31.74	29.79	25.13	20.34	19.28	19.12
9	Measured	17.00	35.61	18.61	32.17	37.50	37.61	31.39	23.72	20.67	20.72
	COBRA-IV	15.78	31.94	16.17	34.17	34.96	32.66	24.93	19.99	20.31	19.74
	CTF	15.60	32.16	16.56	35.91	36.04	33.56	27.91	22.12	20.87	20.69

Table 4-4: CTF results for Case 3 with experimentally measured and COBRA-IV results (colour transition from blue to red indicates temperature increase from low to high)

Window number	Data Type	T_{in}, °C	T_{out}, °C	ΔT, °C (T_{out}-T_{in})	Subchannel number 8	9	10	11	12	13	14
1	Measured										
	COBRA-IV	16.06	32.78	16.73	16.06	16.06	16.06	16.06	16.06	16.06	16.06
	CTF	15.60	32.28	16.68	17.94	18.61	18.48	16.88	15.36	15.38	15.45
3	Measured	16.17	34.06	17.89	17.50	23.56	22.28	18.06	16.28	16.33	16.44
	COBRA-IV	16.06	32.78	16.73	23.58	24.07	23.41	19.59	16.06	16.06	16.06
	CTF	15.60	32.28	16.68	23.39	24.05	23.11	19.85	16.61	15.85	15.70
5	Measured	16.61	36.39	19.78	20.06	28.94	30.89	19.50	16.72	16.72	16.83
	COBRA-IV	16.06	32.78	16.73	29.62	30.58	28.95	22.24	16.06	16.06	16.06
	CTF	15.60	32.28	16.68	28.85	29.49	27.73	22.82	17.85	16.32	15.94
7	Measured	16.56	33.50	16.94	23.61	35.06	35.78	20.89	16.61	16.67	16.83
	COBRA-IV	16.06	32.78	16.73	34.62	36.09	33.52	24.43	16.06	16.06	16.06
	CTF	15.60	32.28	16.68	34.30	34.93	32.36	25.79	19.10	16.79	16.19
9	Measured	15.39	31.50	16.11	27.50	41.17	40.72	27.22	16.11	15.50	15.89
	COBRA-IV	16.06	32.78	16.73	39.05	40.94	37.42	26.42	16.06	16.06	16.06
	CTF	15.60	32.28	16.68	39.75	40.37	36.99	28.77	20.35	17.26	16.43

4.5   Conclusions

Based on the validation work on PNNL test facility using CTF, the following conclusions can be drawn:

1. The validation studies using CTF for the PNNL test facility proved that CTF can be used with confidence for single-phase flow problems.

2. CTF results show that in general, there is good agreement with the data, especially the trends of velocities and temperatures are similar.

3. In occasional circumstances, there is a disparity between the test and the CTF results (both for temperature and velocity), particularly in the vicinity of the wall.

4. It is not possible to get details of the velocity profile for an intra subchannel flow (within a given subchannel flow) from CTF unlike Computational Fluid Dynamics (CFD) analysis.

5. The uncertainties in thermocouple positions near subchannel-8, combined with high temperature gradients near the wall make it more challenging for the code CTF to assess the accuracy of the results.

6. In general, the temperature predictions from CTF have always been higher than those predicted by COBRA-IV. This appears to be an inherent bias, but needs further investigations to further conclude on this.

7. This analysis task of validating CTF for single phase flows has provided sufficient experience that can be used for the further studies on Rig-1, which is going to be purely single-phase and isothermal flows.

CHAPTER 5: MODELLING AND SIMULATION OF FAITH

5.1 Introduction

As explained in the introduction chapter of this thesis, the objective of Project FAITH is to prove that two rigs, one using water (Rig-1) and the other using sodium (Rig-2) as working fluids, can be manufactured through modular construction. These rigs will be used to conduct reactor thermal-hydraulics experiments. Rig-1 is for understanding and validating the flow characteristic through the test section without the complexity or hazards arising from a liquid sodium facility. Rig-2 is for understanding and validating both the flow characteristics and heat transfer within the test section. In Project FAITH, Cammell Laird (CL) will design and manufacture Rig-1 with the support from NNL, and with GE Hitachi providing few specific inputs for the test section details.

The rig will be located in NNL's Workington Rig Hall facility and will be designed and built in a modular manner by CL at CL's facility in Birkenhead. NNL will then carry out the required experiments on the rig, and use the data collected (velocity, pressure) to develop and validate a series of CFD models, which were carried out in parallel to CL's manufacturing efforts. At the time of carrying out this work, NNL/CL is still trying to finalise about the required instrumentation to obtain data from the experiments. CFD analysis has been extensively used to propose velocity and pressure probe locations within the flow domain of the Rig-1. The results from CTF have been compared against CFD results and it is reasonable to accept CFD as a benchmark data at this stage as the experimental measurements were not available.

As part of this MPhil work, subchannel code (CTF) was used in tandem with CFD (Ansys Fluent) mainly to understand the limitations of subchannel codes while capturing the details of the flow and investigations were also made on how CFD results can be used to improve the accuracy of subchannel code predictions. For a full reactor assembly, it is not practical to use CFD codes due to their heavy requirements on computational resources and simulation time but subchannels codes such as CTF provide quick solutions with reasonable accuracy; further the accuracy of the predictions from the subchannels codes can be improved by linking with high fidelity codes (CFD in this study) or measured properties. The current chapter explains on how CFD can be used to enhance the accuracy of CTF.

5.2   Experimental details

NNL have undertaken literature studies to explore the pin layouts and typical flow conditions that are encountered with an SFR and based on those studies the geometry outlined in Preliminary Core Design Studies by E Hoffman, W.S Yang and R.N Hill at the U.S Department of Energy in 2006 (Hoffman, Yang & Hill 2006) was proposed for experimental test section. This report has details relating to a S-PRISM modular plant based on a 1000 MWt reactor. The dimensions of the S-PRISM reactor have been scaled up by a factor of 4 applying similarity theory for the ease of manufacturing process and as well as to provide sufficient space for instrumentation yet without compromising on flow regimes that are of interest. The scaling laws in single phase flows have been well established and an accepted practice. The images showing the test section of the geometry which has 7 fuel pins in a hexagonal pipe are as shown in Figure 5-1 and Figure 5-2. Figure 5-1 shows 3D image of the geometry where the helical wire is wrapped around each fuel pin while the image in Figure 5-2 shows pin wire assembly inside the test section as seen from the top.
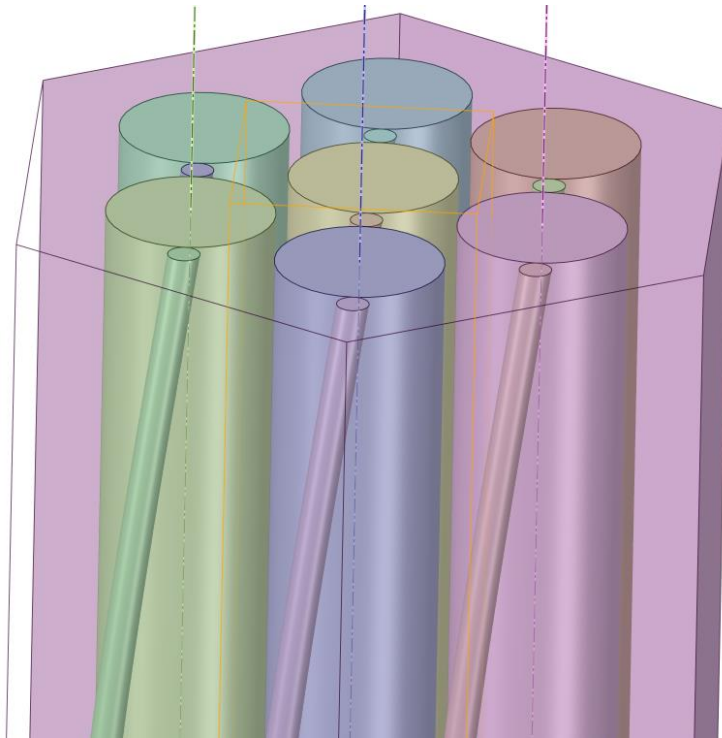
*Figure 5-1: 3D geometry of the test section (Roop, Jonathan & Brendan 2020)*

Wire wrap

Water filled section
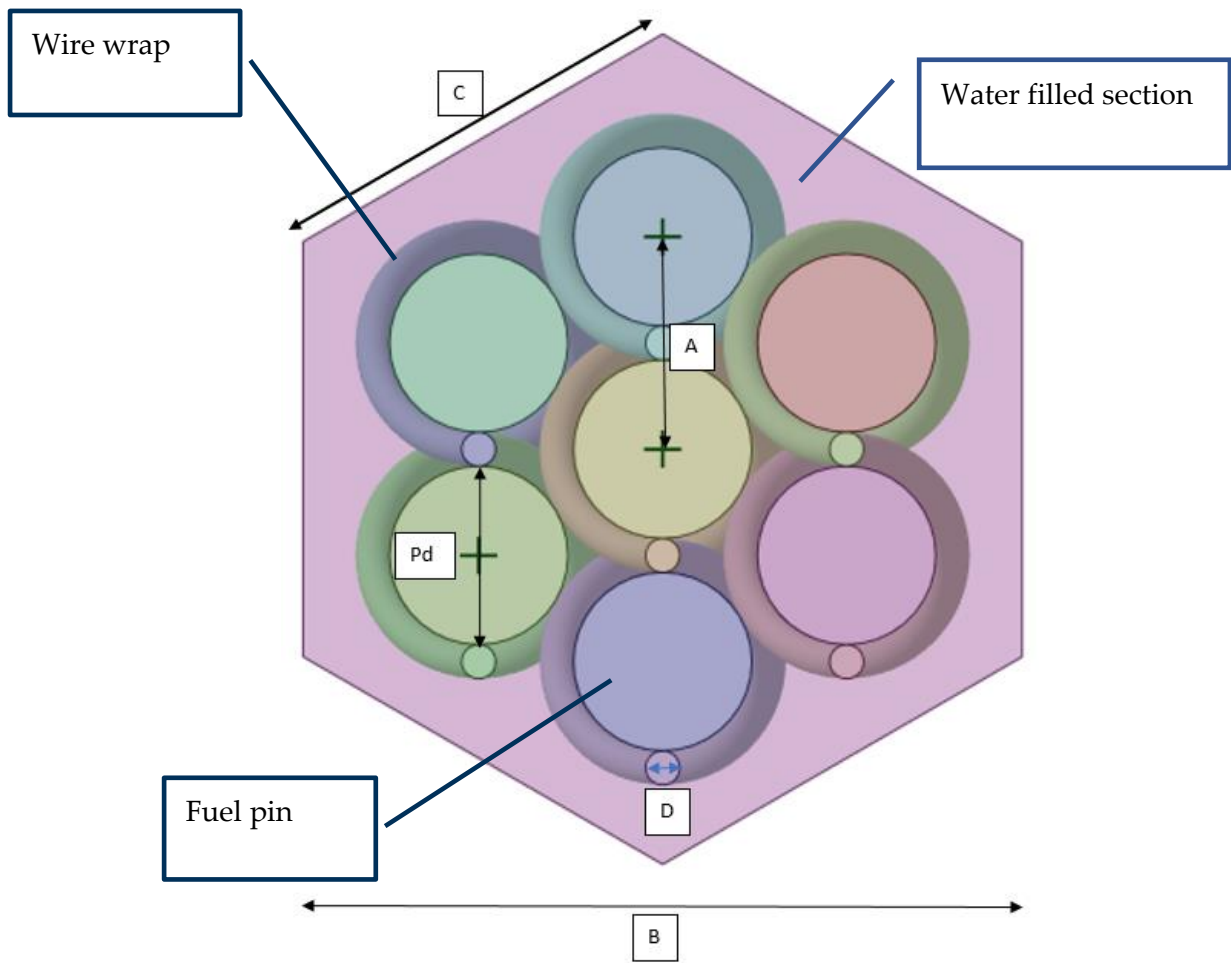
Fuel pin

*Figure 5-2: Plan view of the test section (Roop, Jonathan & Brendan 2020)*
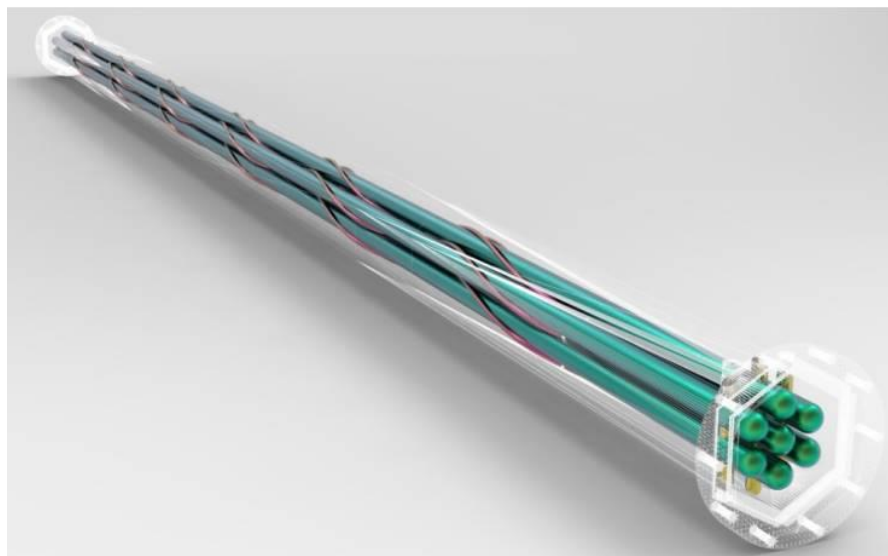
Figure 5-3: Overall view of hexagonal fuel pin assembly as to be manufactured

Figure 5-4: 3D sketch of the modular rig with the test section on the right

5.2.1 Rig dimensions

As explained in the previous section, the rig dimensions are based on a 4 × scale-up of the dimensions from the real fuel assembly which are included in the brackets and as provided below (Roop, Jonathan & Brendan 2020):

➢ Pin external diameter, P_d = 29.76 mm (7.44 mm)
➢ Pin pitch, A = 35.444 mm (8.861 mm)
➢ External wire diameter, D = 5.688 mm (1.422 mm)
➢ Internal width of test element, B = 112.58 mm
➢ Internal length of one side of test element, C = 65 mm
➢ Internal height of one full wire wrap: the 'wrapping pitch', H = 600 mm
➢ Pin length defined by 6 'wrapping pitches' for the test section height = 3600 mm

Manufacturing tolerances for these measurements are around ± 1%. The artistic impressions of fuel pin assembly and the rig (when completed) can be seen in Figure 5-3 and Figure 5-4. The image in Figure 5-3 shows the fuel pins which are in green colour and wrapped helically by the wire shown by the magenta colour, and all the wire-wrapped seven pins are assembled in a hexagonal pipe. Figure 5-4 shows the overall modular rig containing typical pipe network with valves, including the pump, over-head water tank storage, control unit and the test section.

The test rig will be operated across a range of Reynolds numbers by controlling the inlet flow velocity and water temperature. The range of Reynolds numbers cover the operational range that is expected to be seen in SFRs. Subchannel (CTF) and CFD (Ansys Fluent) analyses will be performed on a series of equivalent simulations using the same Reynolds number range, with an intention to have like to like comparison when the measurements will be available.

Table 5-1 presents the range of Reynolds numbers which are required in the rig test section and the corresponding flow velocity at the test section inlet.

Table 5-1: Inlet flow velocity at the test section entrance

Re	5000	10000	25000	50000	75000	100000
Velocity (m/s)	0.24	0.48	1.20	2.39	3.59	4.79

5.3   Modelling approach:

The overall objective of the modelling approach is to investigate how well the subchannel codes such as CTF can be used to represent subchannel flows in an SFR where the cylindrical fuel pins are arranged in a triangular lattice, and the fuel pins are separated from each other by a helical wire wrap. The main parameters of interest in the thermal-hydraulics studies are subchannel wise pressure, temperature and velocity distributions in the sub-assembly. Up to now, these subchannel codes such as CTF have mainly been in use for pressurised water reactors in which the subchannels are predominantly in a square lattice arrangement. A multistage approach has been adapted here with a gradual increase in complexity of modelling, thus testing the capabilities of subchannel codes from standard problems to non-standard problems, thus from the known to the unknown.

During the first stage of multistage approach, a square lattice with fuel rods (of the same size that were in use for Rig-1) that do not contain any wire wrap has been considered

for the subchannel analysis, CTF. CFD analysis has been performed on the same geometry to report pressure drop values for different Reynolds numbers following the best practice guidelines (Patel 2020) on mesh and modelling methods on Rig-1. The results from the codes CTF & Ansys Fluent have been compared against each other. The pressure drops values from CTF code have been developed from empirical frictional correlations used in the code while the pressure drops values from the Ansys Fluent are calculated directly solving the Navier-Stokes equations using numerical methods. The nature of empirical correlations is that they are suitable only for a particular set of geometries and operating conditions within which they are valid. In the present work, a new set of frictional correlations have been developed using the results from CFD (due to non-availability of experimental measurements) over the set of Reynolds numbers as indicated in Table 5-1 and later CTF simulations were performed again using the correlations obtained from CFD and then the results are compared.

The purpose of the first stage (square grid assembly) is to check how good the pressure drops predictions from the standard correlations from CTF compare with the CFD results and it is intentional that the hexagonal pipe with triangular lattice subchannels with the wire wraps were not included in the first state.

During the second stage, the objective is to move towards the realistic scenario, but still only with a gradual increase in complexity. Hence, in the second stage, CTF model was built for a hexagonal pipe with seven fuel pins and no wire wrap around them. This in itself is an additional change for the standard use of CTF where the code is validated for square subchannels.

The objective of the second stage is similar to the first stage except that the triangular lattice is used in place of square and the number of fuel pins are seven instead of nine that were used for a square subchannels. This stage helps to evaluate the performance of CTF moving from square subchannels to triangular subchannels. The results from CTF have been compared against the results from CFD, and also the frictional loss coefficients from CFD have been implemented in CTF to investigate if there are any existing differences (from standard correlations of CTF and CFD) can be minimised by using the data from CFD.

In the final stage, hexagonal pipe with seven pins and wire wraps as used in the experiment was modelled using CTF and as well a CFD model was built for the same

configuration to generate frictional loss coefficients. This dimensionless friction factor is called by various names within the engineering industry. These include resistance coefficient, flow coefficient, Darcy-Weisbach friction factor or Darcy friction factor, to name a few. Within this work, the term adopted for this non-dimensional friction factor is Darcy friction factor which is defined as below:

$$\Delta P = f_D \cdot \left(\frac{L}{D_H}\right) \cdot \frac{1}{2} \cdot \rho \cdot v^2$$

Where ΔP is pressure drop (Pa), f_D is Darcy friction factor, L is length of the pipe (m), D_H is the hydraulic diameter of the test section (m), ρ is the density of water (kg/m³) and v is mean flow velocity (m/s)

5.4 CTF mesh & CFD mesh

The radial mesh distribution of 3 × 3 rod arrangement with square subchannels is presented in the Figure 5-5 and CFD radial mesh can be seen in Figure 5-6 and Figure 5-7. Figure 5-5 shows that the number of radial elements for a CTF mesh is equal to the number of subchannels which is a limitation on the subchannel code. On the other hand, it is evident from the images in Figure 5-6 and Figure 5-7 that the CFD mesh poses no limitation on the number of cells (as long as it is fit for the purpose for the turbulence model that is in use) yet offering greater control on details such as boundary layer, aspect ratio, cells distribution and many parameters that are related to mesh. However, in both the codes, the axial refinement of the mesh can be altered.

The images in Figure 5-8, Figure 5-9 and Figure 5-10 are for a 7-rod arrangement in a hexagonal pipe with triangular subchannels. As with the images for square subchannels case, Figure 5-8 shows the number of radial elements for a CTF mesh and the images in Figure 5-9 and Figure 5-10 show the radial mesh distribution for CFD, the latter figure showing the boundary layer mesh near the wall regions. It can also be noticed from the images that the wire wrap is not included in these figures. The images presented in Figure 5-11, Figure 5-12 and Figure 5-13 include wire wrap for the seven fuel pins which are in triangular lattice arrangement in a hexagonal pipe. This configuration is being manufactured for the Rig- 1.
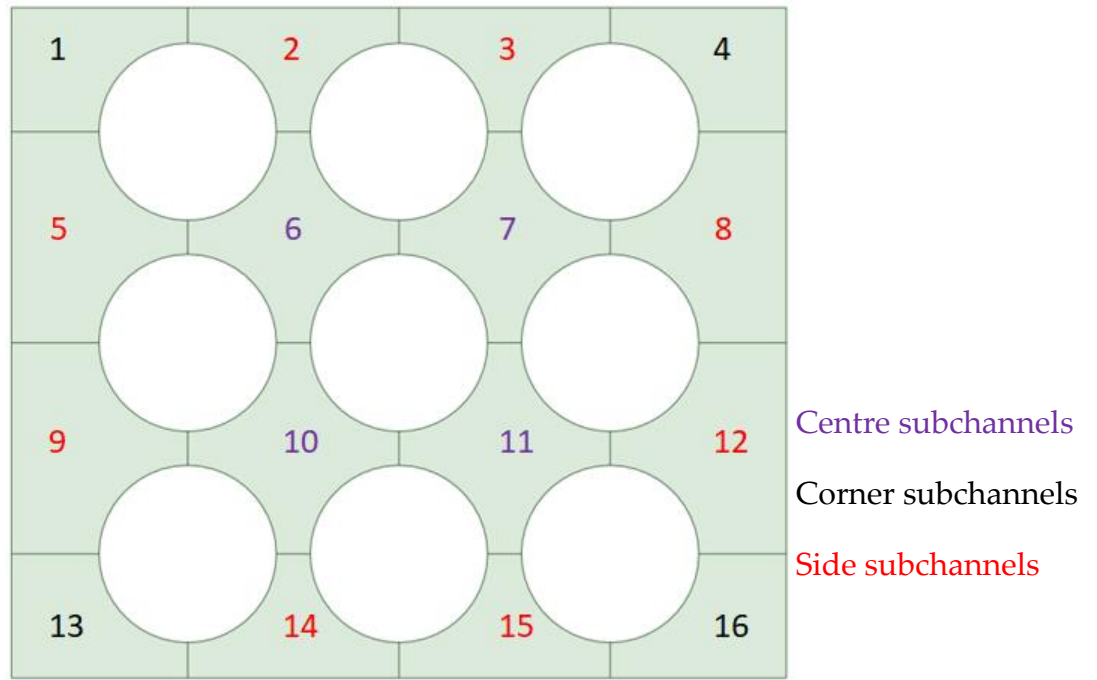
Figure 5-5: CTF mesh - radial distribution of subchannels for a 3 × 3 rod arrangement with square subchannels
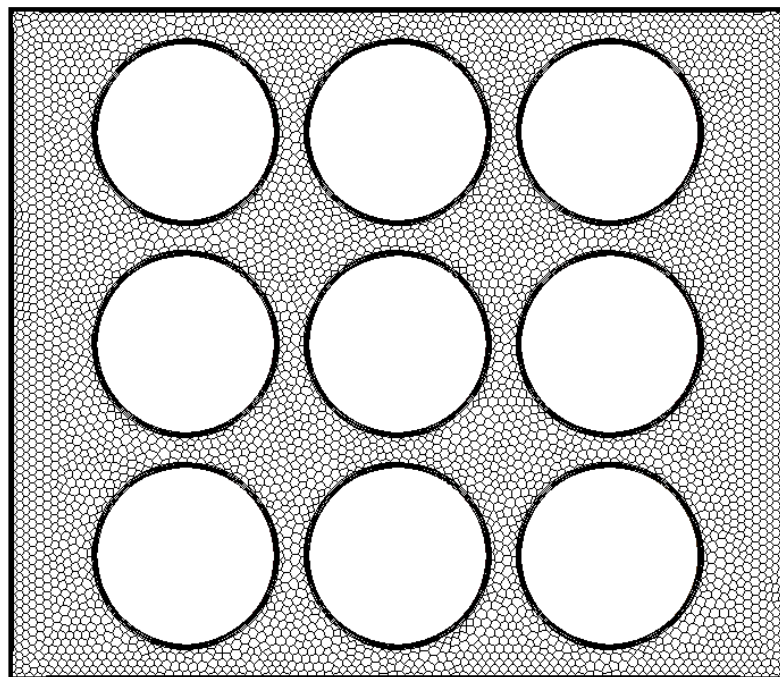
Figure 5-6: CFD mesh - radial distribution of subchannels for a 3 × 3 rod arrangement with square subchannels
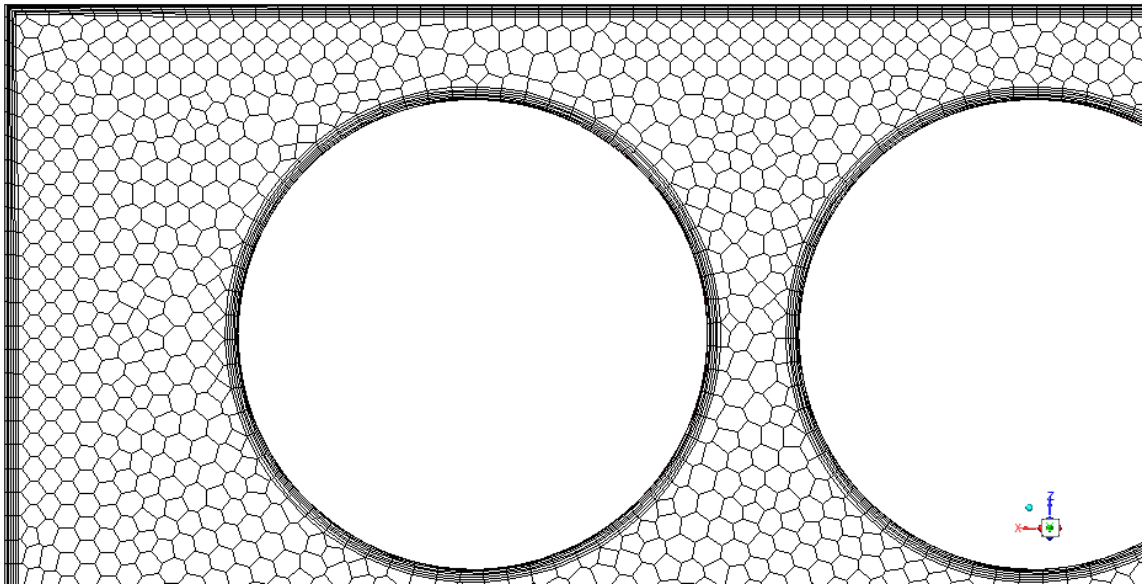
Figure 5-7: CFD mesh - radial distribution showing boundary layer mesh near walls
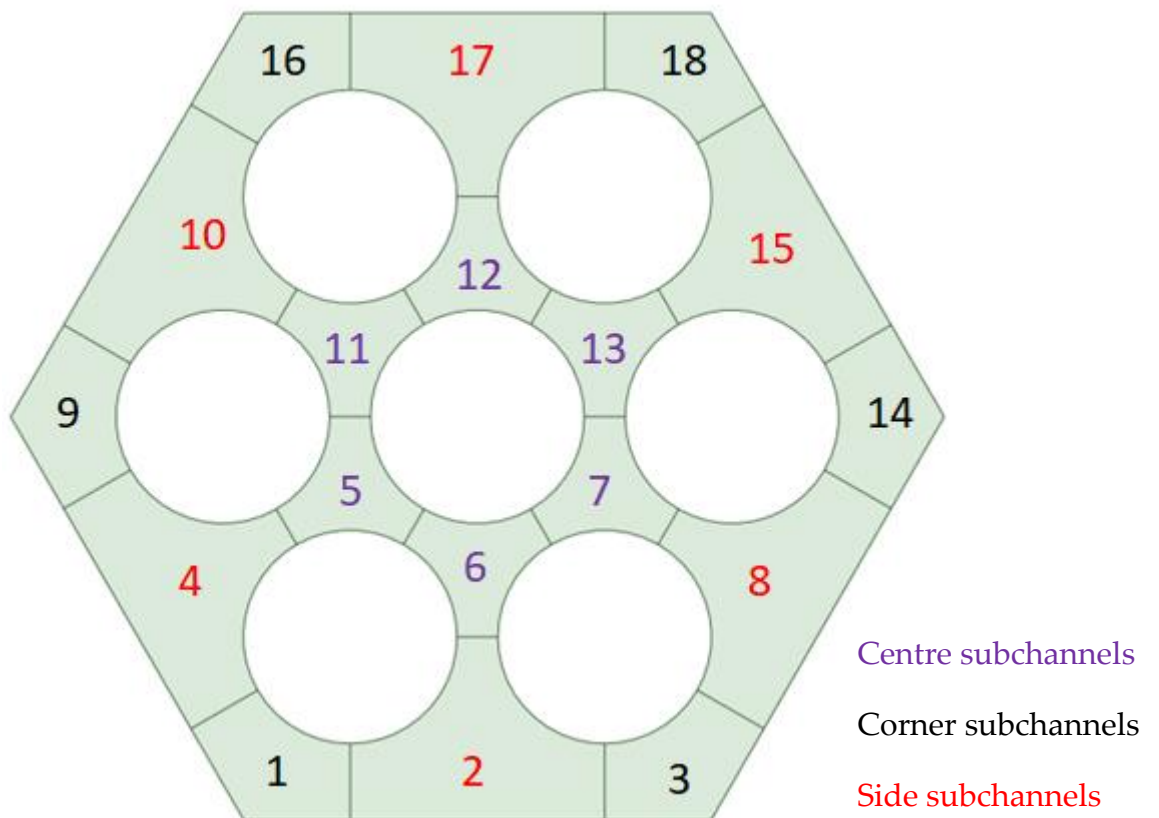
Figure 5-8: CTF mesh - radial distribution of subchannels for a 7-rod arrangement with triangular
*subchannels – without wire wrap*
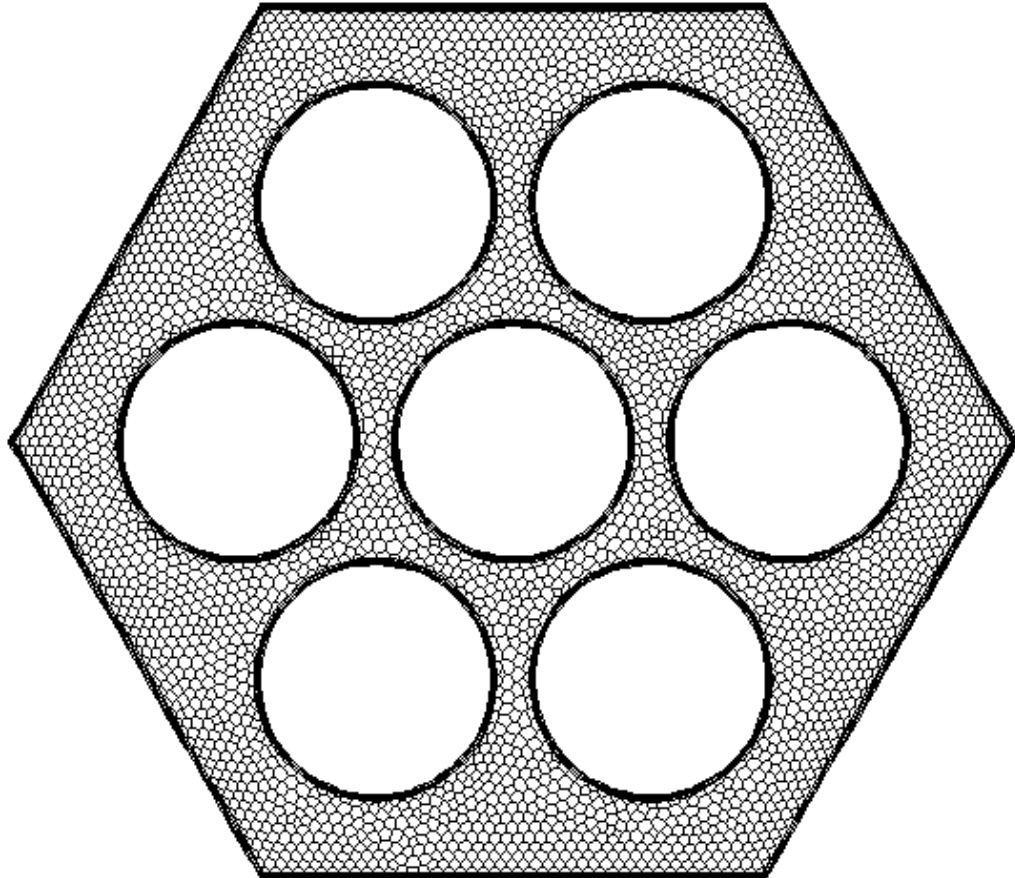
Figure 5-9: CFD mesh - radial distribution of subchannels for a 7-rod arrangement with triangular subchannels
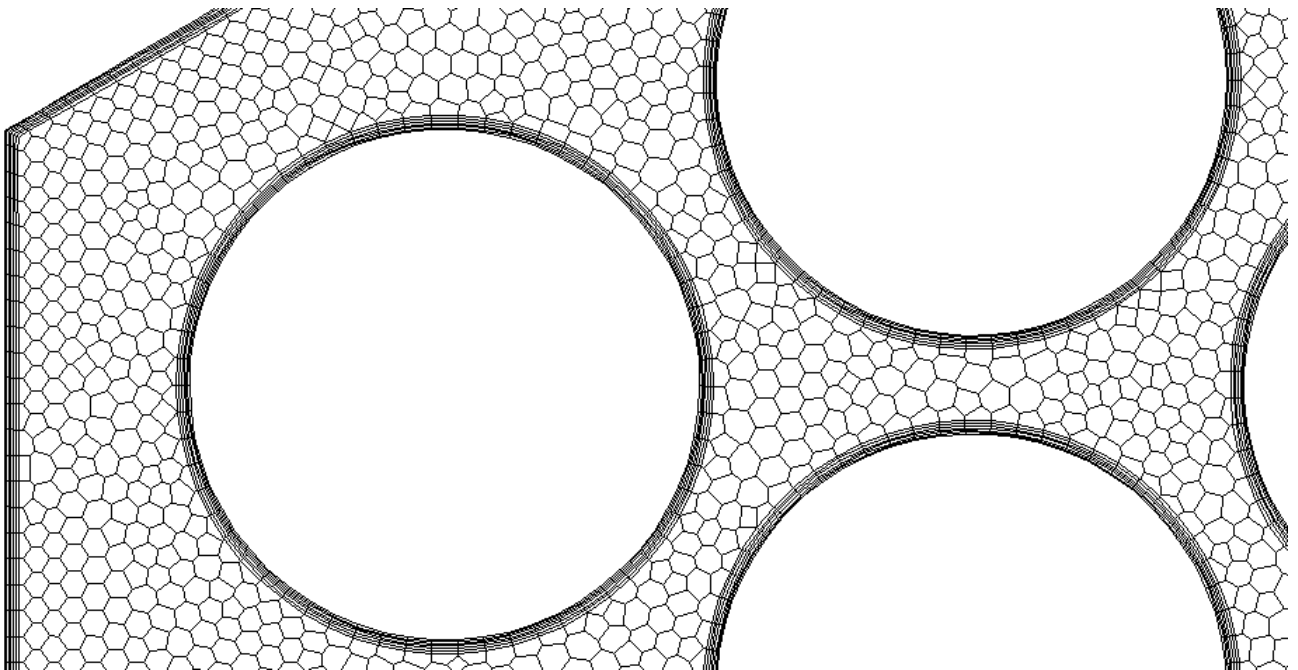

Figure 5-10: CFD mesh - radial distribution showing boundary layer mesh near walls
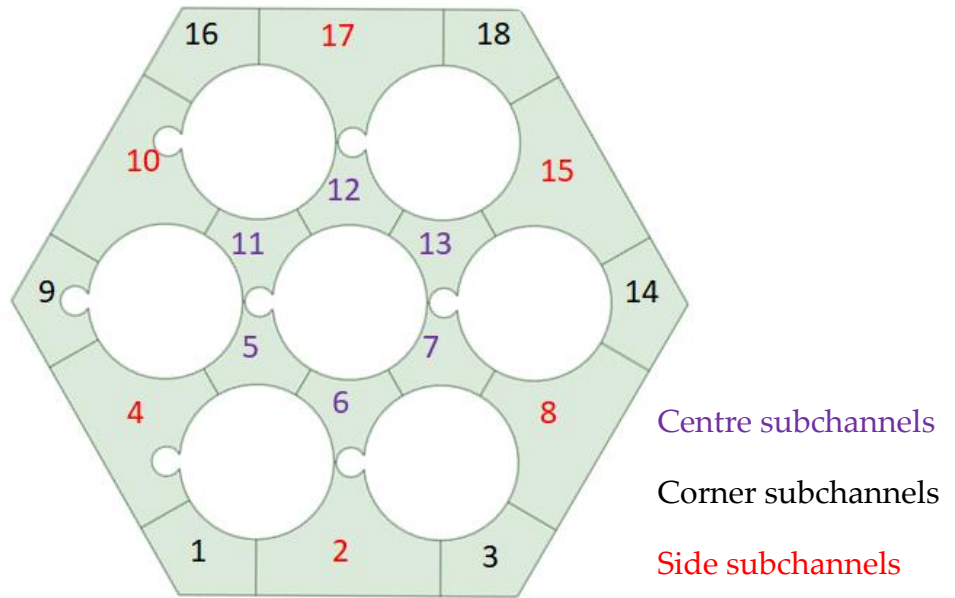
Figure 5-11: CTF mesh - radial distribution of subchannels for a 7-rod arrangement with triangular subchannels – with wire wrap
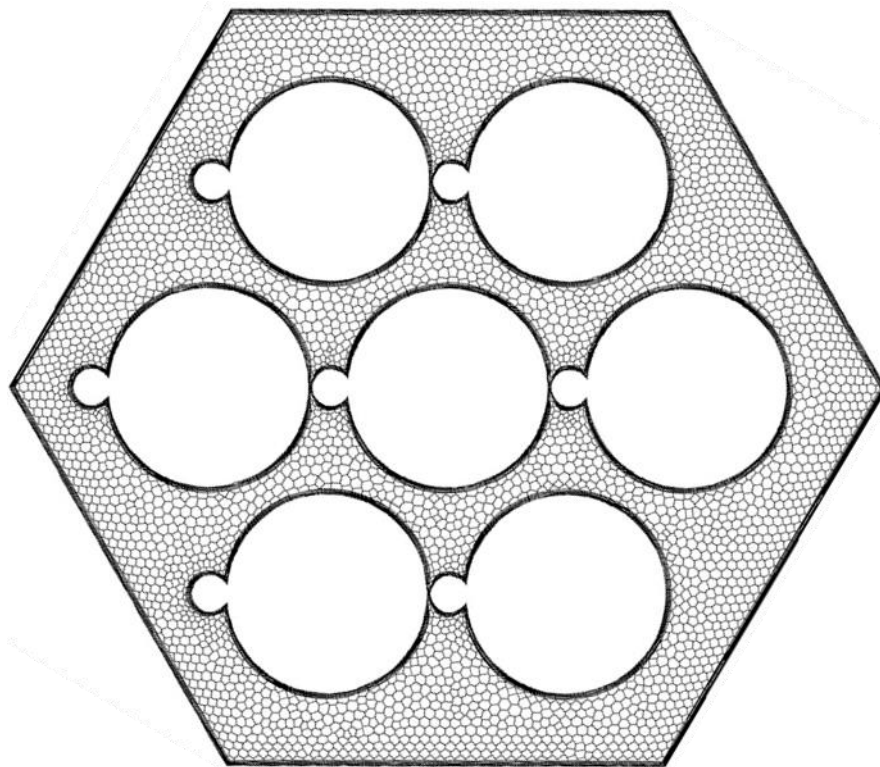

Figure 5-12: CFD mesh - radial distribution of subchannels for a 7-rod arrangement with triangular subchannels – with wire wrap
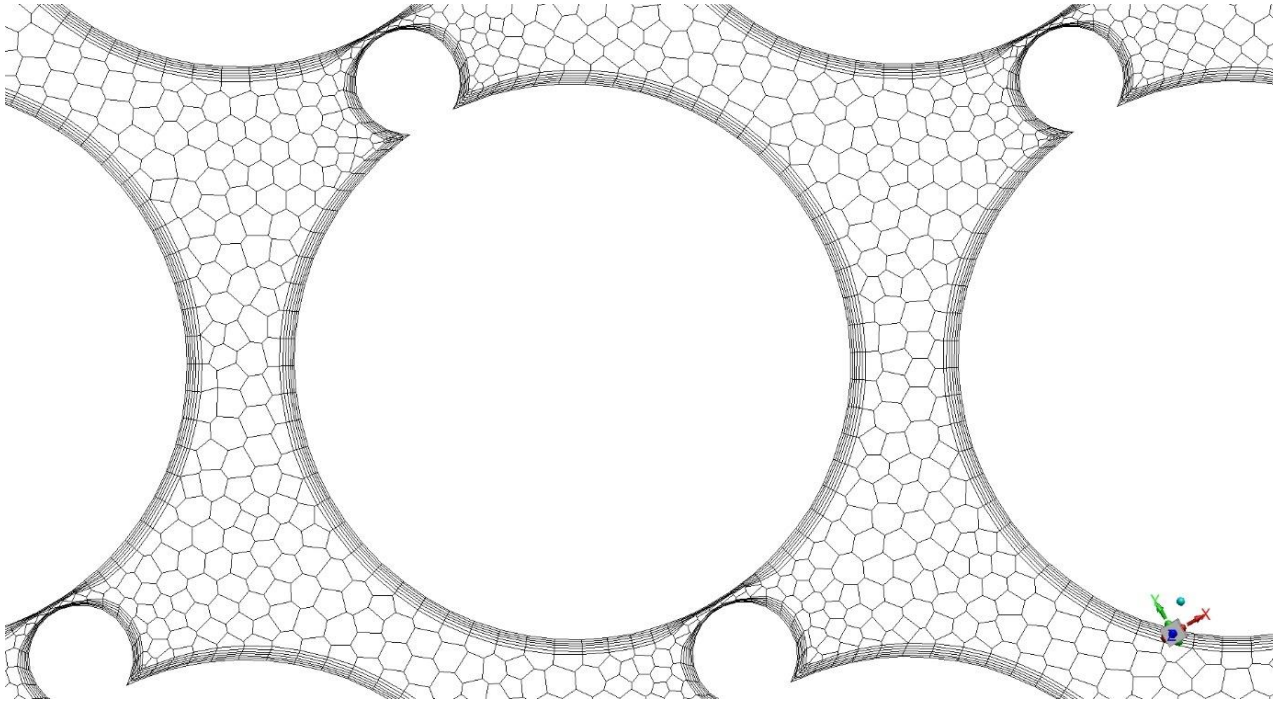
Figure 5-13: CFD mesh - radial distribution showing boundary layer mesh near walls

5.5   Results and discussions

This section presents the findings from all the stages that were described in the modelling approach section. The results include the following:

An X-Y plot of Darcy friction factor, f vs. Reynolds number, Re from CFD output of each stage of the modelling approach i.e., a square lattice with 9 pin (Figure 5-14), a triangular lattice with 7-pin in a hexagonal pipe (Figure 5-16), and triangular lattice with 7-pin in a hexagonal pipe (Figure 5-18) with wire wrap for each pin.

The solid red circles on the X-Y plots are the simulation points, connected in the figure through a red line. The trend shows the characteristic asymptotic reduction of the friction factor with increasing Reynolds number. The power law was used for curve fitting the simulation data and this is visually represented with a dotted black line. The curve fit equation along with the R-squared (R^2) value which is a statistical measure of data fit are shown in the figure.

The next set of plots reported here are X-Y plots of Pressure drop, ΔP vs Reynolds number which can be seen in Figure 5-15, Figure 5-17 and Figure 5-19. Figure 5-15 presents

the results for square lattice with 9 pins, Figure 5-17 shows the results for hexagonal pipe with 7-pin with no wire wrap and Figure 5-19 demonstrates the results for hexagonal pipe with 7-pin and wire wrap. On each of these plots, there are three different series named CFD, CTF- Standard Correlation and CTF-CFD (Power law curve fit). The series data of CFD corresponds to the results of ΔP vs Re, similarly the series data of CTF – Standard Correlation represents the results of CTF simulations using the inbuilt standard frictional correlations for pressure drops. The third series which is titled CTF-CFD (Power law curve fit) are the results of ΔP vs Re obtained from CTF but replacing the standard correlations from CTF code with the power law curve fit equations (from CFD data) for the respective cases.

The hollow blue circles joined by the solid blue line show the data of ΔP vs Re from CFD simulations. The hollow orange triangles connected by the solid orange line indicate data of ΔP vs Re produced from CTF standard frictional correlations and finally the hollow green squares joined by the solid green line show the results of ΔP vs Re from CTF code with the power law curve fit equation (from the CFD data) incorporated in CTF code.

All these plots follow the typical quadratic relation between the pressure drop and Reynolds number in turbulent flow regimes. The average relative error between CTF standard correlations and CFD data is around 25% for the cases without wire wrap and this is regardless of square or triangular array of fuel pin arrangement. However, with a 7-pin in a triangular array and with wire wrap the average relative error between CTF standard correlations and CFD is about 6%. When power law curve fit for pressure drop vs Reynolds number from the CFD results was used for CTF, the aforementioned relative errors have come down to the levels less than 0.5%.

In general, CTF standard correlations tend to overpredict the pressure drops as compared to CFD results. Accurate prediction of pressure drop in fuel assemblies is important in terms of designing the required pump for the flow more efficiently. Furthermore, the radial mesh of the subchannel code, CTF has only 3 channel types that are repetitive in any full fuel assembly; accurate friction factor estimation from high-fidelity models such as CFD and then, further implementation of these friction factor coefficients in subchannels codes such as CTF is an effective way of predicting the fuel assembly

performance. It is worth mentioning that these predictions hold true no matter how large the fuel assembly is, just these frictional coefficients will be enough to predict the performance.

A detailed CFD analysis carried out by Frazer Nash consultancy, UK (Wimshurst 2020) for a 19-pin fuel assembly with wire wrap has predicted similar Darcy friction factor to that for the 7-pin (with wire wrap) fuel assembly carried out for this present work. An additional CTF model was built for a 19-pin fuel assembly as shown in the Figure 5-20. The radial splitting of the CTF mesh with each equal to the subchannel size can also be seen in the image shown in Figure 5-20. The power law curve fit equation for 7-pin fuel assembly with wire wrap (which is essentially Rig-1 geometry) is used for 19-pin fuel assembly to generate pressure drop values at different flow rates and the plots of pressure drop vs Reynolds numbers can be seen in Figure 5-21. The curves in Figure 5-21 follows the same notation for 7-pin curves with hollow orange triangles connected by the solid orange line indicating data of ΔP vs Re produced from CTF standard frictional correlations while the hollow green squares joined by the solid green line show the results of ΔP vs Re from CTF code with the power law curve fit equation (from the CFD data) incorporated in CTF code.

The purpose of doing this 19-pin fuel assembly is to demonstrate to advantage of using subchannel codes for bigger assemblies with good confidence. For instance, in this case, the CFD output of 7-pin which are frictional coefficients at different Reynolds numbers are fed into CTF model for 19-pin and the characteristic curve of ΔP vs Re is produced. Based on what was witnessed for 7-pin case, it can be said that the results for 19-pin match better with CFD results which is the high-fidelity model. Due to the need of intense computational resources and the complexity of generating the accurate representation of mesh/model that is suitable for relevant turbulent models, performing CFD simulations to predict the performance for fuel assemblies having pins 19 and above is not practically feasible. Hence, the approach that is developed here, which is using frictional coefficient from a CFD analysis carried out on sub assembly (7-pin in this context) and subsequently use these friction coefficients in subchannel codes level for bigger fuel assemblies (19-pin in this case) could prove to be more efficient method to predict the pressure drops of bigger fuel assemblies.
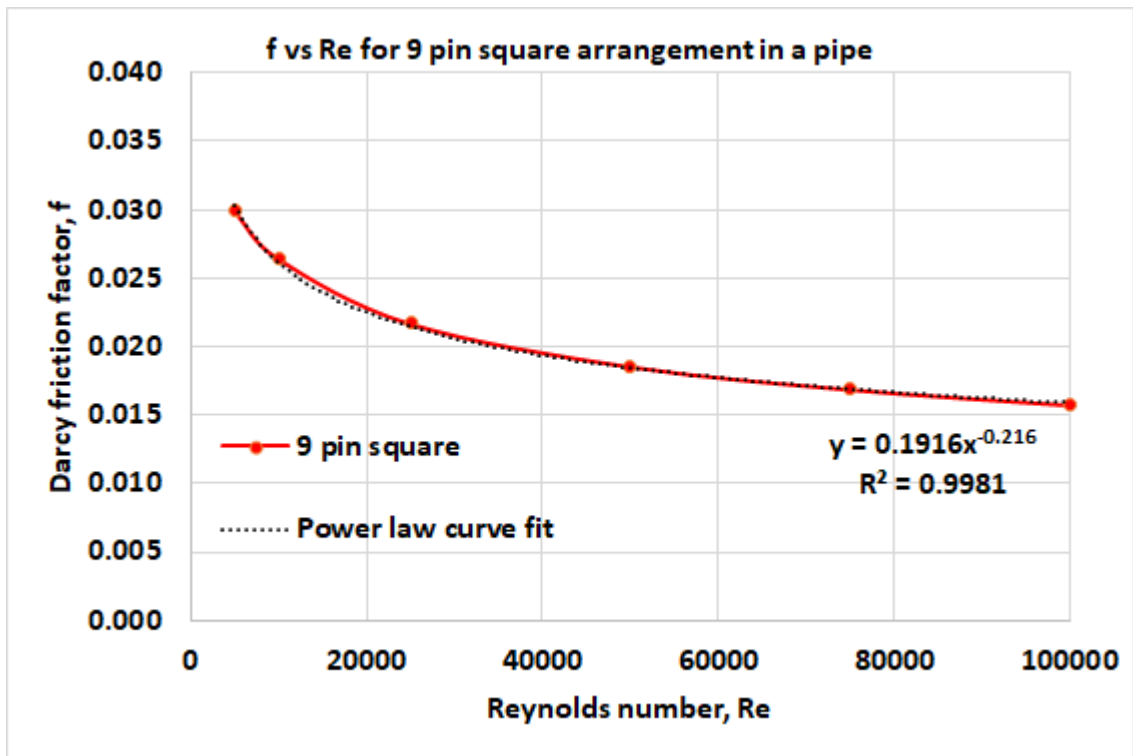
Figure 5-14: Friction factor vs Reynolds number - 9 pin square pipe from CFD results with power law curve fit
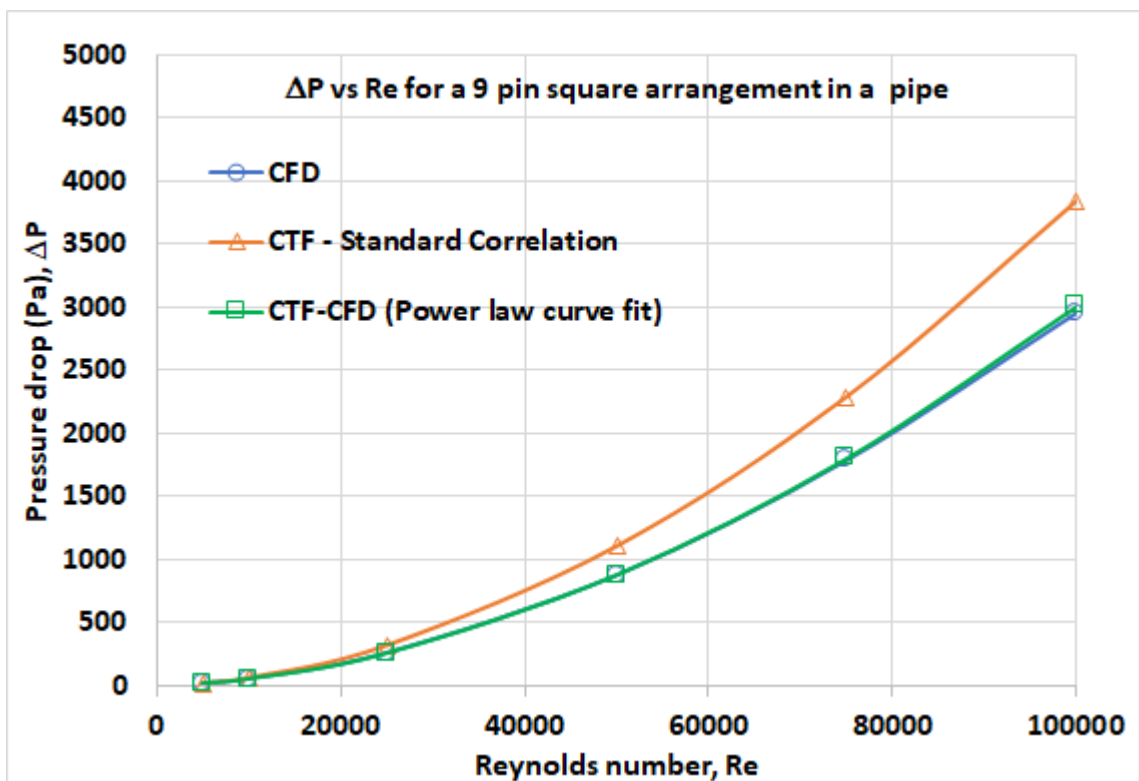
Figure 5-15: Pressure drop vs Reynolds number - 9 pin square pipe showing the effect of the implementation of the power law curve fit (f vs. Re) from CFD in CTF
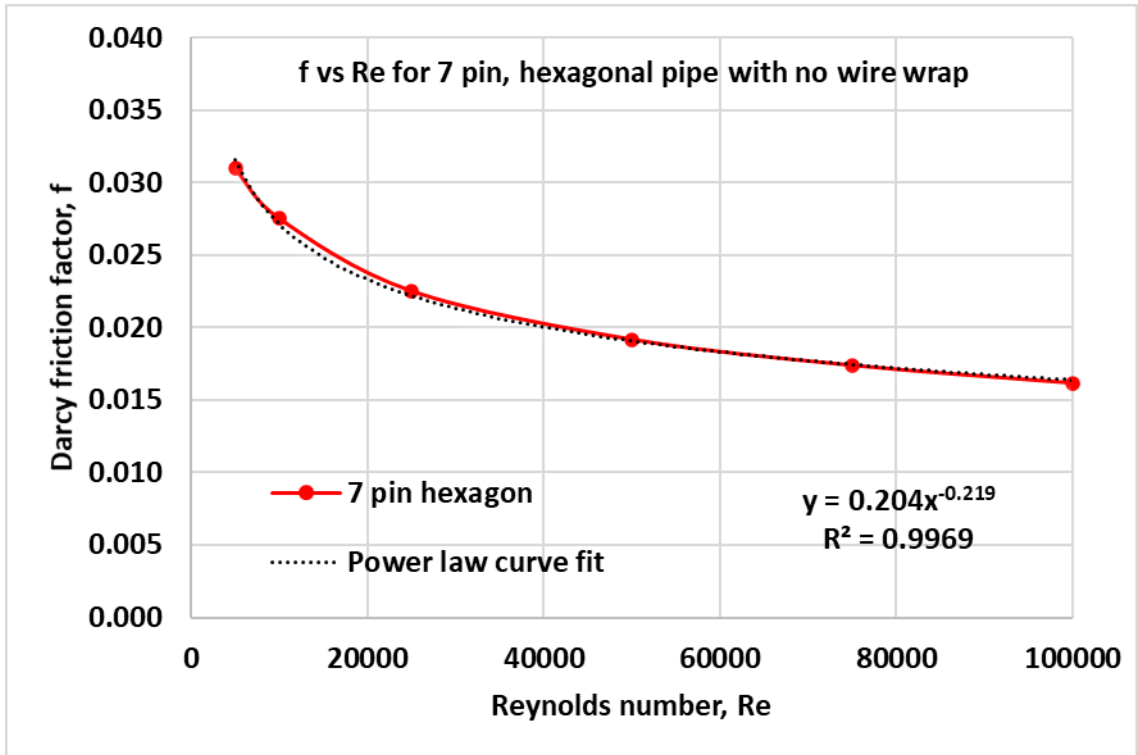
Figure 5-16: Friction factor vs Reynolds number - 7-pin hexagonal pipe with no wire wrap from CFD results with power law curve fit
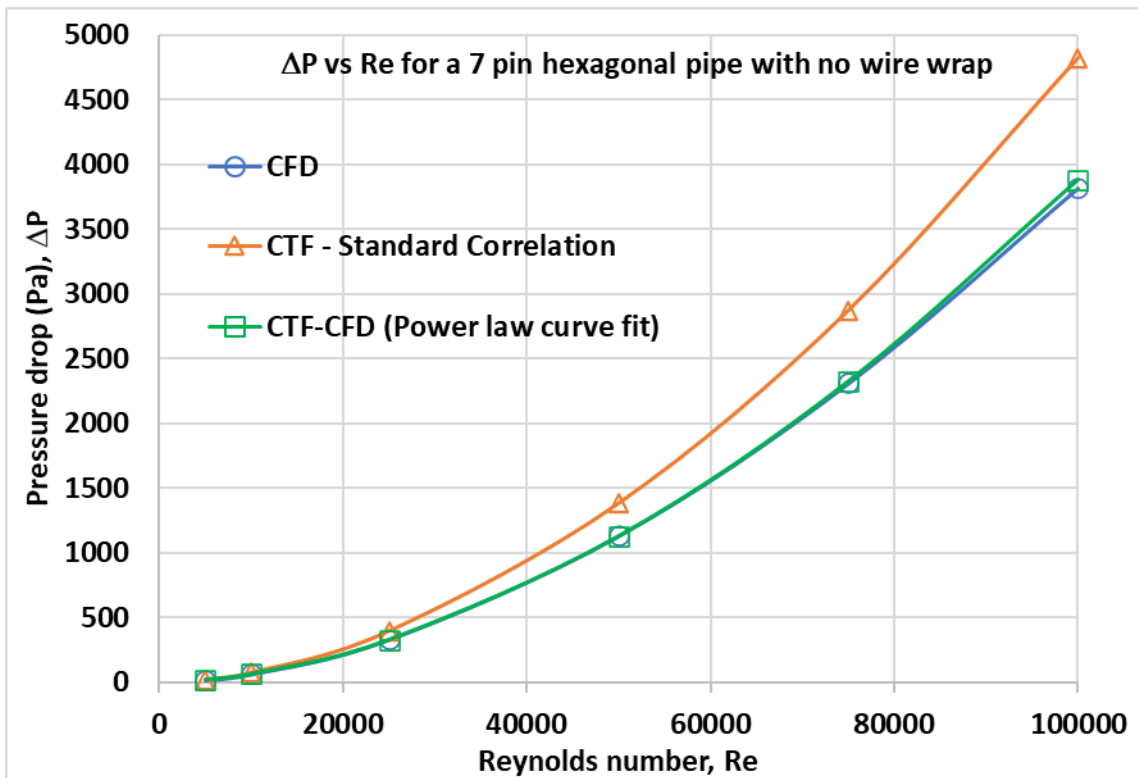
Figure 5-17: Pressure drop vs Reynolds number - 7-pin hexagonal pipe with no wire wrap showing the effect of the implementation of the power law curve fit (f vs. Re) from CFD in CTF
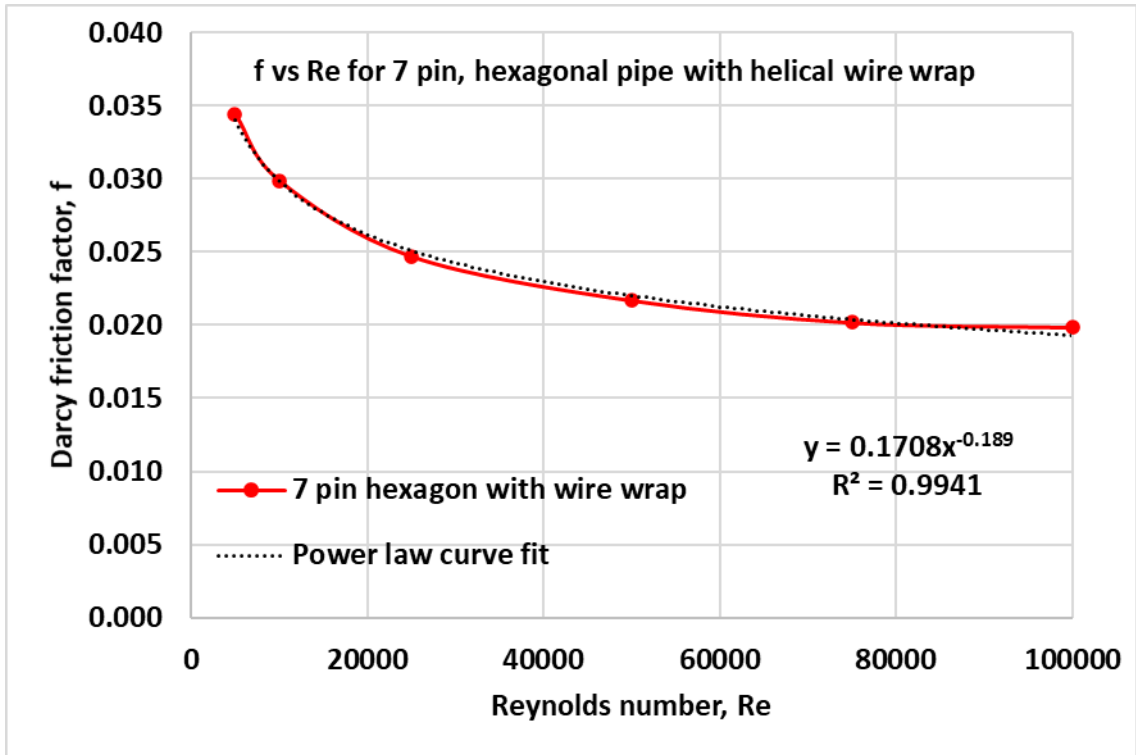
Figure 5-18: Friction factor vs Reynolds number - 7-pin hexagonal pipe with helical wire wrap from CFD results with power law curve fit
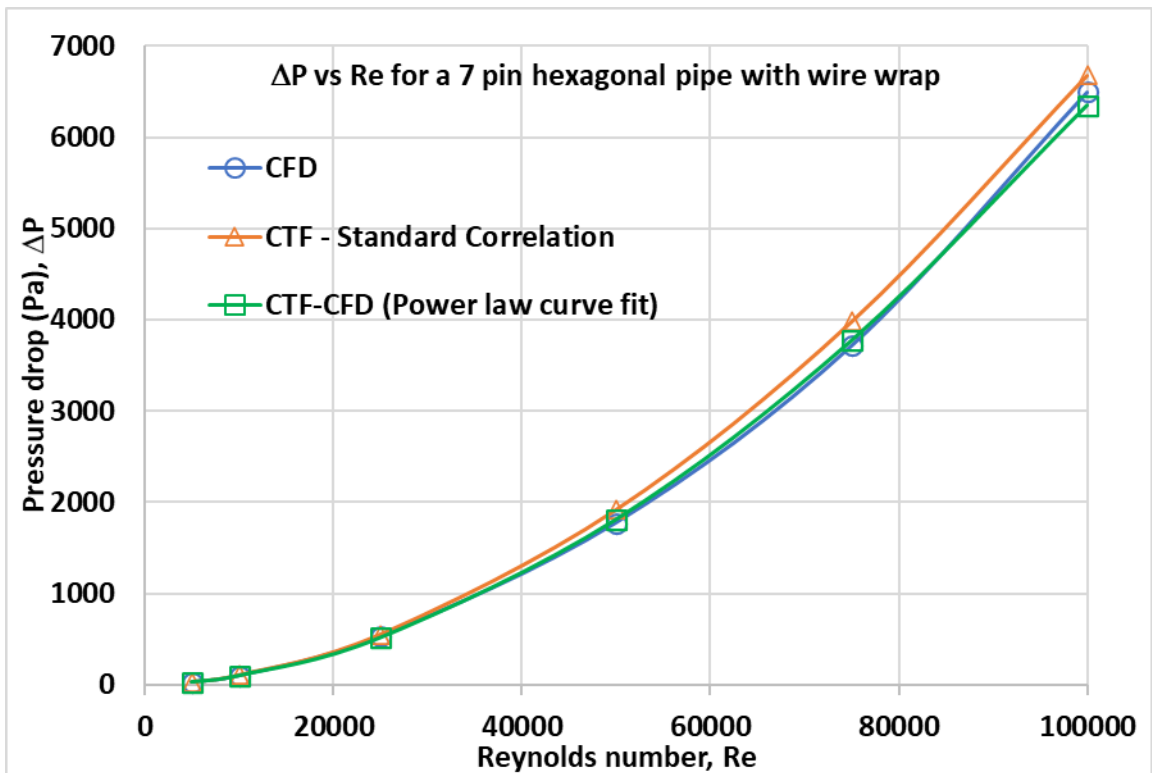
Figure 5-19: Pressure drop vs Reynolds number - 7-pin hexagonal pipe with helical wire wrap showing the effect of the implementation of the power law curve fit (f vs. Re) from CFD in CTF
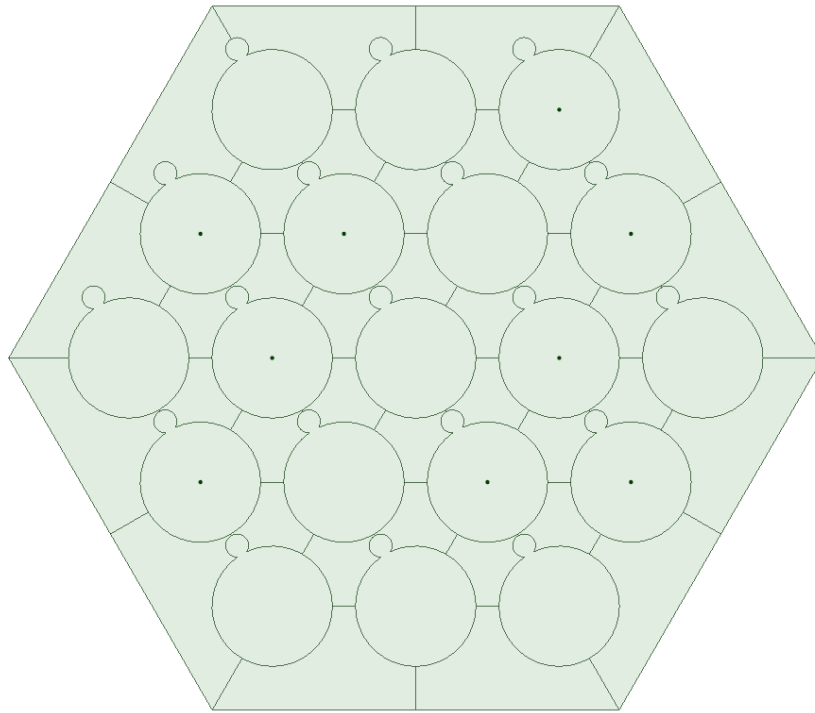
*Figure 5-20: Subchannel splitting of 19-pin fuel assembly, also the radial mesh for CTF*
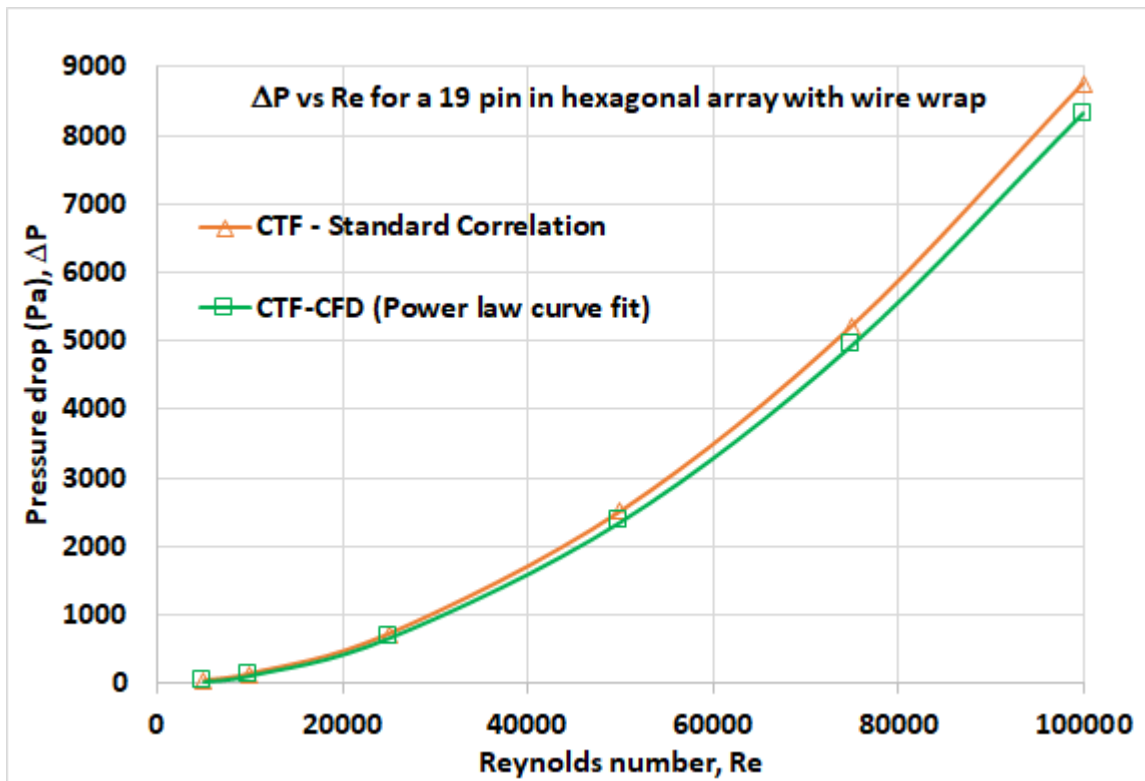
Figure 5-21: Pressure drop vs Reynolds number - 19-pin hexagonal pipe with helical wire wrap using the power law curve fit (f vs. Re) from 7-pin hexagonal pipe CFD analysis.

While the figures above show the averaged values for the whole fuel assembly, of the pressure drop, the following table gives a much deeper insight into the flow thorough the detailed representation of the Reynolds number for each of the calculated sub-channel. This shows on the one hand the power of the coarse mesh CTF solution, but on the other hand the weaknesses of the modelling capability. The power of using coarse mesh such as sub-channel analysis is that it is much quicker as compared a high-fidelity model (for instance CFD) and hence the turnaround time is significantly less for understanding the design performance. For example, using the workstation Dell Precision Tower 7910, with 8 nodes, the typical run time for the CFD analysis is around 6 hours while the single node gives the results from CTF is less than a minute. Additionally, taking advantage of less turnaround time, a great deal of sensitivity studies can be performed which will give good insight into the design aspects.

The weakness is that in the model, the wire is located stationary in the subchannel 9 which leads to reduced Reynolds numbers in this channel. In reality, the wire is wrapped spiralling around the fuel pin, thus it appears in different vertical sections in different places.

A similar effect will not appear in the central subchannels since each of them share half a wire with another channel. However, it is interesting, that there is still a small deviation in subchannel-12, which could be explained with statistical uncertainty and convergence criteria. However, this deviation increases with increasing Reynolds number and stays in the same channel.

There are three combinations of Reynolds numbers predicted in the side sub channels and this is due to the way that the wire is obstructing the flow in those channels as per the given input file for CTF. For instance, full wire is present for subchannels 4 and 10 and hence reduced Reynolds number is predicted. Likewise, there is no wire present for subchannels 8 and 15, consequently predicting higher Reynolds number for flow through them.

Table 5-2: Reynolds number at various subchannels for Rig-1 geometry

Reynolds numbers inside the domain - CTF results						
Inlet	**5000**	**10000**	**25000**	**50000**	**75000**	**100000**
Corner Subchannels						
Channel-1	5525	11049	27623	55246	82869	110496
Channel-3	5519	11038	27594	55188	82782	110380
Channel-9	3924	7849	19622	39243	58865	78489
Channel-14	5519	11038	27594	55188	82782	110380
Channel-16	5519	11038	27594	55188	82782	110380
Channel-18	5519	11038	27594	55188	82782	110380
Average	5254	10508	26270	52540	78810	105084
Centre Subchannels						
Channel-5	3298	6596	16490	32979	49469	65960
Channel-6	3299	6597	16493	32985	49478	65973
Channel-7	3299	6597	16494	32987	49481	65977
Channel-11	3298	6597	16491	32983	49474	65968
Channel-12	3302	6604	16511	33022	49533	66047
Channel-13	3299	6598	16494	32988	49482	65978
Average	3299	6598	16496	32991	49486	65984
Side Subchannels						
Channel-2	5878	11757	29392	58784	88176	117573
Channel-4	5371	10743	26856	53713	80569	107429
Channel-8	6462	12924	32309	64618	96927	129241
Channel-10	5370	10741	26851	53703	80554	107410
Channel-15	6462	12923	32308	64616	96924	129237
Channel-17	5874	11749	29372	58744	88116	117492
Average	5903	11806	29515	59030	88544	118064

Figure 5-22, Figure 5-23 and Figure 5-24 present the typical velocity magnitudes of the flow at 100,000 for 9 pin square array, 7-pin hexagonal without and with wire wrap. Figure 5-22 and Figure 5-23 demonstrate that the flow inside each and every subchannel is highly symmetric. This is comparable to the straight flow patterns inside the subchannels for an LWR since the flow is not disturbed by wire (due to the absence of helical wire wrap). Figure 5-24 shows the more realistic scenario for a fast reactor fuel assembly; the images in this figure clearly point out that there is a clear influence of the wire on the flow distribution and on the flow path lines. The wire follows the helical path and consequently changing the flow area from one position to the other inside the subchannels and further affecting the flow distribution both radially and axially inside the subchannels. Due to the nature of the helical twist, the flow also tends to follow the helical path nearby wire and pin intersection areas, and this can be witnessed in the path lines presented in the image within Figure 5-24.

The current CFD model is for fully developed and periodic flow. This means that the CFD model represents a section of an infinitely long pipe where the flow is fully established and periodic in nature due to the presence of wire wraps. In a realistic case there would be an addition of some transition length which will be required to achieve fully developed flow. For most practical engineering applications, the entrance effects are negligible beyond a pipe length of 10 times the diameter of the pipe (Cengel & Cimbala 2006). Based on this, a rough estimate for Rig-1 geometry is that the first 3 wraps will enable the fully developed region, and wraps 4 and 5 are for measurement regions corresponding to the fully developed region and final wrap (6) is to account for any exit effects (Roop & Brendan 2020). Hence, it can be noted that the results of velocity contours and path lines presented in Figure 5-22, Figure 5-23 and Figure 5-24 are for fully developed flow region of the Rig-1.

The colorbar values (m/s):
6.22, 5.91, 5.60, 5.29, 4.98, 4.66, 4.35, 4.04, 3.73, 3.42, 3.11, 2.80, 2.49, 2.18, 1.87, 1.55, 1.24, 0.93, 0.62, 0.31, 0.00

Contours of velocity magnitude (m/s) for Reynolds number of 100,000 along with path lines
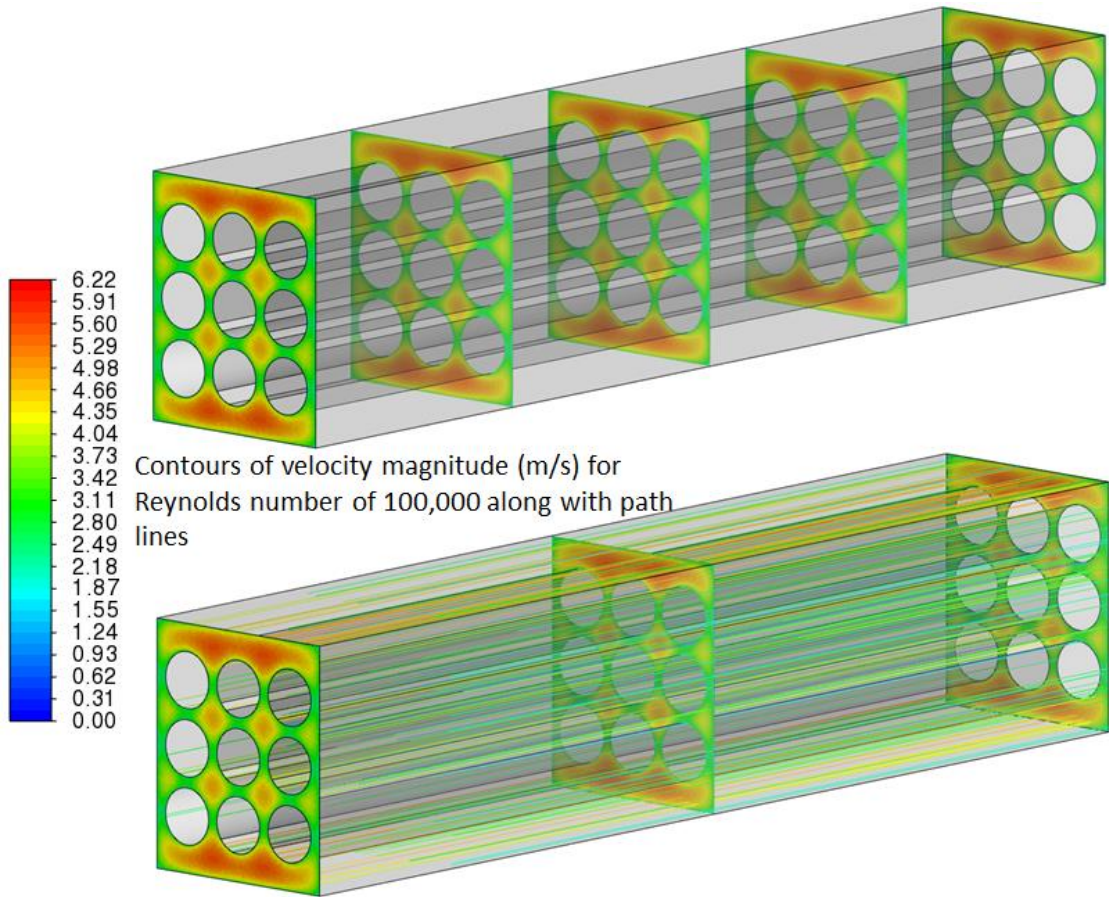
Figure 5-22: Contours of velocity (m/s) & path lines for 9 pin square arrangement in a rectangular pipe

Contours of velocity magnitude (m/s) for Reynolds number of 100,000 along with path lines
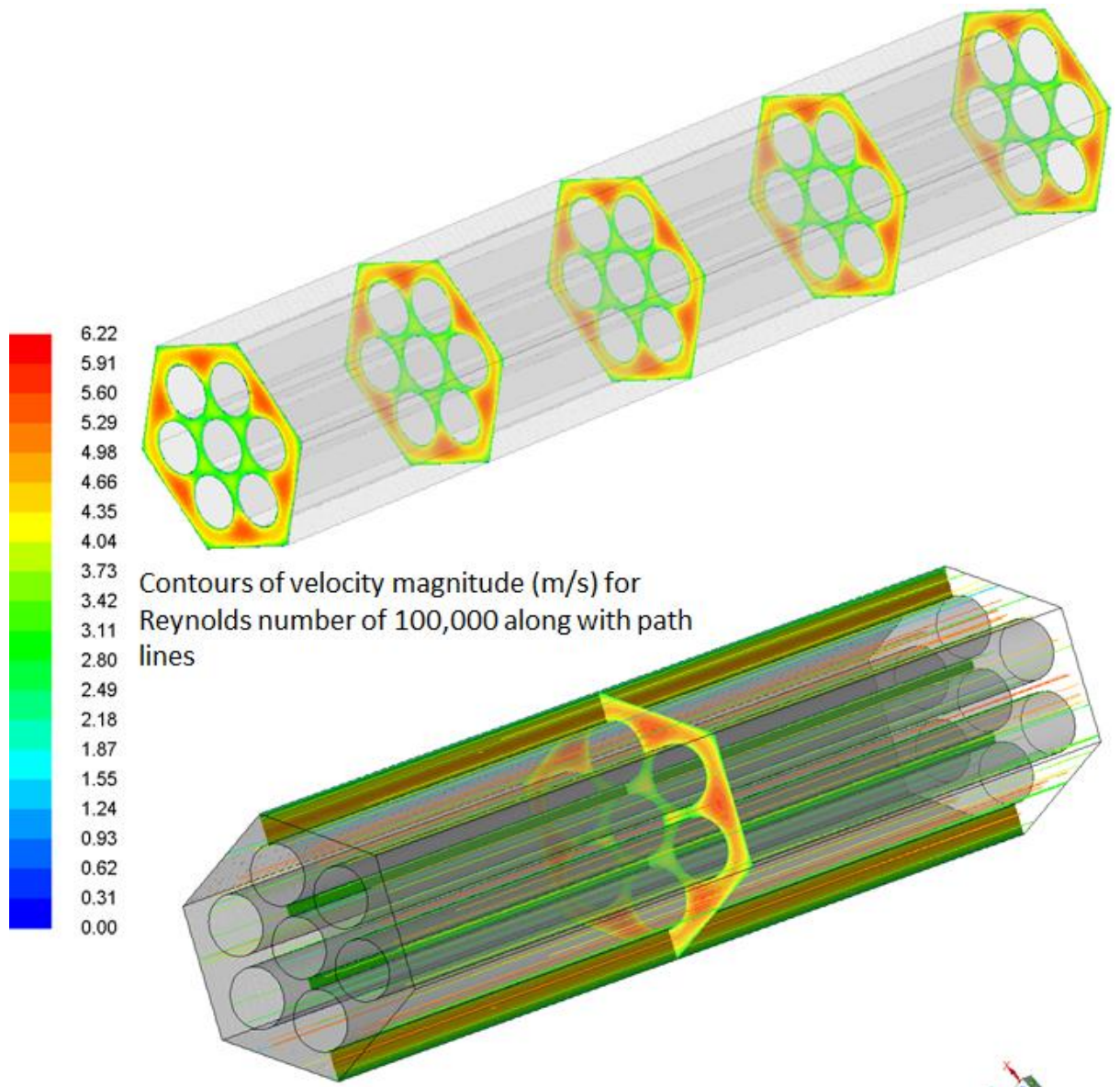
Figure 5-23: Contours of velocity (m/s) & path lines for 7-pin triangular arrangement in a hexagonal pipe
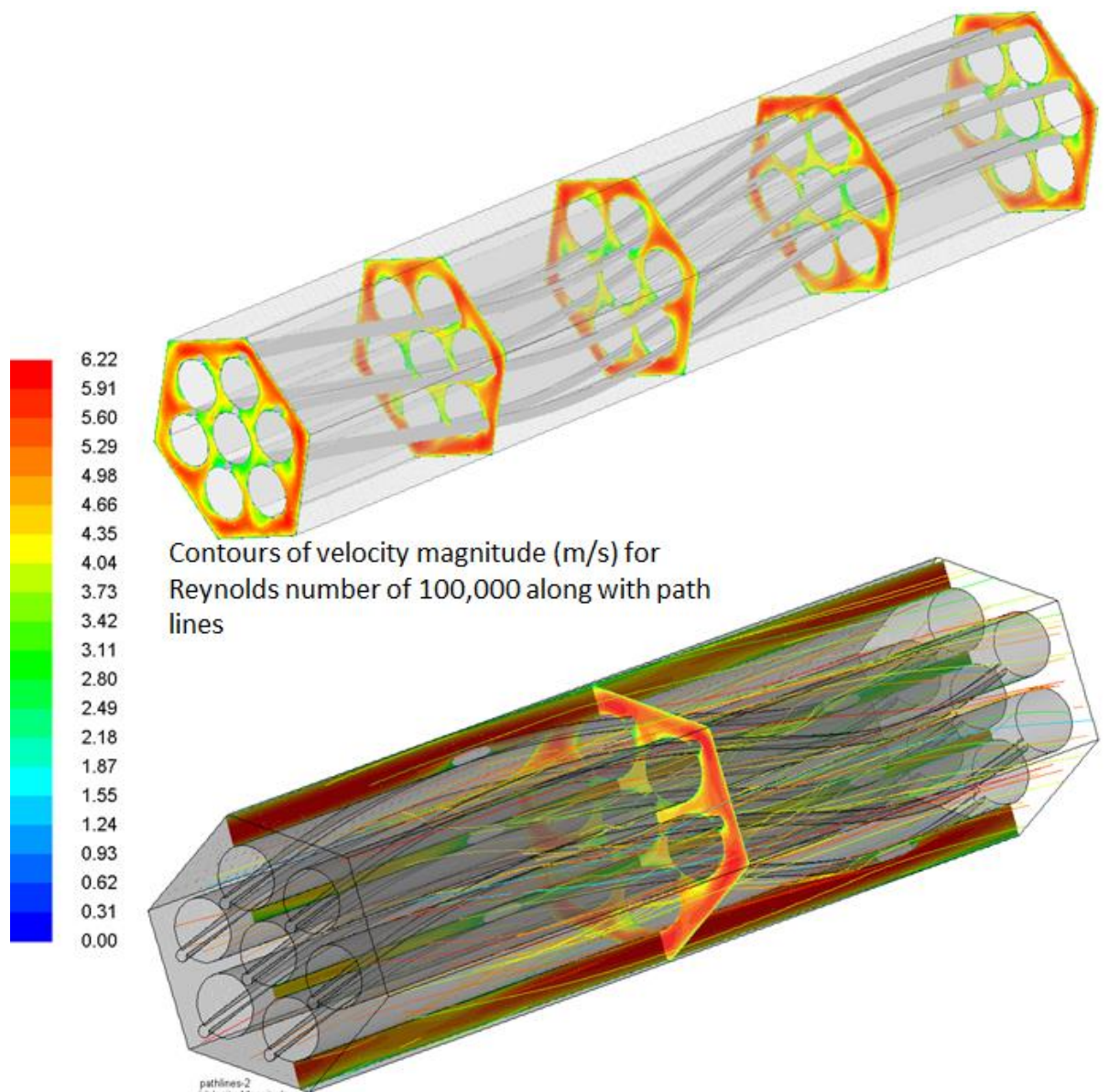
Figure 5-24: Contours of velocity (m/s) & path lines for 7-pin triangular arrangement in a hexagonal pipe – Rig-1 geometry

5.6   Conclusions

From the results of the various analyses activities carried out in this chapter in relation to the Rig-1, the following conclusions can be drawn:

1. A method has been developed to predict the accurate pressure drops for the subchannel code CTF for sub fuel assemblies. This method employs the frictional coefficients obtained from the CFD analysis replacing the standard frictional correlations available within CTF. The method is tested on various pin arrangements ranging from square array to triangular array to the current Rig-1 design that has a

hexagonal pipe with 7 fuel pins with wire wrapped around them, replicating fuel rod structure inside a sodium cooled fast reactor.

2. CTF predictions of pressure drop from its standard frictional correlations tends to overpredict as compared to the CFD results. For 9 pin square array arrangement and 7-pin triangular array arrangement of pins without wire wrap the estimated pressure drops as calculated in the CTF code are about 25% higher as compared to the results from the CFD. For 7-pin triangular array with wire wrap, the CTF standard correlations have predicted around 6% higher pressure drop as compared to the pressure drops from the CFD.

3. When frictional coefficients calculated from the CFD model are applied in the CTF code, the results of pressure drop from CTF for all the cases investigated are overpredicted only by about 0.5% as compared with the data from CFD, and this is an excellent improvement in the accuracy of predictions from the CTF code.

4. In general fuel assembly is characterised by three types of subchannels (centre, side and corner) which are repetitive in nature, thus calculating frictional coefficients for each type would be sufficient to model the full fuel assembly regardless of the size (19-pin or 37-pin or even higher)

5. CFD analysis from the published literature showed that the frictional coefficients for 7-pin and 19-pin in hexagonal arrays are similar. Using the same frictional coefficients (obtained for 7-pin), CTF model was built for 19-pin and pressure drops were found out from the CTF code. The usage of friction factor coefficients, which are obtained from 7-pin hexagonal studies, for 19-pin hexagonal has enabled computationally a better efficient method (than detailed CFD studies) to predict the pressure drops in fuel assemblies for sodium fast cooled reactors' or any other reactors' assemblies.

6. The weakness of the subchannel codes in terms of predicting the varying flow along the helical wire wrap is exposed. While subchannel codes such as CTF gives a lot of insight into the flow details in terms of radial distribution within the subchannels, they still have limited abilities in terms of finding the flow patterns of flows inside a subchannels with pins having wire wrapped around them. CFD is still the best tool to understand and visualise the flow inside subchannels for sodium fast cooled reactors despite its limitations in dealing with transients in complex multi-phase flows.

7. The improved CTF model can be used to do a range of parametric studies which includes slight variations in the geometry (due to manufacturing tolerances etc.) and their effects on the flow at a quicker turnaround time. In addition to this, this improved approach of CTF code can be used for better representation of flows for safety related thermofluidic studies.

CHAPTER 6: CONCLUSIONS AND FUTURE WORK

6.1   Introduction

Project FAITH, which is part of the UK government funded Advanced Manufacturing and Materials (AMM) phase 2 nuclear innovation programmes, provided an excellent opportunity to develop skills in nuclear thermal hydraulics area. These specialised skills in this domain can further be applied to Gen IV reactor studies within the UK. The MPhil project described in this report was developed through this opportunity and represents one contribution FAITH is making to re-establishing UK expertise. During this MPhil program, subchannel code called CTF was used to model the Rig-1 facility which is being built at NNL's Workington facility in a modular manner by Cammell Laird. The current chapter outlines the key activities that have been undertaken during this MPhil program; the major conclusions from the various studies performed and a few recommendations for the future work have been suggested.

6.2   PSBT validation studies

The initial studies include building a CTF model of 5x5 rod bundle in a square lattice which was used for PSBT validation studies and their test cases(Rubin & Avramova 2011b; Rubin, Avramova & Velazquez-Lozada 2016b; Rubin et al. 2012). The output from the code was compared against the measurements. The primary output parameter that was compared was void fraction with the experimental data. CTF results does not correspond well with the measurements for test points with measured maximum void fractions of less than around 0.2, however, CTF underpredicts more consistently for cases where the maximum measured void fraction is greater than 0.5. The reasonable agreement (considering the lower mean errors and standard deviations) with the test data confirmed that the geometry and complex multi-phase flow effects are well captured by the code through the developed input model and accurate settings. The void fraction was also compared with the predicted values from the other codes within the industry. The current CTF model predicts lower mean errors and standard deviations (ranging from 0.018 to 0.05 for standard deviation) than many other codes which were used by various nuclear companies and research institutions. In the absence of measurements for pressure drop data, the simulation values from CTF are compared with the predictions from other codes and it is found that CTF predictions align well with many other

codes. Overall, the comparison of the simulated data with measurements and also with several other industrial codes has reinforced the confidence on applying CTF knowledge to practical systems.

6.3   PNNL validation studies

The next validation case which is more relevant to Rig-1 from the point of view of fully single - phase, representing the flow regimes in sodium fast cooled reactors has been carried out on a 2 × 6 rod bundle where the measured data is available from Pacific Northwest National Laboratory [4]. The experiments comprise a number of cases including isothermal and heated rod scenarios, everything operated at single-phase. These cases were modelled using CTF and results were compared against the experiments. In general, the trends were in good agreement with the measurements, however, the discrepancies between experiments and CTF results were significant in the vicinity of the wall regions. This needs further investigation by using more sophisticated analysis platform such as CFD. Overall, this validation exercise has proved that the subchannel code CTF can be used with confidence for single phase flow problems with heat transfer within sub fuel assemblies.

6.4   Modelling and simulation activities related to Rig-1

Finally, studies were performed using the CTF code on the Rig-1 geometry that has a 7-pin arrangement in a triangular array in a hexagonal pipe. The single-phase flow at normal atmospheric pressures with triangular array arrangement of pins and in addition with the wire wraps around these pins creates as such a non-standard problem for the CTF code. This study focussed on developing a method for obtaining accurate and reliable results from the CTF code for the non-standard cases like Rig-1 geometry. To begin with, a 9-pin in a square array was considered. This geometry is considered to be a standard one for CTF except for the operating conditions which are atmospheric temperature and pressure. Later, two models, which were 7-pin configurations in a triangular array one of them was without wire wrap and the other one was with wire wrap, were considered for the current work. These geometries deviate from the standard problems (forms non-standard problems) for which CTF has been traditionally used. This novel method employs frictional coefficients for the CTF code which are in turn obtained from the detailed CFD analysis on the corresponding geometries for the flow regimes of interest. These frictional coefficients essentially replace the standard frictional

correlations used in the CTF code which will be used to estimate the average pressure drop of the sub-assemblies modelled. It is found that the standard frictional have tended to overpredicted the pressure drops as compared with the results of CFD. Using the newly invented approach, the relative error between CTF and CFD has been reduced from about 25% for both the 9-pin in square array and 7-pin in triangular array without wire wrap to less than 0.5%. Similarly, the relative error for 7-pin in triangular array with helical wire wrap, which is essentially the Rig-1 geometry, has been reduced from around 6% to less than 0.5%. The weakness of the subchannel code CTF has also been discussed within the context of predicting flow details along the length of the subchannels where the flow area keeps changing from one subchannel to the other due to the way the helical wire is wrapped around the pins. While CTF still gives a great insight into the radial distribution of flow for fuel assemblies, and for varying flow areas along the length of the subchannels, it fails to predict the accurate representation of the flow behaviour due its coarse mesh nature. CFD is still the best choice to understand and visualise the flow inside subchannels of these types (pins with helical wire wrap) which are used in sodium cooled fast reactors, but at a significantly higher cost. The improved CTF model approach can be used to do a range of parametric studies which includes slight variations in the geometry (due to manufacturing tolerances etc.) or flow areas of various subchannels (central, corner or side etc.) and their effects on the flow at a quicker turnaround time. This improved approach of CTF code can also be used for better representation of flows for safety related thermofluidic studies.

6.5   Summary of activities undertaken during MPhil work

Furthermore, the key activities that were undertaken during the MPhil programme at University of Liverpool have been summarised in Table *6-1*. It is also worth mentioning that the gained skill set and the knowledge as part of this FAITH programme can be directly transferrable to many other reactor systems that are mentioned in the following table (see Table *6-1*).

Table 6-1: Various activities performed during this MPhil program and the application of the skill set

Activity	Application of the skills set
Relap5 Training - A system level thermal hydraulics code - Basic course	✓ The Relap5 system level thermal hydraulics code finds application in the system level simulations. For example, nuclear reactor core and primary coolant systems, and the entire nuclear power plant.
CTF Training - A subchannel thermal hydraulics code - Basic course	
PSBT - validation studies for multi-phase flow	✓ Subchannel code CTF finds application at reactor core simulations and the details around the subchannels.
PNNL - validation studies for single-phase flow	✓ CFD acts as a high-fidelity model for the subchannel analysis and provides lot of insight into the flow around these subchannels.
Rig-1 flow calculations - single-phase flow (CTF-CFD simulations)	✓ The coupling of CFD to subchannel codes (CTF) or/and system codes (Relap5) has become the research focus in Light Water Reactors, Gen-IV Reactors and including Small Modular Reactor (SMR)/ Advanced Modular Reactor (AMR).
	✓ The acquired skills during this master's programme are directly transferrable to other national nuclear programmes within UK such as UK-SMRs and AMRs, and not just limited to Project-FAITH.

6.6 Future work

1. The current studies have compared the CTF results only with CFD results, this is because the experimental measurements are still not available at the time. Ideally, the CTF results should be compared with measurements.

2. CTF model has certain input mechanisms to account for the changing flow area along the length of the subchannel due to wire-wrap's presence is different to each subchannel. One of the methods is choosing each axial node where the area changes and include wetted perimeter, channel area and gap width. There is also another method where the card group corresponding to spacers is used to account for pressure losses by means of defining pressure loss coefficients. This is a tedious task and normally not recommended to use this approach for the wire wraps, however, this needs more detailed investigations to confirm this.

3. Further investigations need to be carried on testing to split channels to see if the current CTF model could deliver higher fidelity with reasonable increased accuracy. This means the flow area and wetted perimeter of the subchannel region that is available between the pins can further be divided into smaller sections and can be still connected.

4. Heat transfer studies need to be performed, the current work focussed only on isothermal analysis. The estimate of heat transfer calculations is similar to the pressure drops in CTF where in empirical correlations on heat transfer coefficients have been used. Obtaining these heat transfer coefficients from CFD and implementing them in CTF code could maybe further enhance the CTF code performance in terms of accurate predictions on temperatures.

References

Aumiller, D., Tomlinson, E. & Bauer, R. (2001) 'Coupled RELAP5-3D/CFD methodology with a proof-of-principle calculation', *Nuclear Engineering and Design - NUCL ENG DES*, vol. 205, pp. 83-90.

Bertocchi, F., Rohde, M. & Kloosterman, J.L. (2019) *PIV measurements inside a wire-wrapped hexagonal rod bundle: from experiments to governing equations*.

Beus, S. (1972) *TWO-PHASE TURBULENT MIXING MODEL FOR FLOW IN ROD BUNDLES*, Bettis Atomic Power Lab., Pittsburgh, Pa.,

Bubelis, E. & Schikorr, M. (2008) 'Review and proposal for best fit of wire-wrapped fuel bundle friction factor and pressure drop predictions using various existing correlations', *Nuclear Engineering and Design*, vol. 238, no. 12, pp. 3299-3320.

Cengel, Y.A. & Cimbala, J.M. (2006) 'Fluid Kinematics', *Fluid Mechanics Fundamentals and Applications, Mc Graw Hill Higher Education*, p. 327.

Chang, S.-K., Kim, S. & Song, C.-H. (2014) 'Turbulent mixing in a rod bundle with vaned spacer grids: OECD/NEA–KAERI CFD benchmark exercise test', *Nuclear Engineering and Design*, vol. 279.

Chen, S.K., Todreas, N.E. & Nguyen, N.T. (2014) 'Evaluation of existing correlations for the prediction of pressure drop in wire-wrapped hexagonal array pin bundles', *Nuclear Engineering and Design*, vol. 267, pp. 109-131.

Cheng, S.-K. & Todreas, N.E. (1986) 'Hydrodynamic models and correlations for bare and wire-wrapped hexagonal rod bundles—bundle friction factors, subchannel friction factors and mixing parameters', *Nuclear engineering and design*, vol. 92, no. 2, pp. 227-251.

Chun, M.-H. & Seo, K.-W. (2001) 'An experimental study and assessment of existing friction factor correlations for wire-wrapped fuel assemblies', *Annals of nuclear energy*, vol. 28, no. 17, pp. 1683-1695.

Dominguez-Ontiveros, E., Estrada-Perez, C. & Hassan, Y. (2010) Experimental Turbulence Analysis of Fuel Bundle With Spacer Grids, *International Conference on Nuclear Engineering*, vol. 49309, pp. 913-922.

Dominguez-Ontiveros, E. & Hassan, Y. (2009) 'Non-Intrusive Experimental Investigation of Flow Behavior Inside a 5X5 Rod Bundle With Spacer Grids Using PIV and MIR', *Nuclear Engineering and Design*, vol. 239, pp. 888-898.

Fluent, A. (2021) 'ANSYS Fluent 2021 R1 user's guide and theory manual', *Ansys Fluent Inc*.

Gajapathy, R., Velusamy, K., Selvaraj, P., Chellapandi, P. & Chetal, S.C. (2009) 'A comparative CFD investigation of helical wire-wrapped 7, 19 and 37 fuel pin bundles and its extendibility to 217 pin bundle', *Nuclear Engineering and Design*, vol. 239, pp. 2279–2292.

Hoffman, E., Yang, W.S. & Hill, R.N. (2006) *Preliminary Core Design Studies for the Advanced Burner Reactor over a Wide range of Conversion Ratios*, US Department of Energy,

Ikeda, K. & Hoshi, M. (2007) 'Flow Characteristics in Spacer Grids Measured by Rod-embedded Fiber Laser Doppler Velocimetry', *Journal of Nuclear Science and Technology - J NUCL SCI TECHNOL*, vol. 44, pp. 194-200.

In, W.K. (1999) CFD simulation of crossflow mixing in a rod bundle with mixing blades, *Proceedings of the Korean Nuclear Society spring meeting*, KNS, Korea, Republic of, pp. oneCD-ROM.

Kim, J.-B., Jeong, J.-Y., Lee, T.-H., Kim, S., Euh, D.-J. & Joo, H.-K. (2016) 'On the Safety and Performance Demonstration Tests of Prototype Gen-IV Sodium-Cooled Fast Reactor and Validation and Verification of Computational Codes', *Nuclear Engineering and Technology*, vol. 48, no. 5, pp. 1083-1095.

Li, X., Mi, Z., Tan, S., Wang, X., Wang, R. & Ding, H. (2019) 'Experimental investigation of fluid mixing inside a rod bundle using laser induced fluorescence', *Progress in Nuclear Energy*, vol. 110, pp. 90-102.

Masterson, R.E. (2019) *Nuclear Reactor Thermal Hydraulics: An Introduction to Nuclear Heat Transfer and Fluid Flow*, CRC Press.

Merzari, E., Fischer, P., Yuan, H., Van Tichelen, K., Keijers, S., De Ridder, J., Degroote, J., Vierendeels, J., Doolaard, H., Gopala, V.R. & Roelofs, F. (2016) 'Benchmark exercise for fluid flow simulations in a liquid metal fast reactor fuel assembly', *Nuclear Engineering and Design*, vol. 298, pp. 218-228.

Nguyen, T., Goth, N., Jones, P., Lee, S., Vaghetto, R. & Hassan, Y. (2017) 'PIV measurements of turbulent flows in a 61-pin wire-wrapped hexagonal fuel bundle', *International Journal of Heat and Fluid Flow*, vol. 65, pp. 47-59.

Novendstern, E. (1972) 'Turbulent flow pressure drop model for fuel rod assemblies utilizing a helical wire-wrap spacer system', *Nuclear Engineering and Design*, vol. 22, no. 1, pp. 28-42.

Patankar, S. *Numerical Heat Transfer and Fluid Flow, Series in Computational Methods in Mechanics and Thermal Sciences,(1980)*, McGraw-Hill Book Co.

Patankar, S. (2018) *Numerical Heat Transfer and Fluid Flow*, CRC Press.

Patel, N. (2020) 'CFD mesh investigation study for a fuel assembly (4 times scale) as designed for

the water rig for project FAITH', *NNL Reference*, no. 3.

Podila, K. & Rao, Y.F. (2015) *A comparative study of the commercial CFD codes: ANSYS Fluent and STAR-CCM+ to simulate nuclear fuel bundles*, Canada

Quigley, M., McMonagle, C. & Bates, J. (1977) *Investigation of combined free and forced convection in a 2 x 6 rod bundle.[LMFBR]*, Battelle Pacific Northwest Labs., Richland, Wash.(USA),

Rehme, K. (1973) 'Pressure drop correlations for fuel element spacers', *Nuclear technology*, vol. 17, no. 1, pp. 15-23.

Rolfo, S., Péniguel, C., Guillaud, M. & Laurence, D. (2012) 'Thermal-hydraulic study of a wire spacer fuel assembly', *Nuclear Engineering and Design*, vol. 243, pp. 251–262.

Roop, T. & Brendan, P. (2020) 'Project FAITH – Pin Test Section Probe Locations', *NNL Reference*, no. 3.

Roop, T., Jonathan, M.-T. & Brendan, P. (2020) 'Project FAITH Functional Specification - Rig 1', *NNL Reference*, no. 3.

Rubin, A. & Avramova, M. (2011a) *OECD/NRC Benchmark Based on NUPEC PWR Subchannel and Bundle Tests (PSBT). Volume II: Benchmark Results for the Void Distribution Phase*, NEA/NSC/DOC,

Rubin, A. & Avramova, M. (2011b) *OECD/NRC Benchmark Based on NUPEC PWR Subchannel and Bundle Tests (PSBT). Volume II: Benchmark Results for the Void Distribution Phase*, NEA/NSC/DOC,

Rubin, A., Avramova, M. & Velazquez-Lozada, A. (2016a) *International Benchmark on Pressurised Water Reactor Sub-channel and Bundle Tests. Volume II: Benchmark Results of Phase I: Void Distribution*, Organisation for Economic Co-Operation and Development,

Rubin, A., Avramova, M. & Velazquez-Lozada, A. (2016b) *International Benchmark on Pressurised Water Reactors Sub-channel and Bundle Tests. Volume II: Benchmark Results of Phase I: Void Distribution, Organisation for Economic Co-Operation and Development*,

Rubin, A., Schoedel, A., Avramova, M., Utsuno, H., Bajorek, S. & Velazquez-Lozada, A. (2012) *OECD/NRC Benchmark Based on NUPEC PWR Sub-channel and Bundle Test (PSBT). Volume I: Experimental Database and Final Problem Specifications*, Organisation for Economic Co-Operation and Development,

Salko Jr, R., Avramova, M., Wysocki, A., Toptan, A., Hu, J., Porter, N., Blyth, T.S., Dances, C.A., Gomez, A. & Jernigan, C. (2019) *CTF 4.0 Theory Manual*, Oak Ridge National Lab.(ORNL), Oak Ridge, TN (United States),

Shen, Y., Cao, Z. & Lu, Q. (1991) 'An investigation of crossflow mixing effect caused by grid spacer with mixing blades in a rod bundle', *Nuclear Engineering and Design*, vol. 125, pp. 111-119.

Specifications, F.P. (2012) 'OECD/NRC Benchmark Based on NUPEC PWR Sub-channel and Bundle Test (PSBT)'.

Summary Review on the Application of Computational Fluid Dynamics in Nuclear Power Plant Design (2022), INTERNATIONAL ATOMIC ENERGY AGENCY, Vienna.

Sung, Y., Kucukboyaci, V., Cao, L. & Salko, R.K. (2015) 'COBRA-TF Evaluation and application for PWR steamline break DNB analysis', *NURETH-16, Paper*, vol. 13431.

Toti, A. (2018) *Development and Validation of a System Thermal-Hydraulic/CFD Codes Coupling Methodology for Multi-Scale Transient Simulations of Pool-Type Reactors*.

Vaghetto, R., Goth, N., Jones, P., Childs, M., Lee, S., Nguyen, T. & Hassan, Y. (2017) 'Pressure Measurements in a Wire-Wrapped 61-Pin Hexagonal Fuel Bundle', *Journal of Fluids Engineering*, vol. 140.

Versteeg, H.K. & Malalasekera, W. (2007) *An Introduction to Computational Fluid Dynamics: The Finite Volume Method*, Pearson Education Limited.

Wimshurst, A. (2020) 'CFD analysis of Water Rig', *FRAZER-NASH Reference*, no. 1.

Yu, F., Class, A.G., Xiao, J. & Jordan, T. (2017) Coarse grid CFD methodology: flux corrections for individual mesh cells and application to rod bundles, *SE 17th International Topical Meeting on Nuclear Reactor Thermal Hydraulics, Xi'an, Shaanxi, China*.